Université d'Ottawa · University of Ottawa

Combustion Model for a Spark Ignited Lean Hydrocarbon-Air Mixture Near Misfire

by

Angus G. Craig

A thesis presented to the
School of Graduate Studies and Research
in partial fulfilment of the
requirements for the degree of

MASTER of APPLIED SCIENCE
in
MECHANICAL ENGINEERING

Ottawa-Carleton Institute for Mechanical and Aerospace Engineering
Department of Mechanical Engineering
University of Ottawa
Ottawa, Ontario, Canada
May 3, 2002

Abstract

A phenomenological model for a turbulent premixed flame in homogeneous turbulence, which incorporates the conservation of the probability distribution function (pdf) of a scalar, was developed. This was used to simulate the lean burn and misfire limits of combustion within a constant volume chamber.

A one-dimensional numerical approximation of the pdf equation in spherical co-ordinates was obtained using the control volume formulation. The air-fuel premixture in the chamber was divided into particles of equal mass, which in turn were distributed among control volumes considered as spherical concentric shells. Monte-Carlo methods were applied to model the diffusion of particles between and mixing of particles within the concentric spherical shells. The chemical reaction of the mixture used a first order reaction from which a set of ordinary differential equations were solved for the evolution of the temperature and species concentration of each particle. Turbulence was modelled using the rapid distortion theory.

A parametric study was conducted with the present model to show its operation in the misfire region of combustion. There has also been a comparison of mean expansion speeds with the compiled experimental combustion data of Bradley (1992). A suggestion for future research with the established model involves the adoption of the k-ε theory for the development of turbulence-related properties. This would allow comparison to the results obtained with the present rapid distortion theory for turbulence.

Acknowledgments

First, I must express a sincere note of gratitude to Dr. Roger Milane for his generous and unfailing guidance during my time at the University of Ottawa.

I must also acknowledge the support given me by my colleagues at the Emissions Research and Measurement Division of Environment Canada (Environmental Tech Centre; Gloucester, Ontario), in particular, ERMD chief Fred Hendren and engineering head Jacek Rostkowski who both patiently accommodated my irregular schedule.

Lastly, special thanks are due to Kim and her unfailing encouragement - it is to her that I dedicate this thesis.

- A.C.

Table of Contents

List of Figures and Tables

FIGURES

TABLES

Nomenclature

A_b	surface area of burned mass fraction
$A_{pre\text{-}exp}$	pre-exponential to the Westbrook and Dryer single step reaction mechanism
$A(\alpha)$	distribution function (e.g. Dirac delta function) for the mixing model
A	exponent for fuel concentration term in the Westbrook and Dryer single step reaction equation
$A_{1,2}$	first and second moments of $A(\alpha)$
B	activation energy
B	exponent for oxidant concentration term in the Westbrook and Dryer single step reaction equation
C_D	numerical constant for dissipation ε
C_P	constant pressure specific heat
C_ω	empirical constant for mixing rate ω
C_μ	empirical constant for diffusion coefficient Γ_T
D	diffusion rate
Da	Damköhler number
F	fuel mass fraction
f	weighing factor for calculation of values at interface of shells
H	specific enthalpy
K	Karlovitz number (dimensionless flame stretch factor)
k	isotropic turbulent kinetic energy
Le	Lewis number
ℓ	integral microscale length
ℓ_k	Kolmogorov microscale length

ℓ_{tc}	arbitrary length scale (Choi and Huh, 1998) for CFM dimensional consistency
M	mixing term
N	number (quantity) of particles in shell
n_{pairs}	number (quantity) of particle pairs
P	pressure
$\tilde{\mathrm{P}}$	density-weighted average probability density function
R	gas law constant
Re_T	turbulent Reynolds number
R_k	Reynolds number for Kolmogorov microscale
R_ℓ	Reynolds number for integral microscale
R_λ	Reynolds number for Taylor microscale
r	radial (spatial) dimension
Δr_P	radial width (thickness) of shell P
S	source term, rate of productivity of F
S_b	fuel burning speed
S_e	outer spherical surface area of shell P
S_C	source term, rate of productivity of F
S_w	inner spherical surface area of shell P
t	Time
Δt	time-step duration
T	local absolute temperature
$\Im_P$	Production rate of kinetic energy
U	Internal energy
u'	r.m.s. turbulent flow velocity (turbulence intensity)
u'_k	Effective r.m.s. turbulent flow velocity
u_b	mean expansion speed of the flame
u_L	Laminar flame speed
u_t	Turbulent burning velocity
V	Volume
V_b	Volume of burned mass fraction

ΔV_P	Volume of shell P
$\tilde{V}_r$	Density-weighted radial mean velocity
v	Nitrogen concentration
v_T	Kinematic viscosity
$v_{1,2,3,4,5,6}$	Reactant coefficients for the global reaction of carbon dioxide, water, nitrogen, oxygen, carbon monoxide, and hydrogen respectively
w	water concentration
x	fuel species concentration
y	Oxygen concentration
Z	Thermodynamic state
z	Carbon dioxide concentration
z''	Fluctuations of the thermodynamic state

Greek Symbols

α	degree of particle pair mixing (from 0 to 1)
α_F	Carbon parameter for fuel molecule
β	mixing model coefficient for degree of property exchange
β_F	Hydrogen parameter for fuel molecule
Γ_T	Turbulent diffusion coefficient
δ_L	Laminar flame thickness
δ_F	Nitrogen parameter for fuel molecule
ε	Dissipation rate of kinetic energy
ϕ	fuel-air equivalence ratio
ζ_F	Oxygen parameter for fuel molecule
θ	angle of inclination in spherical co-ordinates
φ	angle of rotation in spherical co-ordinates
λ	Taylor microscale length
ρ	Density
$\langle\rho\rangle$	local mean density
σ	scalar fluctuations in flow

σ_k	Empirical constant for kinetic energy k
σ_ε	Empirical constant for dissipation ε
σ_ϕ	Turbulent Schmidt number
τ, τ_a	Integral time scale
τ_c	transit time scale
τ_K	Kolmogorov time scale
ω	mixing frequency

Superscripts

$'$	Difference (fluctuations) from conventional mean value
0	value at time, t
$*$	value at time, $t + \Delta t$

Subscripts

b	burned (products)
$diff$	diffusion
E	outer shell neighbouring P (in a positive direction along r)
e	referring to a outward (radially) direction from shell P
$e-$	leaving shell P through outer surface
$e+$	enterng shell P through outer surface
I	burning particle
L	laminar flow condition
min, max	scalar bounds
P	shell of current interest
R	radial direction from centre of sphere
t, T	turbulent flow condition
U	unburned (reactants)
W	inner shell neighbouring P (in a negative direction along r)
w	referring to an inward (radially) direction from shell P
$w-$	leaving shell P through inner surface
$w+$	entering shell P through inner surface
0	value at time of ignition

Others

$\langle\,\rangle$	conventional mean value
$\tilde{}$	Favre averaged mean value

Chapter 1

Introduction

The motivation to study the combustion phenomenon and its products takes on a greater importance as the world community attempts to identify processes that contribute to global climate change. Recently (1997), at the Kyoto Climate Change Conference for global-warming conference, Canada's federal government pledged to reduce its national CO_2 emissions by 6% from its 1990 levels by the year 2012. With the burning of fossil fuel continuing to dominate the energy economy, it is clear that combustion research must take on a bigger significance if Canada is to meet its emission commitment.

The effect of the conventional internal combustion engine, with its carbon-based fuel, on the elevated levels of CO_2 release is substantial. Lean-burn spark-ignition internal combustion engines offer the attractive prospect of higher thermal efficiency (i.e. less pumping effort from a wider throttle setting) and lower

CO_2 emissions. Unfortunately, combustion with a lean mixture is much slower than with a stoichiometric mixture and, in effect, works against engine fuel economy. This occurs because, to accommodate the relative slowness of the lean burn energy release, ignition timing is advanced and thus imparts counter-productive work to the compression stroke. The future of lean burn in automobiles rests with the need to encourage combustion to progress quickly enough to avoid the inefficiency of extreme spark advance (Schäfer et al, 1995). Another problem with engine lean burn involves the combustion temperatures and the excess of oxygen that together increase emissions of nitrogen oxides (NOx). This regulated exhaust pollutant is proving difficult to control with current abatement technology. It is therefore apparent that more knowledge is needed to assist the development of lean burn combustion in conventional engines.

In this study, a numerical model for combustion that simulates a turbulent premixed flame in a lean hydrocarbon fuel-air gaseous mixture is to be presented. The purpose of this computational study is to predict the progress of a flame in a given environment (similar to that of an internal combustion engine) and help in the understanding of the combustion mechanism and its misfire limits.

1.1 Model Approach

Heywood (1978) has presented a detailed, authoritative classification of combustion models. Combustion models for spark ignition engines are classified

as either phenomenological or multi-dimensional. In the phenomenological approach, empirical knowledge of the basic engine processes is collected and quantified to interact coherently as the model. In multi-dimensional models, the conservation of mass, momentum, species and energy are solved numerically to obtain spatial variations of velocity, temperature, and species concentration.

In this study, the intent is to model and interpret the combustion results in a lean burn environment. This intention is to be pursued by creation of a phenomenological model with the conservation equation of the probability density function (pdf) of a scalar. The Monte Carlo technique is employed as the numerical method for the solution of the discretized governing equation. Pope (1979, 1980) has made thorough use of the Monte Carlo technique to model isothermal flows and combustion. It will be shown in the formulation of Chapter 3 that this approach will have computational advantages by avoiding the necessity of numerical modelling of the source and the convection terms.

The formulation involves the discretization of the governing equation (the pdf conservation equation of a scalar) for one-dimensional spherical flame propagation in a closed vessel. A control-volume method divides the volume of the closed vessel into concentric 'shells'. It is practical that the thermodynamic space defined by the 'shells' be sub-divided into a number of distinct particles each having equal mass. In the version of this method used by Pope, these particles are without mass; however, the present study will affix a mass to each

particle. It is further proposed that these particles could be considered as either unburned, burning, or fully-burned. The expansion velocity is therefore taken into account by the particles with their variable density. This has suitable application with enclosed environments, such as IC engines.

Ignition energy released by a centrally issued spark is equally distributed to a few adjacent particles. Subsequently, the thermodynamic state of these burned and the outlying unburned particles is calculated using the first law of thermodynamics and the volume constraint of the closed combustion chamber.

Turbulence intensity is a property assigned to each particle within the chamber and is calculated during ignition, using the rapid distortion theory for a spherical eddy in a homogeneous turbulent field (Borgnakke et al, 1980). After the ignition event, the development of the turbulence intensity property can be induced according to the rapid distortion theory or the k-ε model (Launder et al, 1972).

The effect of diffusion is achieved by the movement of particles between adjacent shells based on quantitative and directional restrictions. That is, a number of randomly selected particles within each shell (based on the average turbulent intensity) are directed to their adjacent shells.

The mixing process is modelled as in a partially stirred reactor where pairs of particles are chosen, at a frequency determined by the turbulence intensity, to mix.

This binary mixing of particles is assumed to occur instantaneously, and allow the two particles to separate immediately after mixing. The resulting particle pairs will have species concentration, turbulence, temperature, and volume based on a mixing distribution function for the property exchange. It is recognized that such an instantaneous consummation is in conflict with the presumption that mixing models should describe a continuous process that leads to complete mixing. The mixing model of Curl (1963), in yielding complete mixing, produces a sudden jump in thermodynamic space, and therefore may produce faulty results. As a result Pope (1982) proposed several mixing models, including a modified Curl model, which describe intermediate stages before complete mixing. However all of these are discontinuous in nature and do not produce the necessary Gaussian behaviour according to Kosaly (1986). Dopazo (1994) has proposed a continuous model that is not completely satisfactory - especially in homogeneous isotropic turbulence (Norris and Pope, 1994). Lately Correa (1995) has tested all three models (Curl, modified, IEM) and concluded that all three gave adequate results at high frequency of mixing and that all three are unsatisfactory. Pope (1985) proposed a model that accounts for the fact that the composition field in the neighbourhood of a particle influences its mixing. In the absence of a fully satisfactory mixing model, the Curl model (Curl, 1963) has been adopted as a first approximation. This is because the objective is not to test mixing model but to develop this pdf model to predict combustion in confined volume and to show how reasonable the results are irrespective of the shortcomings of the mixing model.

The burning of particles will take place when a burned particle is mixed with an unburned, or a burning one. As with the experimental observation by Namazian et al (1980), all three types of particles; namely unburned, burned, and burning particles, can coexist in the partially stirred reactor.

The evolution of composition and temperature of the burning particles is described by a set of chemical rate equations for all species applied to each burning particle. Using the first law and assuming perfect gas behaviour, an expression for the rate of temperature rise is derived. These equations are solved simultaneously. The results give the species concentration and temperature of each burning particle and subsequently the pressure of the system with each time-step of the simulation.

1.2 Objectives of the Present Study

In this thesis, the objectives are:

1. To formulate a phenomenological model for flame propagation in an air-hydrocarbon fuel gaseous mixture. The direction of the formulation is to respect the conservation of properties (i.e. mass, fuel fraction, volume, and temperature) in a thermodynamic space. A process of discretization of the property conservation equation in a control volume numerical method will provide the basis of analysis. The control volumes will be composed of

particles which each possess the properties mass, fuel fraction, volume, and temperature.

2. To construct an algorithm and conduct a series of computer simulations of the numerical model with a range of input parameters so to predict combustion progress in a given lean burn environment.

3. To compare the results of the computer simulation with published experimental values. This discussion is to be pursued with a focus on the flame speeds, mass burn fraction, and pressure development for the combustion of a lean fuel-air mixture.

4. To determine what aspects of the numerical model might be improved upon in future study.

Successful completion of the above list will be useful in understanding the mechanism and misfire limits of internal combustion. However, it is noted that the numerical modelling does not replace any engine experiments. The purpose of this study is to assist researchers in understanding the results of engine experiments, and to direct future experiments. For this reason, it is recognized that experiment and numerical modelling should always complement one another.

Chapter 2

Literature Survey

2.1 General Overview

Flame propagation in turbulent flow of a premixed solution of gaseous fuel and oxidant is described by any one of several types: wrinkled flame based on laminar flame speed, entrainment controlled based on laminar flame speed and flame propagation in vortex tubes, and microvolume mixing (also known as a mixing-controlled or distributed reaction regime) at relatively higher turbulence intensities. Bradley (1992) has presented data on flame propagation from various sources as a function of the following non-dimensional terms: u_t/u_L, u'/u_L, and $\mathrm{K}\cdot Le$; where u_t is the turbulent flame speed, u_L is the laminar flame speed, u' is the turbulent intensity, K is the Karlovitz number, and Le is the Lewis number. Misfire with the advent of quenching starts to occur when $\mathrm{K}\cdot Le = 0.215$ and, as $\mathrm{K}\cdot Le$ increases, the probability of misfire increases until total quench is assured at

$K \cdot Le = 6.0$. Poinsot et al (1991) have obtained a regime of flame propagation based on a mixing-controlled condition when $K \cdot Le \geq 5.3$.

2.2 Regimes of Premixed Turbulent Combustion

In Glassman (1987), it is stated that, "The interaction of turbulence and chemistry constitute the field of turbulent reacting flows and is of importance whether flame structures exist or not." The Glassman reference reviews the influences and regimes of burning with premixed combustion as a specific, exothermic example of turbulent reacting flows.

The influence of turbulence on combustion is quantified by the use of characteristic lengths (based on the time with which the phenomenon occurs). If a chemical effect is completed over a distance smaller than a mechanical effect (e.g. velocity of the flow) then turbulence is inconsequential to the process. However, if the opposite is true, as in a turbulent flow reactor, then the flame structure will demonstrate an affected chemical reaction and heat release rate. In the extreme case of a 'stirred reactor', the combustion products rapidly mix with reactants in a time much shorter than the burning time. The latter two examples are considered ones in which no contiguous flame structure exists.

Glassman describes regimes of the burning reaction as a function of the root-mean-square (r.m.s.) turbulent velocity fluctuations, u', and the aforementioned characteristic length scales, these length scales being the Kolmogorov length (or

microscale), ℓ_k, which represents the smallest dimension in which dissipation absorbs turbulence, the Taylor length, λ, which relates the occurrence of strain in a viscous medium, and the integral length, ℓ_0, which represents the dimension of the largest eddies of the flow.

If δ_L and u_L represent the thickness and flame speed of a premixed laminar flame respectively, then as turbulence is increased in the reacting flow, successive flame regimes are created and destroyed per Glassman (1987) as follows:

(i) stable laminar flame (smooth thin reaction zone)

(ii) wrinkled flame (thick, bushy reaction zone), $\delta_L < \ell_k$ with flame speed u_L

(iii) severe wrinkling, $\ell_k < \delta_L < \lambda$ where the local flame speed is u_L

(iv) flamelets in eddies (contiguous reaction zone destroyed), $\lambda < \delta_L \leq \ell_0$

(v) distributed reaction zone, $\delta_L > \ell_0$

A definitive chart, shown in Figure 1-1, which delineates the premixed turbulent combustion regimes. The velocity ratio u'/u_L of the flow is plotted against the various turbulent Reynolds number scales. These Reynolds numbers are derived using the characteristic lengths and kinematic laminar viscosity ν as: $R_t = u'\ell_0/\nu$, $R_\lambda = u'\lambda/\nu$, and $R_k = u'\ell_k/\nu$. Here the distributed reaction zone is considered to

exist with very intense turbulence ($u' >> u_L$), and then only above and to the left of the Klimov-Williams line ($\ell_k = \delta_L$).

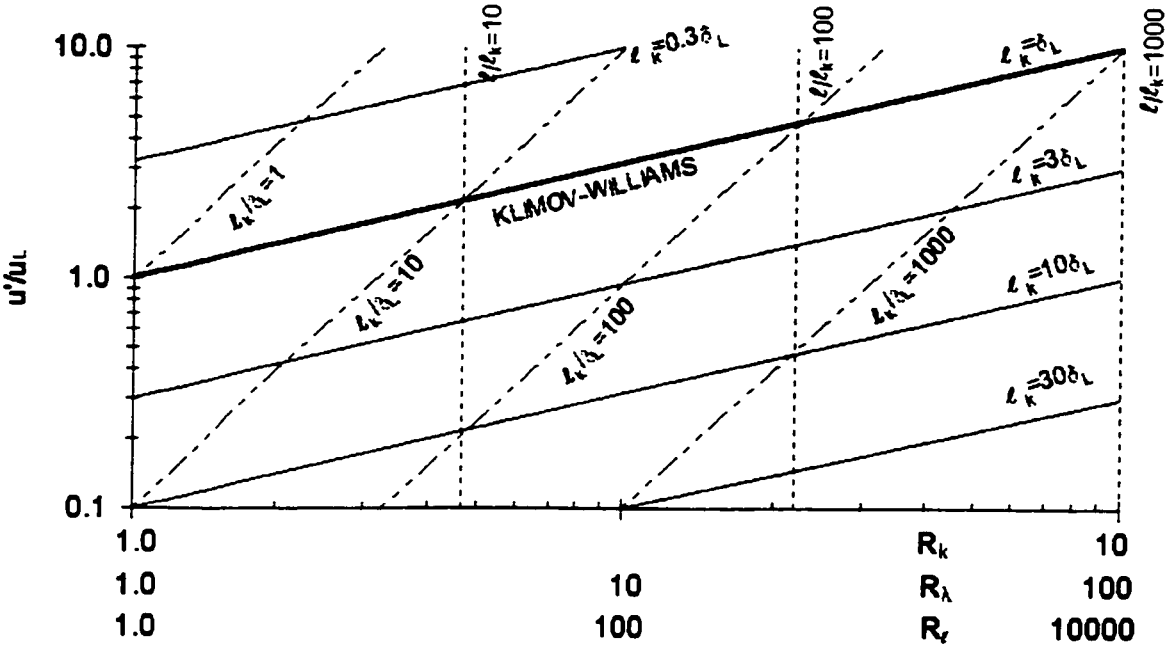

Figure 2-1. Characteristic Parameters of Premixed Turbulent Combustion – Glassman (1987)

In his study of turbulent combustion modelling, Borghi (1988) used the following characteristics to delineate flame regimes:

(i) the turbulent kinetic energy k

(ii) Kolmogorov time τ_K

(iii) the time microscale τ

(iv) the transit time τ_c which is a measure of the time for the fluid to traverse the laminar flame thickness δ_L.

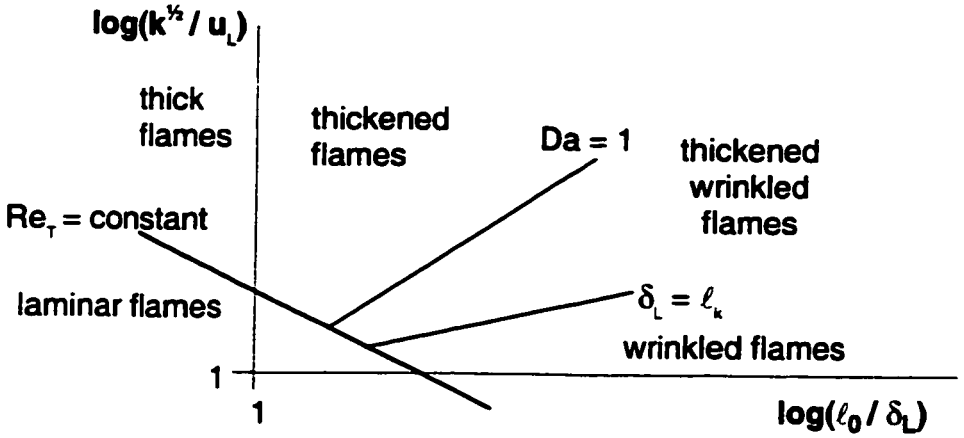

Figure 2-2. Premixed Burning Regimes – Borghi (1988)

The representative plot of Figure 2-2 shows that, as with the plot of Figure 2-1, the onset of severe flame wrinkling is predicted by $\ell_k = \delta_L$. Physically, the line of constant Reynolds number ($\mathbf{Re}_T = 1$) represents a boundary separating turbulent from laminar flames where $\mathbf{Re}_T$ is to be considered equivalent to R_ℓ, the Reynolds number for the integral microscale. The ratio of time scales is defined by the Damköhler number, $Da = \tau/\tau_c$. Here, the line of constant Damköhler ($Da = 1$) represents a relevant parameter in the turbulence-chemical interactions of the flame. Above this transition boundary (where $Da < 1$ and $k^{1/2}$ is sufficiently high),

the combustion is controlled by turbulence as in a well-stirred reactor and is not typical of the wrinkled flames in a conventional internal combustion engine. Borghi (1988) acknowledges that turbulence is not the same at all locations of a reaction. This means that, in practice, there will be different flame regimes at different locations of a combustion process. In the case of spark-ignited internal combustion engines, the operation is predominated by wrinkled flame regimes.

Abdel-Gayed and Bradley (1989) identified the flame regimes after correlating a large collection of experimental data on premixed turbulent burning velocities with the dimensionless number Karlovitz stretch factor. This flame stretch factor, K, is defined as:

$$K = \left(\frac{u'}{\lambda}\right)\left(\frac{\delta_L}{u_L}\right) \qquad [2.1]$$

where, as before, u' is the r.m.s. turbulent velocity, λ is the Taylor microscale length, δ_L is the laminar flame thickness, and u_L is the laminar burning velocity. Abdel-Gayed and Bradley recognized that the effect of strain is enhanced with the incidence of a higher thermal diffusion in a flow. Data reflecting lower values of the non-dimensional Lewis number, *Le* (a measure of mass diffusivity relative to thermal diffusivity) would then demonstrate reduced flame strain. In a later publication on the same subject, Bradley (1992) presented the plot of Figure 2-3 where the flame regimes were quantified in terms of the K·Le product. In this plot u_k' is the effective r.m.s. turbulent flow velocity acting on the flame and u_l is

the turbulent burning velocity. Poinsot (1991) found that the 'fragmented flame front' or a severely distributed reaction zone was found to exist as $K \cdot Le$ values exceeded 5.3. A complete flame quench (combustion extinguishment) was obtained when $K \cdot Le$ exceeded 6.0. Figure 2-3, because it is based on an extensive compilation of empirical data, provides an important reference for all premixed burning studies. It shows the transformation of a flame from a laminar to a fragmented reaction and ultimately to a quenching condition as $K \cdot Le$ increases.

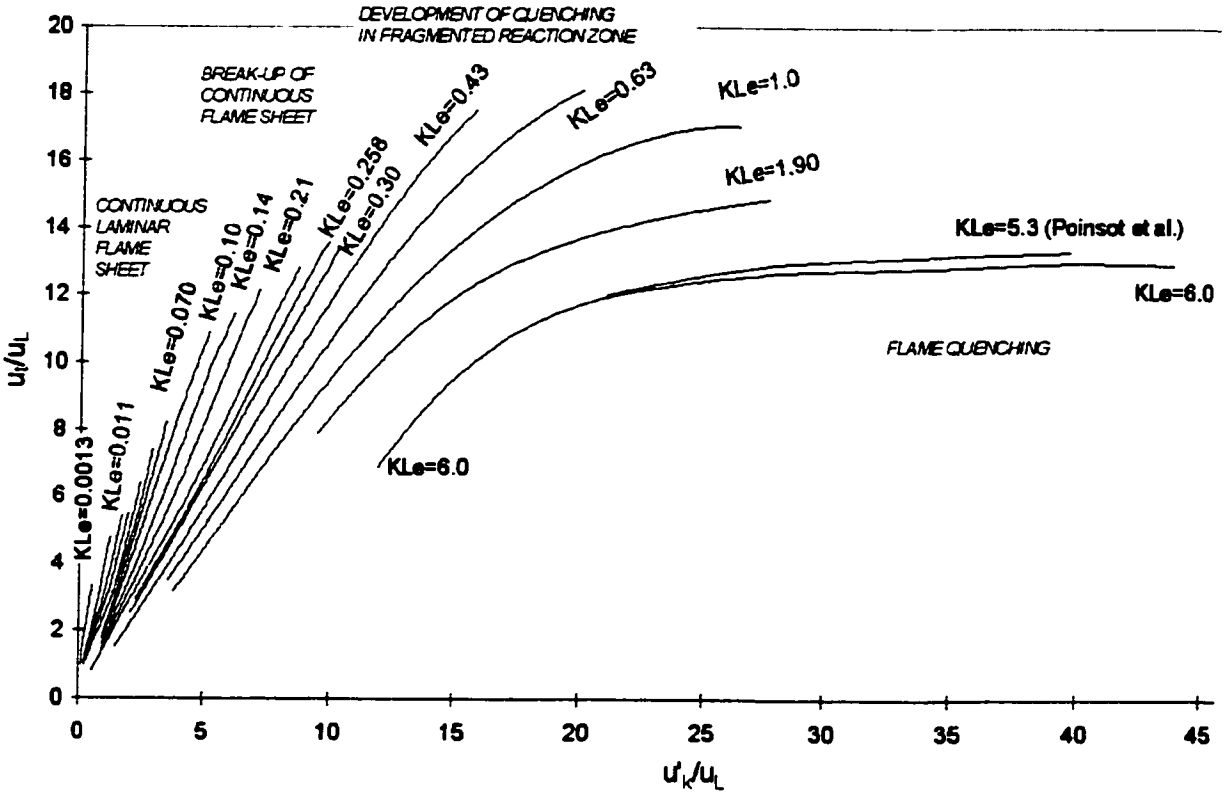

Figure 2-3. Premixed Burning Regimes – Bradley (1992)

A concise combustion regime diagram in Figure 2-4 is presented by Bray and Peters (1994) makes use of the Karlovitz and Damköhler non-dimensional numbers as defined above. It shows that regimes of flame propagation in IC (internal combustion) engines as having flame structure that extends into the flamelet and distributed reaction zone regimes.

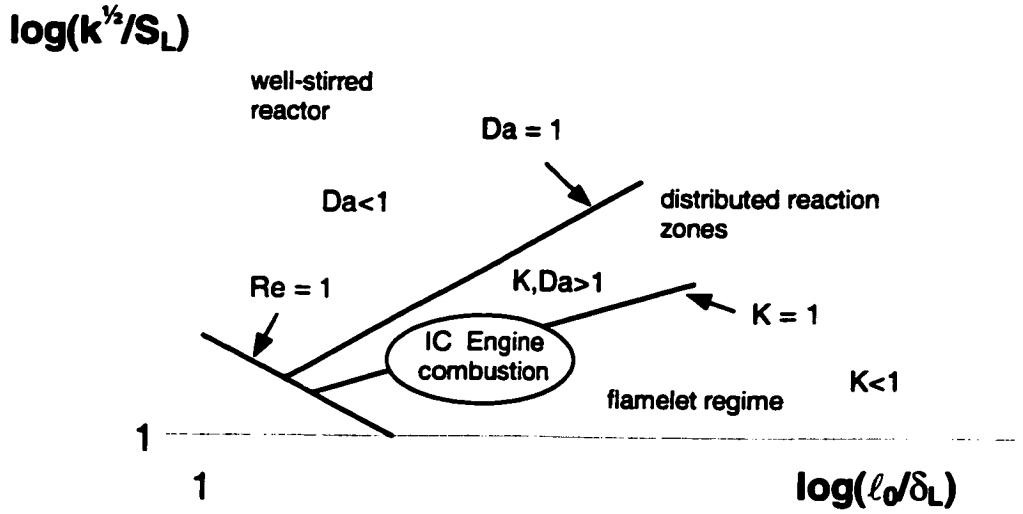

Figure 2-4. Premixed Burning Regimes – Bray and Peters (1994)

The relevance of a flame structure's burning regimes and the incidence of quenching for premixed combustion were recently interpreted by Chen et al (1996). In this research, the flame stretch from the turbulence within conventional spark-ignition internal combustion engines and gas turbines is said to extend the combustion from the flamelet regime into the distributed-reaction-zone

regime. Within the distributed-reaction-zone regime, local quenching is again found to be the result of further increases in turbulence.

Heywood (1988) has described engine operation at high speeds with low loading to reflect combustion within a distributed reaction regime. This can be accounted for by the low laminar flame speed values and high residual gas concentration from previous combustion events.

In summary, the properties and burning regimes of premixed combustion have been presented. The distributed reaction zone regime is shown to define lean burn at the threshold of misfire. With the focus of this research being that of the simulation of lean burn, beyond the realm of conventional engine operation, assignment of the numeric inputs must coincide with those of combustion in a distributed reaction regime. That is, initial turbulence and chemistry properties should correspond to $K > 1$ (Bray and Peter), $Da > 1$ (Bray and Peter), $\delta_L > \ell_0$ (Glassman), and $K \cdot Le > 5.3$ (Bradley) from the surveyed literature.

Chapter 3

Formulation of the Governing Equation

3.1 Discretization of the Governing Equation

Flame propagation in a closed spherical vessel with central ignition is symmetrical about the centre of the vessel. Therefore, the governing equation for the probability density function (pdf) is to be considered one-dimensional for this application, and the pdf varies in the radial direction only. A spherical co-ordinate system is adopted to present the governing equation for the pdf in thermodynamic space,

$$\underbrace{\frac{\partial}{\partial t}\left(\langle\rho\rangle\tilde{P}\right)}_{\text{temporal change}} + \underbrace{\frac{1}{r^2}\frac{\partial}{\partial r}\left(\langle\rho\rangle r^2\tilde{V}_r\tilde{P}\right)}_{\text{convection}} = \underbrace{\frac{1}{r^2}\frac{\partial}{\partial r}\left(\Gamma_T r^2\frac{\partial\tilde{P}}{\partial r}\right)}_{\text{diffusion}} - \underbrace{\langle\rho\rangle\left(\frac{\partial}{\partial Z}\left(\tilde{P}S\right)\right)}_{\text{source}} + \underbrace{\langle\rho\rangle\langle M\rangle}_{\text{mixing}} \qquad [3.1]$$

where $\tilde{P}$ is the density-weighted average probability density function (pdf) of a thermodynamic variable Z, $\tilde{V}_r$ is the density-weighted radial mean flow velocity,

Γ_T is the turbulent diffusion coefficient, **S** is the source term, M is the mixing term, and $\langle\rho\rangle$ is the mean density.

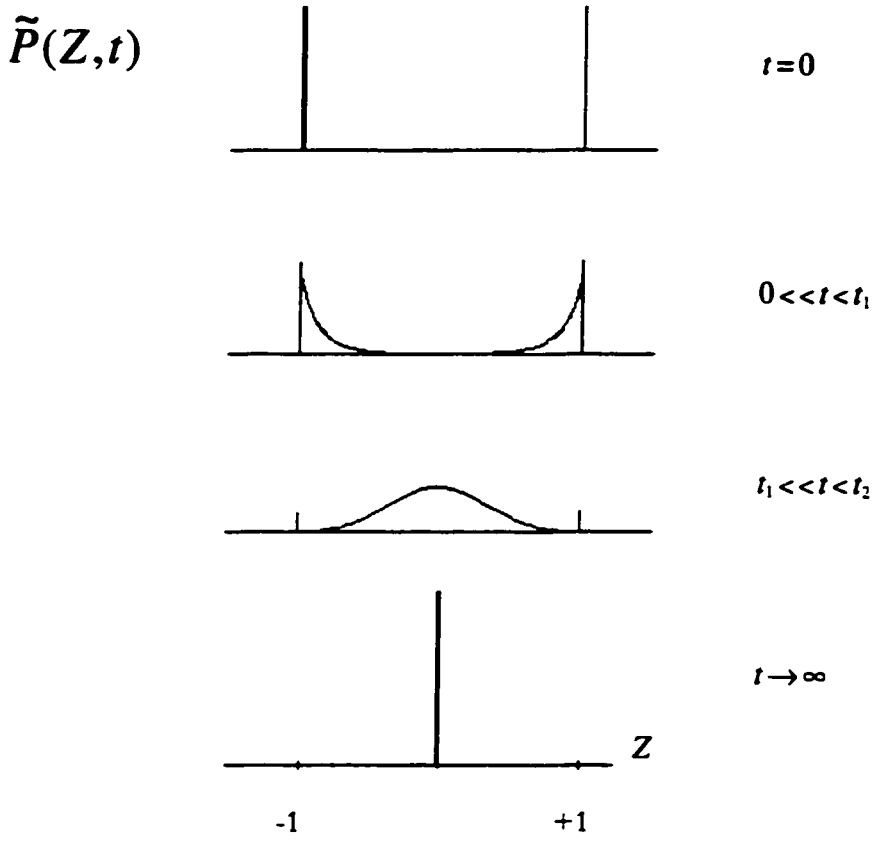

Figure 3-1. Evolution of pdf $\tilde{P}$ in Time – Pope (1979)

3.1.1 Evolution of PDF

The pdf $\tilde{P}$ for the thermodynamic variable Z is one that continually evolves in time. Consider the example shown in Figure 3-1 of a turbulent flow with zero mean. At time $t=0$, the scalar field is assumed to be binary, that is, the initial pdf

is composed of only the two spikes at $Z=-1$ and $+1$. As time passes, to t_1 then t_2, the influence of the diffusion from Eq. [3-1] serves to distribute $\tilde{P}$ between the bounds of $Z=-1$ and $+1$. Eventually, with time approaching infinity ($t \rightarrow \infty$), $\tilde{P}$ is seen to assume a singular value spike which reflects uniform property Z throughout the thermodynamic space.

In this study, the properties composing Z are the fuel mass fraction F, internal energy U, and volume V. Using the above pdf evolution example to represent combustion in a closed chamber, one of the two spikes at time $t=0$ (just after the ignition event) could represent the property Z of the burned gases in the spark gap, and the other spike the property Z of the unburned gases in the remainder of the vessel. With the passage of time towards full combustion, the effects of chemical reaction, mixing, and diffusion would serve to diminish the variation in the thermodynamic properties among the combustion gases. When combustion is finally completed ($t \rightarrow \infty$), the resulting property Z would be homogeneous throughout the combustion chamber.

3.1.2 Control-Volume Formulation

The numerical method adopted to solve Eq. [3.1] is the control-volume formulation using explicit values. In this approach depicted in Figure 3-2, the one-dimensional domain is divided into a series of non-overlapping control

volumes in the radial direction (..., ww-w, w-e, e-ee, ...), each surrounding a grid point (..., W, P, E, ...). The outer face of the outermost shell is fixed at the wall of the spherical vessel. From this shell arrangement, the differential equation is then integrated over each control volume assuming a uniform value of the pdf. This results in a discretization equation for the pdf, $\tilde{P}$, for each of the control volume. To derive this discretization equation, the grid system shown below in Figure 3-2 is adopted.

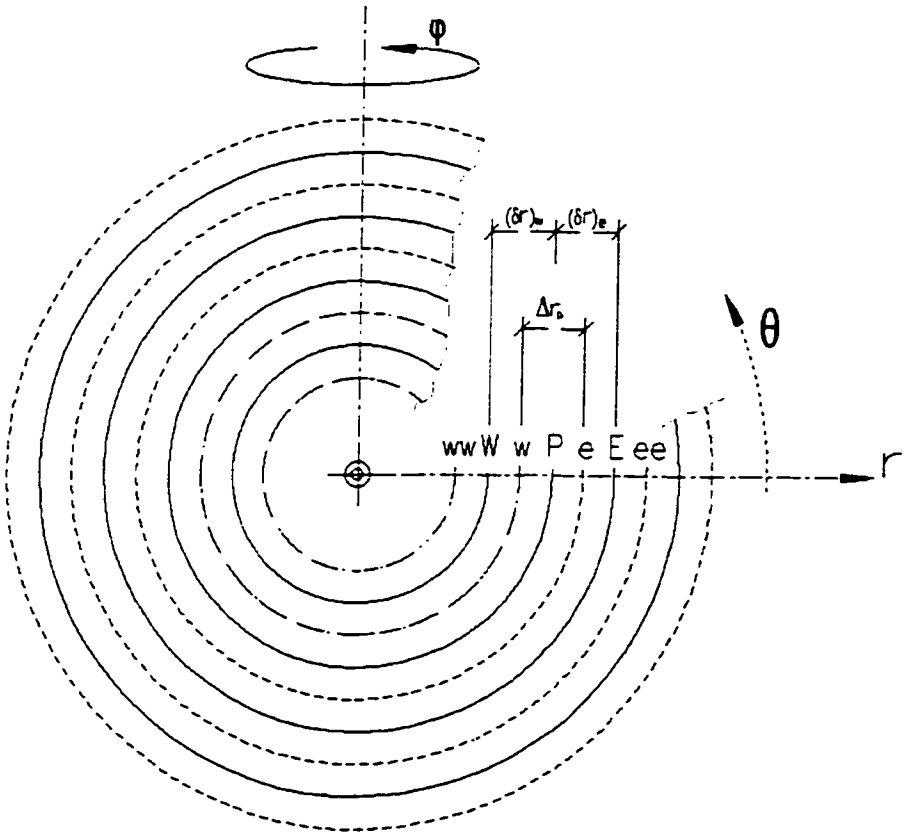

Figure 3-2. Grid Point Cluster

Concentric circles are drawn, with solid lines depicting the locations of the grid points and dashed lines forming the boundaries. For the purpose of this writing, the control volumes between these neighbouring pairs of dashed lines will be called 'shells'. Because the problem can be considered symmetric about the angle of rotation φ and the angle of inclination θ, the grid system is simplified in a one-dimensional fashion as shown in Figure 3-3.

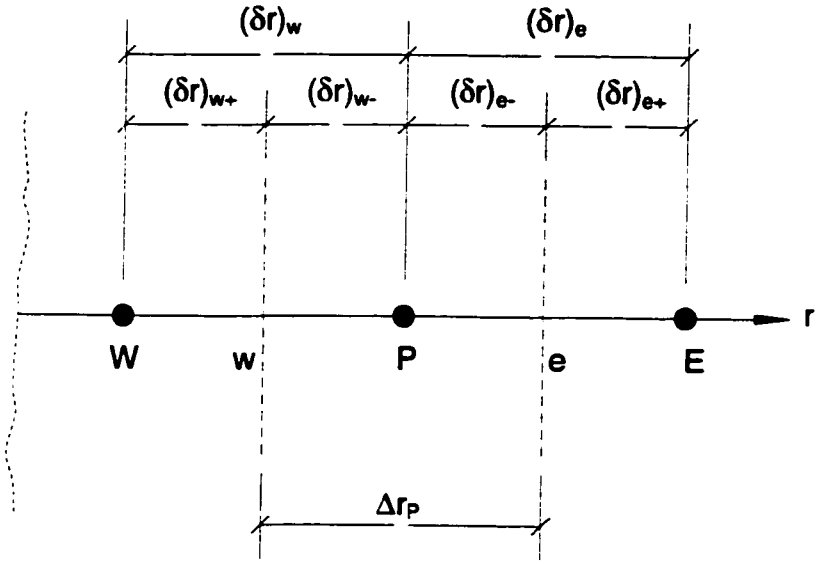

Figure 3-3. Grid Point Cluster in One-Dimensional Radial Space

Here, shell P (the hatched region) is located between neighbouring shells W (the western or inner control volume) and E (the eastern or outer control volume). The dashed lines (w and e) represent the interfaces with these neighbouring shells. It is between the dashed lines (concentric shells) labelled w and e that the governing equation is integrated in space for shell P.

The integration is from face w to e in an outwardly radial direction using the spherical co-ordinate system. Integration is also necessary through time (i.e. from t to $t+\Delta t$) as a one-way co-ordinate. Explicit values, as opposed to implicit values, are applied to provide numerical solution to the integration. This course requires less of the computer resource and its accuracy will be discussed in Chapter 5 by investigating the effect of the time-step on results.

The following integral is the basis for the numerical solution of the governing equation, Eq. [3.1], after multiplying the governing equation by $4\pi r^2$ to account for the spherical surface of the shells:

[3.2]

Using a superscript 0 to represent values at time t and a superscript 1 to represent the value at time $t+\Delta t$, the first term (temporal change) on the left hand side is integrated explicitly assuming a uniform pdf $\tilde{P}$ over the shell P as:

[3.3]

$$\int_w^e \int_t^{t+\Delta t} 4\pi r^2 \frac{\partial}{\partial t}\left(\langle\rho\rangle \tilde{P}\right) dt\, dr = \langle\rho\rangle_P^0 \left[\tilde{P}^1 - \tilde{P}^0\right] \Delta V_P$$

where the volume of shell P is known to be

[3.4]

$$\Delta V_P = \int_w^e 4\pi r^2 dr$$

which is written as

$$\Delta V_P = \frac{4\pi}{3}\left[r_e^3 - r_w^3\right]. \qquad [3.5]$$

The explicit value has been assumed for the density $\langle\rho\rangle_P^0$ in Eq. [3.3].

The second term (convection) on the left-hand side of Eq. [3.2] is integrated using an explicit scheme as:

$$\int_w^e\int_t^{t+\Delta t} 4\pi\frac{\partial}{\partial r}\left(\langle\rho\rangle r^2\tilde{V}_r\tilde{P}\right)dtdr = \left[\langle\rho\rangle_e^0 S_e\tilde{V}_{r_e}^0\tilde{P}_E^0 - \langle\rho\rangle_w^0 S_w\tilde{V}_{r_w}^0\tilde{P}_W^0\right]\Delta t \qquad [3.6]$$

where S_e and S_w represent the spherical surface area at faces e and w respectively.

The first term on the right hand side (diffusion) is also integrated using an explicit scheme as:

$$\int_w^e\int_t^{t+\Delta t} 4\pi\frac{\partial}{\partial r}\left(\Gamma_T r^2\frac{\partial\tilde{P}}{\partial r}\right)dtdr = \left[\Gamma_{T_e}^0 S_e\frac{\left(\tilde{P}_E^0 - \tilde{P}_P^0\right)}{(\delta r)_e} - \Gamma_{T_w}^0 S_w\frac{\left(\tilde{P}_P^0 - \tilde{P}_W^0\right)}{(\delta r)_w}\right]\Delta t \qquad [3.7]$$

where the terms Γ_{T_e} and Γ_{T_w} at the faces e and w, respectively, are expressed as:

$$\Gamma_{T_e} = \left[\frac{1-f_e}{\Gamma_{T_P}} + \frac{f_e}{\Gamma_{T_E}}\right]^{-1} \qquad [3.8]$$

and

$$\Gamma_{T_w} = \left[\frac{1 - f_w}{\Gamma_{T_P}} + \frac{f_w}{\Gamma_{T_W}} \right]^{-1} \qquad [3.9]$$

and where Γ_{T_E}, Γ_{T_P}, and Γ_{T_W} are the diffusion coefficients based on the properties of shells E, P, and W respectively. The weighing factors f_e and f_w are defined (in reference to Figure 3-3) as:

$$f_e = \frac{(\delta r)_{e+}}{(\delta r)_e} \qquad [3.10]$$

and

$$f_w = \frac{(\delta r)_{w+}}{(\delta r)_w}. \qquad [3.11]$$

The second term on the right hand side representing the source term is integrated assuming $\tilde{P}$ of uniform value over the shell P as:

$$\int_w^e \int_t^{t+\Delta t} 4\pi r^2 \langle \rho \rangle \left(-\frac{\partial}{\partial Z}\left(\tilde{P}S\right) \right) dt\,dr = \left[-\frac{\partial}{\partial Z}\left(\tilde{P}S\right) \right]^0 \langle \rho \rangle_P^0 \Delta t\, \Delta V_P \qquad [3.12]$$

The solution is dealt with directly using the Monte Carlo technique.

The third term on the right hand side representing the mixing term is integrated assuming uniform M over the shell P as:

$$\int_w^e \int_t^{t+\Delta t} 4\pi r^2 \langle \rho \rangle M dt dr = \langle \rho \rangle_P^0 M^0 \Delta t \, \Delta V_P \qquad [3.13]$$

As with the source term, this mixing term is solved directly using the Monte Carlo technique.

3.2 The Monte Carlo Method

As mentioned above, the Monte Carlo method will be used to simulate technique the terms of the discretized equations.

The discretized equation from the previous is obtained by substituting Eq.[3.3], Eq.[3.6], and Eq.[3.7] into Eq.[3.2] and rearranging as:

$$\underbrace{\left(\tilde{P}^1 - \tilde{P}^0\right)}_{\text{temporal change}} + \underbrace{\frac{\left(\langle \rho \rangle_e^0 S_e \tilde{V}_{r_e}^0 \tilde{P}_e^0 - \langle \rho \rangle_w^0 S_w \tilde{V}_{r_w}^0 \tilde{P}_w^0\right) \Delta t}{\Delta V_P \langle \rho \rangle_P^0}}_{\text{convection}} = \underbrace{\left[\Gamma_{T_e}^0 S_e \frac{\left(\tilde{P}_E^0 - \tilde{P}_P^0\right)}{(\delta r)_e} - \Gamma_{T_w}^0 S_w \frac{\left(\tilde{P}_P^0 - \tilde{P}_W^0\right)}{(\delta r)_w}\right] \frac{\Delta t}{\Delta V_P \langle \rho \rangle_P^0}}_{\text{diffusion}} - \underbrace{\left[\frac{\partial}{\partial Z}\left(\tilde{P} S\right)\right]^0 \Delta t}_{\text{source}} + \underbrace{M^0 \Delta t}_{\text{mixing}} \qquad [3.14]$$

In the Monte Carlo method, the concentric shells described in Section 3.1.2 are to be composed of particles of equal mass, each having a thermodynamic state Z. A depiction is shown in Figure 3-4. The physics of particle movement,

interaction, and property evolution will be handled by a reworking of each term in Eq. [3.14].

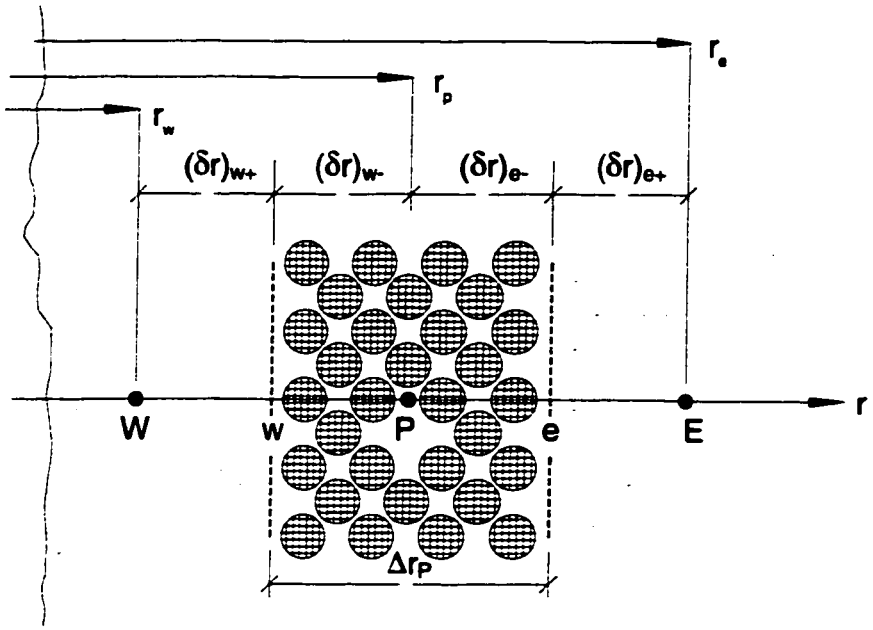

Figure 3-4. Grid Point Cluster with Compositional Particles

3.2.1 Convection Term

Before ignition, the mean flow is assumed nil in the spherical vessel. After ignition, the burned gases are radially expanded and the unburned gases are radially compressed. This creates a radial mean velocity that contributes to the convection term. It is noted that the radial velocity fluctuations contribute to the diffusion term as in conventional turbulence modelling. The solution of the convection term is not needed if the interfaces move with the local radial mean velocity. With reference to shell P of Figure 3-4, the shell thickness, Δr_p, the radii

of its interfaces, r_w and r_e, and the location of the grid point r_p are changing in time. Except, of course, for the outermost shell whose outer boundary is fixed at the wall of the spherical vessel.

3.2.2 Diffusion Term

There are two directions in which the diffusion of particles can occur according to Figure 3-4: either inward (negatively along r) or outward (positively along r). This is better understood referring to the corresponding term in the discretized equation where the superscript 0 has been dropped for simplicity.

[3.15]

$$\underbrace{\left[\frac{\Gamma_{T_E}}{\langle\rho\rangle_P}\frac{S_e}{\Delta V_P}\frac{\left(\tilde{P}_E-\tilde{P}_P\right)}{(\delta r)_e}-\frac{\Gamma_{T_w}}{\langle\rho\rangle_P}\frac{S_w}{\Delta V_P}\frac{\left(\tilde{P}_E-\tilde{P}_P\right)}{(\delta r)_e}\right]\Delta t}_{\text{net diffusion into shell P}}=\underbrace{\left[\frac{\Gamma_{T_E}}{\langle\rho\rangle_P}\frac{S_e}{\Delta V_P}\frac{\tilde{P}_E}{(\delta r)_e}\Delta t\right]}_{\text{entering P from E}}$$
$$\underbrace{-\left[\frac{\Gamma_{T_E}}{\langle\rho\rangle_P}\frac{S_e}{\Delta V_P}\frac{\tilde{P}_P}{(\delta r)_e}\Delta t\right]}_{\text{leaving P for E}}$$
$$\underbrace{-\left[\frac{\Gamma_{T_w}}{\langle\rho\rangle_P}\frac{S_w}{\Delta V_P}\frac{\tilde{P}_P}{(\delta r)_w}\Delta t\right]}_{\text{leaving P for W}}$$
$$\underbrace{+\left[\frac{\Gamma_{T_w}}{\langle\rho\rangle_P}\frac{S_w}{\Delta V_P}\frac{\tilde{P}_W}{(\delta r)_w}\Delta t\right]}_{\text{entering P from W}}$$

In the Monte Carlo solution, the evaluation of the pdf, $\tilde{P}$, in shell P is represented by sampling from an ensemble of particles and moving them in and out of the shell as described by the following equation:

[3.16]

$$\text{net diffusion of particles into shell P} = \underbrace{\left[\frac{\Gamma_{T_E}}{\langle\rho\rangle_P}\frac{S_e}{\Delta V_P}\frac{\tilde{P}_E}{(\delta r)_e}\Delta t\right]}_{n_{c+}\text{ particles}} - \underbrace{\left[\frac{\Gamma_{T_E}}{\langle\rho\rangle_P}\frac{S_e}{\Delta V_P}\frac{\tilde{P}_P}{(\delta r)_e}\Delta t\right]}_{n_{c-}\text{ particles}} - \underbrace{\left[\frac{\Gamma_{T_w}}{\langle\rho\rangle_P}\frac{S_w}{\Delta V_P}\frac{\tilde{P}_P}{(\delta r)_w}\Delta t\right]}_{n_{w-}\text{ particles}} + \underbrace{\left[\frac{\Gamma_{T_w}}{\langle\rho\rangle_P}\frac{S_w}{\Delta V_P}\frac{\tilde{P}_W}{(\delta r)_w}\Delta t\right]}_{n_{w+}\text{ particles}}$$

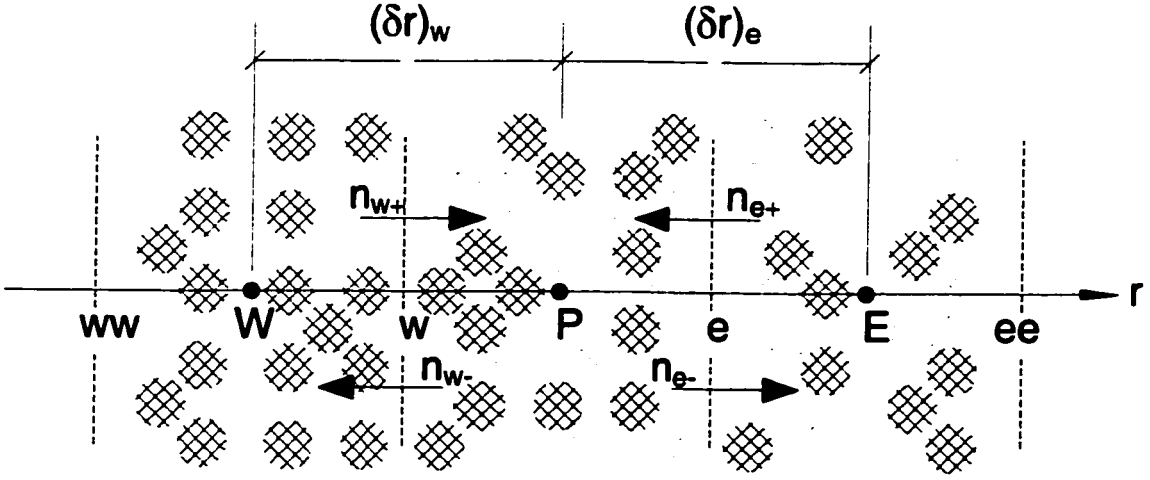

Figure 3-5. Grid Point Cluster showing Diffusion of Compositional Particles

As depicted in Figure 3-5, the numbers of diffusing particles either leaving or entering shell P (delimited by faces w and e) from t to $t+\Delta t$ are expressed by n_{e-}, n_{e+}, n_{w-}, and n_{w+}. The number of particles, n_{e-} represents those leaving shell P and entering shell E through interface e,

$$n_{e-} = \frac{S_e}{\Delta V_P \delta r_e} \frac{\Gamma_{T_r}}{\langle \rho \rangle_P} N_P \Delta t \qquad [3.17]$$

The number of particles, n_{e+} represents those travelling in the opposite direction through interface e,

$$n_{e+} = \frac{S_e}{\Delta V_P \delta r_e} \frac{\Gamma_{T_r}}{\langle \rho \rangle_P} N_E \Delta t . \qquad [3.18]$$

Conversely, the number of particles, n_{w-} represents those leaving shell P and entering shell W through interface w,

$$n_{w-} = \frac{S_w}{\Delta V_P \delta r_w} \frac{\Gamma_{T_r}}{\langle \rho \rangle_P} N_P \Delta t . \qquad [3.19]$$

Lastly, the number of particles, n_{w+} represents those travelling in the opposite direction through interface w,

$$n_{w+} = \frac{S_w}{\Delta V_P \delta r_w} \frac{\Gamma_{T_w}}{\langle \rho \rangle_P} N_W \Delta t \,. \qquad [3.20]$$

In the above expressions for the quantities of diffusing particles, ΔV_P is the volume of shell P. The total particle counts within shells W, P, and E are N_W, N_P, and N_E respectively. The inner and outer surface areas of the shell at interfaces w and e are represented by S_w and S_e, respectively.

The diffusion terms of Eq. [3.17] through to Eq. [3.20] have the general form,

$$n \equiv \frac{S}{\Delta V \delta r} \frac{\Gamma_T}{\langle \rho \rangle} N \Delta t \,. \qquad [3.21]$$

It can be shown that they are identical to the term's used in Pope (1979) for a one-dimensional Cartesian co-ordinate (x-direction) using $\delta r = \delta x$ and $\Delta V = S\,\delta x$ as follows,

$$n \equiv \frac{S}{S\,\delta x\,\delta x} \frac{\Gamma_T}{\langle \rho \rangle} N\,\Delta t \equiv \frac{\Gamma_T}{\langle \rho \rangle} N \frac{\Delta t}{(\delta x)^2} \,. \qquad [3.22]$$

3.2.3 Mixing Term

The mixing term, $M^0 \Delta t$, describing the transfer of thermodynamic variables between mixing particles, without chemical reaction, makes use of the binary

mixing model. In this model, pairs of particles destined for mixing are randomly picked in time-step Δt. The number of binary mixing particle pairs (n_{pairs}) is given by the scalar mixing model,

$$n_{pairs} = \beta \, \omega \, N_P \, \Delta t \qquad [3.23]$$

where ω is the mixing frequency to reach scalar uniformity, and β is a function of the mixing model. After mixing it is necessary to calculate new thermodynamic properties for each of the mixing particles. This is discussed in the next section. The volume of the mixing pairs and the pressure do not change because mixing is assumed to occur under static or 'frozen' conditions.

3.2.3.1 Mixing Models

Lei and Milane (1990) adopted Curl's mixing model (complete mixing) where two mixing particles have identical properties after mixing. The compositional and thermodynamic state $Z = Z(F,U,V)$ of the particles after mixing is assumed as the arithmetic averages of the original thermodynamic states of the particles.

$$Z_1^* = Z_2^* = \frac{(Z_1 + Z_2)}{2} \qquad [3.24]$$

where subscripts *1* and *2* denote the original particles and superscript '*' denotes the particles after the mixing. As described in section 3.1 of this study, the

variables describing the thermodynamic state of a particle Z are its fuel mass fraction F, internal energy U, and volume V.

Other partial mixing models may be used where the degree of mixing is described with a single variable α such that the thermodynamic state of particle 1 is,

$$Z_1^* = \left[(1-\alpha)Z_1 + \frac{\alpha(Z_1+Z_2)}{2}\right] \qquad [3.25]$$

and of particle *2* is

$$Z_2^* = \left[(1-\alpha)Z_2 + \frac{\alpha(Z_1+Z_2)}{2}\right]. \qquad [3.26]$$

The value of α has an upper bound of 1 for complete mixing and a lower bound of 0 for no mixing. The value of α is governed by a distribution function $A(\alpha)$ such that,

$$\int_{\alpha=0}^{1} A(\alpha)\, d\alpha = 1. \qquad [3.27]$$

3.2.3.2 Binary Mixing Frequency

For a homogeneous non-reactive flow, the rate of decay of the standard deviation of the scalar fluctuations σ is,

$$\frac{d\sigma}{dt} = -\omega\sigma \qquad [3.28]$$

where ω is the inverse of the scalar-decay time scale given as,

$$\omega = C_\phi\left(\frac{\varepsilon}{k}\right) \qquad [3.29]$$

and ε is the dissipation rate of turbulent kinetic energy k. The ratio $\frac{\varepsilon}{k}$ is the inverse of the turbulent decay time scale that will be given by a turbulent model. Pope (1982) assigned a value of 2 for C_ϕ; however, he reported that reasonable values for C_ϕ can vary from 0.6 to 3.1. Sensitivity of the results to the value of this variable will be assessed in the Results and Discussion section of Chapter 5.

Pope has further shown that for a mixing model governed by a distribution function $A(\alpha)$, the rate of decay of the standard deviation of the fluctuations in the thermodynamic state, $\sqrt{\overline{z''^2}}$, is given as,

$$\frac{d\sqrt{\overline{z'^2}}}{dt} = -\beta\omega\left(a_1 - \frac{1}{2}a_2\right)\sqrt{\overline{z'^2}} \qquad [3.30]$$

where a_1 and a_2 are the first and second moments of the distribution function $A(\alpha)$ given as

$$a_1 = \int_{\alpha=0}^{1} \alpha A(\alpha) d\alpha \qquad [3.31]$$

and

$$a_2 = \int_{\alpha=0}^{1} \alpha^2 A(\alpha) d\alpha \qquad [3.32]$$

By comparing Eq. [3.28] and Eq. [3.30], the coefficient β is given as,

$$\beta = \left(a_1 - \frac{1}{2}a_2\right)^{-1} \qquad [3.33]$$

The factor β is a function of the mixing model. Two mixing models are considered: complete mixing and partial mixing. In the case of complete mixing, the distribution of $A(\alpha)$ is described by the Dirac delta function,

$$A(\alpha) = \delta(1-\alpha) \qquad [3.34]$$

which has the following properties,

$$A(\alpha)=0 \text{ for } \alpha \neq 1$$
$$=\infty \text{ for } \alpha = 1$$

The first and second moments of the delta Dirac distribution are given as $a_1 = 1$ and $a_2 = 1$. This results in $\beta_{complete} = 2$.

In the case of partial mixing, the variable α is assigned a value according to a uniform random number generator. The distribution function is defined as $A(\alpha)=1$ and the moments of this distribution are calculated as $a_1 = \frac{1}{2}$ and $a_2 = \frac{1}{3}$ which results in $\beta_{random} = 3$.

3.2.4 Source Term

The source term, $-\left[\frac{\partial}{\partial Z}(\tilde{P}S)\right]^0 \Delta t$, is simulated deterministically by following the species concentration due to chemical reaction in each particle. This is expressed as the ordinary differential,

[3.35]

$$\frac{dF}{dt} = S$$

where F the fuel fraction and S is the rate of production of F. The single step reaction mechanism from Westbrook and Dryer (1981) is adopted as,

$$S = -A_{pre-exp} \exp\left(\frac{-B}{RT}\right) x^a y^b, \qquad [3.37]$$

where T is the local absolute temperature, $A_{pre-exp}$ is a pre-exponential constant, B is the activation energy, R is the gas law constant, x is the fuel concentration, y is the oxidant concentration, and both a and b are empirical constants.

Chapter 4

SUPPORTING MODELS

4.1 Method of Solution

With the discretization in hand, it is now possible to formulate a numerical procedure to solve the governing equation. Such a procedure involves 'marching' the combustion process in the chamber through time. The sequence starts with a central spark-ignition followed by the outward propagation of the flame and the eventual termination of combustion due to the complete consumption of the reactants or the flame being quenched.

4.2 Ignition Model

The centremost shell in the simulated combustion chamber is dimensioned such that its diameter would constitute a practical spark gap. The ignition event is modelled by instantly and completely burning all the particles in the central shell. These now fully-burned particles can be said to represent the kernel for

subsequent flame development and propagation. The thermodynamic states of the particles after ignition are calculated using the procedure as developed by Lei and Milane (1990).

4.3 Flame Propagation

With the ignition process complete, the propagation of the released combustion energy is accomplished by the diffusion and mixing of the fully-burned particles into the unburned surrounding particles. The chemical reaction progress for each individual particle can then be assessed.

4.3.1 Diffusion Model

The movement of individual particles within the combustion chamber is modelled by incorporating the Monte Carlo based diffusion equations, Eq [3.17-20]. In the Δt time period, n_{diff} particles are randomly picked from the N_P particles in shell P (see Figure 3-3) and moved to adjacent shells (either inward or outward) as

$$n_{diff} = \frac{S}{\Delta V_P \delta r} \frac{\Gamma_T}{\langle \rho \rangle_P} N_P \, \Delta t \qquad [4.1]$$

where S is the spherical surface area at the diffusion interface, ΔV_P is the volume of shell P, δr is the midpoint of shell P to the midpoint of the destination shell, $\langle \rho \rangle_P$ is the mean density of shell P, and Γ_T is the turbulent diffusion coefficient at

the interface e or w. Furthermore, that particles are limited to one diffusion movement from a shell P per global time-step, Δt.

The turbulent diffusion coefficient is given as:

$$\Gamma_T = \frac{C_\mu}{\sigma_\phi}\frac{k^2}{\varepsilon}\langle\rho\rangle \qquad [4.2]$$

where C_μ is an empirical constant equal to 0.09, σ_ϕ is the turbulent Schmidt number, k is the turbulent energy, and ε is the mass specific rate of turbulent energy dissipation. The sensitivity of the results to σ_ϕ will be evaluated by assigning values of 0.7 and 1.0. The value of Γ_T at interfaces e or w is calculated using Eq. [3.8] and Eq. [3.9], respectively.

4.3.2 Mixing Model

During binary mixing, a particle intermingles and exchanges property $Z = Z(F,U,V)$ with another particle. For example, the particles' fuel mass fraction F_n defines if they are unburned ($F_n = F_0$), burning ($O < F_n < F_0$), or fully-burned ($F_n = 0$). The fuel mass fraction is therefore directly related to each particle's burning status and, accordingly, to its ability to release heat due to combustion. The effect of mixing will mean that the burn particles can be spread into the unburned particles by exchange of fuel mass fraction to become a burning particle. The complete mixing model will be adapted in this thesis.

The mixing of individual particles within the shell P is modelled by incorporating the Monte Carlo based mixing equations of Section 3.2.3. Within a given shell P, the number of particle pairs selected during time-step is given as,

$$n_{pairs} = \beta \omega N_P \Delta t \qquad [4.3]$$

where β=2 for complete mixing as described in Section 3.2.3.2. The n_{pairs} sre selected randomly from the N_P particles.

4.3.3 Reaction Rate Model

The global reaction equation for the air-fuel mixture within a burning particle is written as (Ferguson, 1986):

$$\psi\phi C_{\alpha_F} H_{\beta_F} O_{\zeta_F} N_{\delta_F} + (0.21O_2 + 0.79N_2) \rightarrow \upsilon_1 CO_2 + \upsilon_2 H_2O + \upsilon_3 N_2 + \upsilon_4 O_2 + \upsilon_5 CO + \upsilon_6 H_2 \qquad [4.4]$$

where ψ is the molar fuel-air ratio and ϕ is the fuel-air equivalence ratio within a particle. A convenient approximation by Hires et al (1976) used in the lean combustion (ϕ<1) of this study is

$$\upsilon_1 = \alpha_F \phi \psi \qquad [4.5]$$

$$\upsilon_2 = \frac{1}{2}\beta_F \phi \psi \qquad [4.6]$$

$$\upsilon_3 = 0.79 + \frac{1}{2}\delta_F \phi \psi \qquad [4.7]$$

$$\upsilon_4 = 0.21(1-\phi) \qquad [4.8]$$

$$\upsilon_5 = 0 \qquad [4.9]$$

$$\upsilon_6 = 0 \qquad [4.10]$$

It is noted that the concentrations of CO in Eq. [4.9] and H_2 in Eq. [4.10] are considered negligible. As a first approximation in this thesis it is assumed that the excess of oxygen and the low adiabatic flame temperatures at ϕ=0.6 favours the creation of CO_2 and H_2O without the subsequent dissociation of these products into CO and H_2 respectively.

The fuel species evolution of such a burning particle, i, can then be determined by its temperature T_i, volume V_i, and species concentrations x_i (fuel) and y_i (oxygen) according to the previously noted Westbrook and Dryer (1981) mechanism,

$$\frac{dx_i}{dt} = -A_{\text{pre-exp}} \exp\left(\frac{-B}{RT_i}\right) x_i^{\,a} y_i^{\,b} \qquad [4.11]$$

Here $A_{pre\text{-}exp}$, B, a, and b are experimental constants specific to the particular fuel.

The rates of change of the concentrations of oxygen, y_i, carbon dioxide, z_i, water, w_i, and nitrogen, v_i, are related to that of the fuel, x_i, by using the coefficients of the above global reaction equation as,

$$\frac{dy_i}{dt} = (\upsilon_4)\frac{dx_i}{dt} \qquad [4.12]$$

$$\frac{dz_i}{dt} = -(\upsilon_1)\frac{dx_i}{dt} \qquad [4.13]$$

$$\frac{dw_i}{dt} = -(\upsilon_2)\frac{dx_i}{dt} \qquad [4.14]$$

$$\frac{dv_i}{dt} = -(\upsilon_3)\frac{dx_i}{dt} \qquad [4.15]$$

4.3.4 The Thermodynamic State of a Particle

The temperature of a burning particle is calculated using the first law of thermodynamics applied to the individual particle i,

$$\frac{du_i}{dt} = q_i - P\frac{dv_i}{dt} \qquad [4.16]$$

where u_i, q_i, v_i are specific quantities for the particle i of internal energy U_i, heat transfer Q_i, and volume V_i. It is possible to express the internal energy of the particle in terms of the internal energies of its various species, and relate the change of internal energy of each species (X) to the specific heat at constant volume C_{rx} as,

$$du_X = C_{v_x}\, dT_i \qquad [4.17]$$

An equation for the rate of change of temperature of the burning particle is derived (Lei, 1989) which uses the same subscripts as in Section 4.3.3,

$$\frac{dT_i}{dt} = \frac{\frac{dx_i}{dt}(RT_i - U_i) + N_i \frac{RT_i}{P}\frac{dP}{dt}}{C_{v_i} + (N_i)(R)} \qquad [4.18]$$

where N_i refers to the number of moles in particle i and

$$U_i = M_x u_x + \upsilon_4 M_y u_y + \upsilon_1 M_z u_z + \upsilon_2 M_w u_w + \upsilon_3 M_v u_v,$$

$$C_{v_i} = M_x x_i C_{vx} + M_y y_i C_{vy} + M_z z_i C_{vz} + M_w w_i C_{vw} + M_v v_i C_{vv},$$

$$N_i = x_i + y_i + z_i + w_i + v_i.$$

In these equations, M refers to the molecular weight in [*grams/mole*] and u is the specific internal energy of the subscripted species fuel (x), oxygen (y) carbon

dioxide (z), water (w) and nitrogen (v). The specific heats are calculated using the expression proposed by Hires et al (1976).

4.4 Turbulence Model

The rate equation for turbulent kinetic energy is given as,

$$\frac{dk}{dt} = \Im_P - \varepsilon \qquad [4.19]$$

where ε is the rate of turbulence dissipation given as $\varepsilon = C_D \frac{k^{3/2}}{\ell}$, $\Im_P$ is the rate of turbulence production, ε is the rate of turbulence dissipation, and ℓ is the integral scale. In isentropic turbulence with zero shear flow, the production of turbulent kinetic energy is generated by the expansion and compression of the gases as $\Im_P = \frac{2}{3}\frac{k}{\rho}\frac{d\rho}{dt}$ is adapted in this study as a first approximation.

4.4.1 Rapid Distortion Theory

In rapid distortion theory, the dissipation is assumed negligible in comparison to production (i.e. $\varepsilon << \Im_P$). This results in (Borgnakke et al, 1980)

$$k = k_0 \left(\frac{\rho}{\rho_0} \right)^{\frac{2}{3}} \qquad [4.20]$$

where $k_0 = \left(\frac{3}{2}\right)(u_0')^2$ is the initial turbulent kinetic energy before ignition, ρ_0 is the initial density, ρ is the initial density, and ρ is the density of the shell. Also, assuming constant eddy diffusivity, $k^{1/2}\ell$ =constant , the integral scale is

$$\ell = \ell_0\left(\frac{\rho_0}{\rho}\right)^{\frac{1}{3}} \qquad [4.21]$$

The mixing frequency, Eq. [3.29], calculated for each shell is,

$$\omega = C_\phi\left(\frac{\varepsilon}{k}\right) \qquad [4.22]$$

which is expressed as a function of ρ by substituting Eq. [4.19] and Eq. [4.20] and then rewriting as,

$$\omega = C_\phi C_D \frac{\sqrt{k_0}}{\ell_0}\left(\frac{\rho_0}{\rho}\right)^{\frac{2}{3}} \qquad [4.23]$$

The turbulent diffusion coefficient is given by Eq. [4.2],

$$\Gamma_T = \frac{C_\mu}{\sigma_\phi}\frac{k^2}{\varepsilon}\langle\rho\rangle. \qquad [4.24]$$

Substituting for k and ε using Eq. [4.19] and Eq. [4.22] gives,

$$\Gamma_T = \frac{C_\mu}{\sigma_\bullet C_D} \ell_0 \sqrt{k_0} \,. \qquad [4.25]$$

This value is shown to be identical in value for all shells in time.

4.5 Flow-Charting of the Models

With the necessary composite models now presented, it is possible to arrange them into a sequence that then imitates the actual combustion process. The flowchart in Figure 4-1 shows the overall combustion model as arranged for this computer-based study.

4.6 Time Restriction to the Numerical Modelling

The iterations necessary to propagate the theoretical flame as shown in Figure 4-1 must be assigned a global time-step Δt that allows the models to evolve. As previously discussed, the diffusion, mixing, and chemical reaction of a particle take place in fractional steps. Therefore, Δt should be as short as possible for accurate combustion simulation of the concomitant processes. However, the expense of excessive computing time dictates the necessity of adopting a value for Δt that is a balance between a numerical accuracy and computational efficiency.

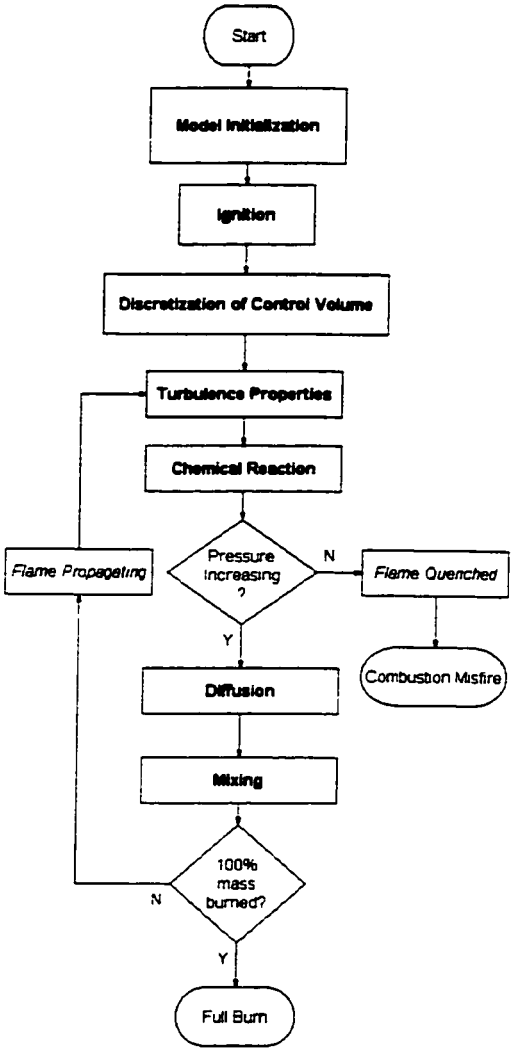

Figure 4-1. Main Flow-Chart of Combustion Model

4.6.1 Time Restriction Related to the Diffusion Process

In the case of diffusion, the number of particles transferred between neighbouring control volume shells for diffusion during Δt should not exceed the total number N_P existing within the shell of interest. The solution must be one relating the time-

step to the control volume thickness (traversal dimension) δr. Using the same nomenclature as the previous chapter's discretized diffusion term (Section 3.2.2), it is possible to adopt a scenario for a given control volume. That is, a shell can never be emptied of particles by the diffusion process within any given time-step, i.e.

$$n_{e-} + n_{w-} \leq N_P \qquad [4.26]$$

To apply this concept to the current model, the algorithm was programmed to flag individual diffused particles to avoid subsequent random selections for diffusion within the same global time-step.

The time restriction criterion Δt_{max} can be established by substituting Eq. [3.17] and Eq. [3.18] in Eq. [4.23],

$$\Delta t_{\text{diffusion max}} \leq \left(\frac{S_e}{\Delta V_P \delta r_e} \frac{\Gamma_{T_e}}{\langle \rho \rangle_P} + \frac{S_w}{\Delta V_P \delta r_w} \frac{\Gamma_{T_w}}{\langle \rho \rangle_P} \right)^{-1}. \qquad [4.27]$$

4.6.2 Time Restriction Related to the Binary Mixing Process

The time restriction due to binary mixing is simply a check to ensure one is not expecting to mix n_m particles which exceeds the total N_P particles in a given control volume, i.e.

$$n_m \leq N_P \qquad [4.28]$$

where

$$n_m = 2\beta\omega N_P \Delta t \qquad [4.29]$$

The maximum mixing time $\Delta t_{\text{mixing max}}$ then would allow all a given shell's particles to be mixed (i.e. $n_m = N_P$). This mixing time restriction is then derived as,

$$\Delta t_{\text{mixing max}} \leq \frac{1}{2\beta\omega}. \qquad [4.30]$$

4.6.3 Time Restriction Related to the Reaction Process

The concern with the chemical reaction model (single-step reaction mechanism) is the possibility that time-step will be too coarse to allow the species evolution to be accurately calculated. In reality it is known that the rate of chemical reaction is generally much greater than that of diffusion and mixing. For this reason it is necessary to adapt a predictor-corrector solver to evolve the reaction mechanism at an optimal smaller time-step for each burning particle within the global time-step, Δt_{global}, of the algorithm's iteration. The computer code of Lei (1988) includes the established method called CHEMEQ by Young and Boris (1977) that uses Euler's predictor and the trapezoidal rule as the corrector. It is therefore

acceptable to assume that the maximum global time-step Δt_{max} for the combustion algorithm's iteration need only consider the rate-controlling processes of diffusion and mixing.

4.6.4 Iteration Refinement of the Time Restriction

As the algorithm is driven through time, the iteration of each time-step should be refined as the above time restrictions demand. The minimum Δt_{global} from diffusion and mixing is then adopted as the ensuing iteration's global time-step. That is,

$$\Delta t_{global} \leq \text{Minimum}\left[\Delta t_{mixing\,max}, \Delta t_{diffusion\,max}\right] \qquad [4.31]$$

By refining the Δt_{global} as necessary during the computational process, the computational time is reduced without losing any of the respective models' influence.

Chapter 5

Results and Discussion

A major part of this study has been the development of the computer code that provides numerical solution to the conservation of the probability density function. The code, described in Appendix B, integrates all of the models and geometrical constraints discussed in the previous sections.

Successful flame propagation with the operation of the computer algorithm was obtained when the input parameters to the model served to disperse energy from the ignited particles at the time of ignition. This propagated energy would be released into the surrounding, unburned fuel-air mixture where the chemical reaction rate would be fast and combustion could proceed.

A misfire in the modeled combustion was obtained if the inputted parameters served to propagate the energy from the ignited particles at an excessive rate. This rapid dispersion of the energy would not permit a fast enough chemical reaction rate to sustain the heat release. In the misfire case, the combustion's

burned mass fraction and pressure would not increase with time thereby indicating a flame quench in the model.

Once the operation of the code was established, results from variations of input parameters (i.e. diffusion, mixing, and chemical reaction coefficients) were evaluated. The effects of the degree of mixing, diffusion, and chemical reaction could then be compared qualitatively with experimental data. An optimized solution to variations of the input parameters would be one that demonstrates the expected flame behavior while making efficient use of available computer run time. The plotted results for all computer runs pertaining to the following discussion are presented in Appendix A. It should be noted here that any 'fuzziness' in the plotted computer generated data is the resolution with which output was calculated along the discrete time-steps.

5.1 Estimating a Flame Speed

In the present algorithm, the ability to explicitly calculate the flame speed, u_f, in the algorithm of the combustion is possible. This is because the shadow (or leading edge) of the flame is not simulated. To generate values that approximate the speed of the flame propagation, it is necessary to relate the shadow or visible area of the combustion's leading edge.

From previous study, Heywood (1988) has shown the importance of u_b, which represents the mean expansion speed of the burned gas and ensuing enlargement of the burning area. He has submitted results from a cylinder pressure data for combustion near stoichiometric conditions (ϕ=0.98) which demonstrated the growth of the flame radius, r_f, and the burned gas radius, r_b, during the rapid burning or fast chemical reaction phase. It is during this phase that $r_f - r_b$ (roughly half the thickness of the turbulent flame) is seen to be approximately constant and therefore supposes that u_f and u_b can be considered equal. This consequence in the published experimental data allows the present study to indirectly fashion the necessary flame speed u_f by presuming it to be the same as u_b which is defined as follows,

[5.1]

$$u_b = \frac{\partial V_b / \partial t}{A_b}$$

where V_b is the spherical volume of the gases which constitute the burned mass fraction of the combustion and A_b represents the corresponding spherical surface area of this volume. The derivation of the collective volume of the burned gases is readily available with each time-step of the algorithm. By calculating the rate of change of the volume of this sphere, the mean expansion speed of the burned gas, u_b, is then obtained.

A reservation to this argument for the equivalent relationship between u_f and u_b comes when considering that conditions for the present study are at the limit of the lean burn where ϕ=0.625, away from stoichiometry ($\phi = 1.0$). It is accepted that the flame thickness may not remain constant over the fast chemical reaction phase of lean burn thus diminishing the accuracy of the above approximation for u_f.

The Heywood study has also defined the burning speed of the fuel as,

[5.2]

$$S_b = \frac{\partial m_b / \partial t}{\rho_u A_b}$$

where m_b is the mass of the fully burned gases which constitute the burned mass fraction of the combustion, and A_b is defined as above. The burned mass fraction is calculated directly in each time-step, and by tracking the rate of change of the burned mass fraction, the burning speed, S_b, of the combustion is then easily obtained.

5.2 Effect of the Input Parameters: Constants of the Model

The baseline input parameters taken from empirical values found in the literature are tabulated in Appendix C.

The baseline combustion properties (i.e. fuel type, equivalence ratio, and initial reactant temperature, pressure, and turbulence parameters) were taken from

experimental measurements conducted by Petrov and Talantov (1959). It is with these experimental values, where the $K \cdot Le$ product approaches the quenching limit of 6.0, that aspects contributing to combustion misfire can be best revealed.

Constants for the single-step chemical rate equation [4.11] were those proposed by Westbrook and Dryer (1981) which are particular to the fuel. These inputs consist of a pre-exponential coefficient $A_{pre\text{-}exp}$, the activation energy B, and exponents values a and b for the fuel and air concentration terms respectively. There is some perceived freedom to adjust the pre-exponential coefficient or the activation energy. This is because the authors, in using the mechanism, were attempting to predict laminar flame speeds in the absence of available data for the corresponding flame thickness.

Ultimately, with all the baseline criteria in place, the computer code simulated a misfire as shown with the pressure and burned mass fraction plots of Figures A-1 and A-2 respectively. This consequence is not surprising considering that the Petrov and Talantov data are close to the quenching limit cited by Bradley (1992). From the misfire result of the baseline data, the sensitivity of the results to the various parameters is then investigated to account for their influence on the combustion event.

5.2.1 Effects of the Pre-exponential and Activation Energy Constants on the Chemical Reaction Rate

The most direct way of influencing the combustion to advance beyond the baseline misfire is to either lower the activation energy, B, required by the chemical reaction or increase the pre-exponential, $A_{pre\text{-}exp}$, of the chemical rate equation. Westbrook and Dryer (1981) showed that the fuel benzene has values of $2\times10^{11}[cal./sec.]$ and $30000[cal./sec.]$ for $A_{pre\text{-}exp}$ and B respectively. Figures A-1 to A-4 show plots of the pressure, burned mass, burning speed, and burning particle fraction over time when $A_{pre\text{-}exp}$ is decreased from 2×10^{12} down to $2\times10^{11}[cal./sec.]$ and B is decreased from 35000 down to $25000[cal./mol.]$.

The maximum activation energy, B, to obtain a full burn in the chamber is seen to be $26000[cal./mol.]$ where any higher value does not allow for a fast chemical reaction to bring the combustion to full burn. As B is lowered in value to $25000[cal./mol.]$, the time to fully burn the mixture becomes shorter. A similar effect was found by increasing the pre-exponential $A_{pre\text{-}exp}$ from the combustion limiting value 9×10^{11} up to $2\times10^{12}[cal./sec.]$. Simulated misfires are in evidence when $A_{pre\text{-}exp}$ or B take on values below $9\times10^{11}[cal./sec.]$ and above $26000[cal./mol.]$ respectively.

The pressure plot of Figure A-1, when changing the $A_{pre\text{-}exp}$ or B value, demonstrated the same characteristics as the burned mass fraction plots of Figure A-2 above a burn mass fraction of 10%. At the point where the burning rate

maximizes, the chamber combustion pressure was found to have a value of 3.0[*atm.*]. This observation is in agreement with the research of Rassweiler and Withrow (1938) who were able to demonstrate a correlation between the profiles of burned mass fraction and pressure within a closed combustion chamber.

The plots of S_b, the particles' burning speed, in Figure A-3 show that S_b/u_L maximizes as $A_{pre\text{-}exp}$ or B approach their limiting values of 9×10^{11}[*cal./sec.*] or 26000[*cal./mol.*] respectively. This demonstrates that adjustment in the activation energy or pre-exponential values does not influence the profiles or maxima of the expansion speed plots near the misfire limit. As $A_{pre\text{-}exp}$ or B take on values promoting full combustion, the S_b/u_L profiles are seen to have reduced maxima from those near the misfire limit. The plots maximize corresponding to approximately 40% mass burn.

The burning particle fraction plots in Figure A-4 show that fewer particles retain the burning condition for a shorter time as $A_{pre\text{-}exp}$ or B move from their combustion limiting values.

An observation common to all of the full burn combustion runs is that once the burn mass reaches 10 %, there is little difference in the observed burning rate and combustion time to full burn.

Therefore, other constants, namely the diffusion constant σ_ϕ and mixing constant C_ϕ should be varied to change the profile of the plotted results.

One set of $A_{pre\text{-}exp}$ and B values will be adopted for the computer runs of the next section, that is, $A_{pre\text{-}exp}=2\times10^{11}[cal./sec.]$ and $B=25000[cal./mol.]$. This combination assures the sustenance of a fast chemical reaction rate while still in the proximity of the misfire region for combustion. As shown above, the combination of $A_{pre\text{-}exp}=2\times10^{11}[cal./sec.]$ and $B=30000[cal./mol.]$ recommended by Westbrook and Dryer (1981) would not provide a fast enough chemical reaction rate for the present model

5.2.2 Effect of Constants in the Mixing and Diffusion Expressions

The influence of mixing and diffusion on the flame propagation affects the rate at which energy is transferred among neighbouring particles and between neighbouring shells in the chamber.

The rate of particle diffusion between the shells of the modeled combustion chamber is dependent on the value of the diffusion coefficient Γ_T given as:

$$\Gamma_T = \frac{C_\mu}{\sigma_\phi}\frac{k^2}{\varepsilon}\langle\rho\rangle$$

The diffusion rate can then be adjusted directly to the ratio of the empircal constants $\frac{C_\mu}{\sigma_\phi}$ that, according to Pope (1976), can have values between 0.129 and 0.09. This corresponds to σ_ϕ having a range of value between 1.0 and 0.7 where C_μ has been cited with a value of 0.09.

Figures A-5 to A-8 show plots of pressure, burned mass fraction, burning speed, and burning particle fraction when σ_ϕ is varied from 0.5 up to 2.0, thereby reducing the rate of diffusion of particles between the shells.

The degree of mixing is prescribed by the mixing frequency ω of particles within a local shell to reach scalar uniformity given as:

$$\omega = C_\phi\left(\frac{\varepsilon}{k}\right)$$

The mixing rate can therefore be seen to be directly proportional to the empirical constant C_ϕ that, from the literature, can have values from 0.6 to 3.1.

Figures A-9 to A-12 show plots of pressure, burned mass fraction, burning speed, and burning particle fraction when C_ϕ is varied from 3.0 down to 0.1 thereby reducing the rate of mixing among particles.

A common effect with the reduction of the diffusion or mixing rates is an extension of necessary time to achieve full burn. The influences of the diffusion constant σ_ϕ and mixing constant C_ϕ are similar in that they serve to moderate the rate of the pressure increase and burned mass fraction development. Burning speeds exhibit a longer profile in time with a reduced maximum value under slower diffusion and mixing among the particles. Burning particle counts are seen to diminish during combustion runs as the rates of diffusion and mixing are reduced.

In general, the effect of reducing the diffusion or mixing rates is to slow the completion of the combustion process and moderates the values of the burning speed and burning particle counts. At the extreme of this influence, that is where C_ϕ has a value of 0.1, the burning process is lengthened in time by a factor of 10 and the S_b/u_L maximum is reduced by a factor of 10.

5.2.3 Effect of the Quantity of Shells and Particles on Results

A basis for any numerical study is the effect of grid refinement on the accuracy of the results. The simulated combustion data reviewed above were produced with a combustion space of 23 concentric shells and 107440 compositional particles. By presenting data from models with half or double the shell or particle counts, a reasonable model should generate results with close agreement when all other variables are fixed.

Figures A-13 to A-16 compare plotted results from a grid refinement of the baseline values. This is represented by runs where there are 12, 23, and 45 shells and there are 53720, 107440, and 214880 particle counts. In all all but one of the above cases, the results show close conformity. The exception came when the shell count was increased to 45 without a corresponding increase in the number of particles and resulted in a comparative time delay in the onset of the fast chemical reaction.

The loss of accuracy demonstrated in the run with 45 shells could be accounted for by the 'thinning' of the particle counts within the most central

spherical shells. Following ignition, the diffusion and mixing of the centrally-ignited articles may be adversely affected with less populated adjacent shells to propagate the released energy. For this reason, an increase the total number of shells in the pursuit of numerical accuracy should be accompanied by a corresponding increase in the total number of particles.

The effect of refinement, with the provision that sufficient particles be available to populate all shells, provides confidence in the grid size numerical accuracy offered by the model.

5.2.4 Effect of Time-Step Refinement

As detailed in the control-volume formulation of Section 3.1.2, the differentiation of the governing equation in time was achieved by way of explicit values. That is, values at time t were used to derive the subsequent values at time $t+\Delta t$. This numerical method is understood to be more computationally expeditious than the use of implicit values, but not necessarily more accurate.

A study of time-step refinement would test the validity of the explicit scheme. As the time-step is decreased, the computed values at time t will approach those of $t+\Delta t$ and, in the limit, represent implicit values. Figures A-17 to A-21 plot results from a numeric refinement of the global time-step. The comparison is represented by runs where Δt_{GLOBAL} during each iteration of the algorithm is divided by factors of 2 (the current), 4, and 8. In all cases, the results show close conformity. This observation supports the implementation of the

implicit scheme for the purpose of reduced computer run times without compromising numeric accuracy.

5.3 Comparison with the Compiled Results of Abdel-Gayed, Bradley, and Lawes (1987)

As detailed from the relevant literature review of Chapter 1, the assumption of flame quenching came with the $K \cdot Le$ product approaching 6.0. Combustion runs in the above plots of Figures A-1 to A-16 made use of conditions which reflected a lean burn premixture and a $K \cdot Le$ product equal to 5.94.

The results of the model were tabulated in a format consistent with previous research, with the intention of validating the combustion model in the lean burn combustion limit. With the modeled combustion having a point-source ignition and an enclosed chamber, it was necessary to incorporate the relationship between the effective r.m.s. turbulent velocity acting on a flame, u_k', and r.m.s. turbulent velocity, u'. This would allow the tabulation to account for the relevant frequency range of the turbulent power spectrum during the growth of the kernel from a point source ignition. It has been shown by Abdel-Gayed et al (1985) that as the kernel grows the propagation of the flame is first influenced by the higher frequencies of the turbulent spectrum and, with time, increasingly lower frequencies. Figure 5-1 shows this correspondence, that is, how the influence of

the velocity fluctuations in the flame front can be tied to a dimensionless time scale and subsequently used to derive the necessary u_k'.

The calculation to derive the integral time scale τ_a for the stirred bomb combustion from Abdel-Gayed et al (1987) is as follows:

$$\tau_a = \frac{\ell_0}{u_0'}\sqrt{\frac{\pi}{8}} \qquad [5.3]$$

where ℓ_0 and u_0' are the initial values of integral length scale and r.m.s. turbulent velocity respectively. Using the combustion time t as the independent axis, a range of values of $\frac{u_k'}{u_0'}$ corresponding to $\frac{t}{\tau_a}$ is found by interpolating within the plot of Figure 5-1. The specific values of u_k' are then returned by multiplying the dimensionless ratio $\frac{u_k'}{u_0'}$ through by u_b'.

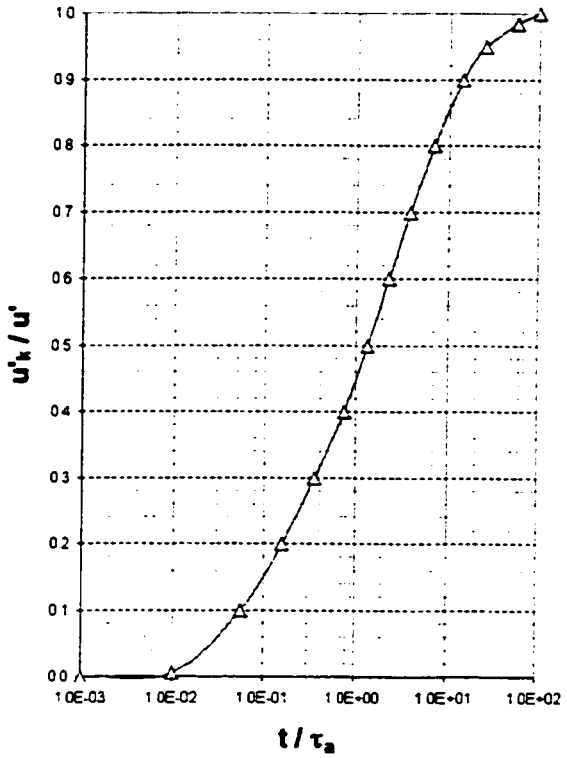

Figure 5-1. Development of Effective R.M.S. Turbulent Velocity and Strain Rate with Dimensionless Time – Abdel-Gayed et al (1987)

With the above interpolation now shown to yield values of u_k', it is possible to relate u_k' to t and consequently plot u_k' against the mean expansion speed u_b to its maximum value.

By plotting a dimensionless relationship between u_k' and u_b with respect to the laminar flame speed u_L, the results of the combustion algorithm can be compared to the lean burn limit characteristic ($K \cdot Le = 6.0$) of Figure 2-3. Figure A-17 shows this correlation up to where the reacting mass (burning and fully

burned particles) reaches 80%. These plotted relationships demonstrate how, as the empirical constant C_ϕ of the mixing rate takes on values near 2.0, the simulated results approach those of experiment.

The plots of Figure A-17 are an effort to present the extent to which the combustion has engulfed the premixture. This may in fact then simulate the propagation of an enclosed flame. In this study then, it is most desirable to compare data to the corresponding experimental data by considering the development where this engulfed mass of the premixture approaches 90%.

5.4 Comparison with the Experimental Results of Checkel and Ting (1993)

Interest in the effect of moderate changes in the premixture equivalence ratio, ϕ, and the variety of fuel has been discussed earlier. Heywood (1988) observed the equivalence of flame speed u_f and burning speed u_t near stoichiometry (ϕ=0.98). The present study models combustion in a different regime at the limit of the lean burn where ϕ=0.625. This citation alone provides tenuous support to the $u_f \sim u_t$ assumption.

The work of Checkel and Ting (1993) with a constant volume chamber provides opportunity to weigh the impact of variation in the equivalence ratio as it

relates burning velocity to turbulence intensity. In these experiments, using fuel methane, the change of ϕ from a near-stoichiometic condition (ϕ=0.96) to a much leaner burn of ϕ=0.76 was assessed. A conclusion made was that over the range $0 < u_k'/u_L < 12$ of normalized turbulent intensity, there could be found a linear relationship between u_b and u_k' in the spherical flame of the experiment. This relationship was observed to be exact in value for both the lean and the near-stoichiometric premixture. A further interesting result was that this linear relationship is independent of the variety of hydrocarbon fuel used

Table 5-1 : Comparison of Results at 2.2[atm.] from the Present Model and the Checkel and Ting (1993) Experiment

Data Source	premixture fuel : air by mass	spherical flame diameter [cm]	Range of linearity	slope of linearity $\frac{u_b/u_L}{u_k'/u_L}$
Present Study, Figure A-17 (C_ϕ=2.00)	0.625 : 1.0 (benzene : air)	2.78	$5 < u_k'/u_L < 14$	0.50
Checkel and Ting (1993)	0.760 : 1.0 (methane : air)	2.70	$0 < u_k'/u_L < 12$	0.27

Referring to plotted results of the present study in Figure A-17, there can be seen a linearity along the normalized u_b versus u_k' plots in the range $5 < u_k'/u_L < 14$. The slope of the linear relationship for each plot is seen to increase from 0.2 to

0.5 with the value of mixing constant C_ϕ increasing from 0.1 to 2.0. A detailed comparison is shown in Table 5-1.

It is consequently shown that the present study presents data that follows the linearity of combustion highlighted by Checkel and Ting (1993). Their experimental observations on the independence of the hydrocarbon fuel and the equivalence ratio to an enclosed chamber are quite valuable to the present study. With the present fuel being a hydrocarbon (benzene) and the present equivalence ratio lean of stoichiometric conditions (ϕ=0.625), the present model can thus be said to correspond to experiment with a fair deal of confidence. This agreement with experiment also lends credence to the Heywood approximation for u_f in the present study.

5.5 Review of the CFM Numerical Study of Choi and Huh (1998)

The comparison of the data from the present study results to that of other numerical simulations is another desirable method to validate the established model. Recently, Choi and Huh (1998) made a detailed study on the ability of the coherent flamelet model (CFM) to correlate with the experimental data for turbulent burning velocity published by Checkel and Thomas (1986) and Abdel-Gayed et al (1987).

The study of Choi and Huh used two forms of the flame production term in their numerical models called CFM-1 and CFM-2 to predict u_b. In the CFM-1 version, the flame production term is related to rate of strain (previously provided as $\sqrt{\varepsilon_0/\nu_T}$ in Section 5.4). The CFM-2 version uses a different the flame production term is related to turbulent intensity as u'/ℓ_{ic}. A problem with the CFM application, as cited by the authors, was the acceleration experience in u_b near the wall as combustion nears completion. Their remedy to this situation was to incorporate an annihilation term which slowed combustion as the mass burned fraction approached 100% in the wall at the limit of the flame travel.

The CFM models simulated spark-ignited premixed combustion by dividing the process into the three distinct phases of ignition, laminar flame propagation, and turbulent flame propagation. Ignition is established by the formation of an initial flame kernel that expands spherically and is then considered to propagate as a laminar flame. The transition to the turbulent propagation is arbitrarily chosen to occur when the flame radius reaches a set fraction of ℓ. The transport equations of the CFM models use a conservation of property technique to allow numerical solution in time.

The necessary input parameters and output configurations were applied to the CFM models that they might simulate the combustion scenarios of published experimental results. To compare numerical results with the research of Checkel and Thomas (1994), the CFM models were programmed to evolve the normalized

ratio of S_b/u_L to where $P/P_0 = 2.2$. The desired data set from the collection of Abdel-Gayed et al (1987) was to be modeled using constant turbulence and in the combustion regime where the break-up of the flame sheet was assured (i.e. $0.07 < \mathrm{K} \cdot Le < 0.7$).

In general, the CFM models were shown to simulate the experimental results. Their application of arbitrary tuning constants allowed the predicted u_b to match a reference condition. From agreement with the experimental reference, the simulations could adopt different input combustion conditions and gauge their correspondence to other sets of experimental data. The CFM-2 that related u'/ℓ_{ic} to flame production best followed the behavior both the Abdel-Gayed et al and the Checkel et al data.

The present study focussed on $\mathrm{K} \cdot Le \sim 6.0$ region where flame quench prevails. For this reason, there was no ability for a numerical comparison with the numerical results of the CFM technique. Despite this deficiency, the study by Choi and Huh offers some useful ideas for future study with the present model. The use of an annihilation term for improved combustion simulation near the outer wall and the use of the arbitrary tuning constants to establish agreement with a reference experimental value are seen as effective methods of promoting model success.

Chapter 6

Conclusions and Recommendations

6.1 Conclusions

The objectives described in section 1.2, pertaining to this work, have been completed. The concluding remarks are summarized below

1. A numerical model was developed to study the combustion of a lean premixture in a closed vessel at the threshold of misfire. It has the capability to simulate the fundamental phenomena that constitute combustion, that is, chemical reaction, diffusion, and mixing. A discretization of the property conservation equation in a control volume numerical method was the basis of analysis for the model.

2. Numerical simulations have been performed which demonstrate combinations of the necessary chemical reaction, diffusion, and mixing input parameters that allow for combustion to propagate in a constant volume vessel.

3. The results suggest that a fast reaction rate among the burning particles of the simulation can only be sustained if the rates of mixing or diffusion between particles are reduced from those suggested in the literature.

4. The closest agreement with the compiled experimental results of the mean expansion speed, u_b, from Bradley [1992] was best achieved when activation energy, B, and mixing rate coefficient, C_ϕ, are set to values near 25000[*cal./mol.*] and 2.0 respectively. In addition, the simulated propagation of the enclosed flame was best presented when 80% of the premixture mass had been engulfed by the chemical reaction of the combustion.

6.2 Recommendations

In further work to the present study, the following recommendations should be considered:

1. A concern of the accuracy of the approximation of the flame speed u_f must be expressed. It has not been confirmed with experimentation that at the limits of the lean burn, away from stoichiometric mixtures, that the flame thickness will remain constant. A more involved study to confirm the derivation u_f in the region of the lean burn limit would serve to improve the interpretation of the model output.

2. One clear shortcoming in the established model was seen with the loss of accuracy demonstrated by the 'thinning' of the particle counts within the most

central spherical shells. To improve the accuracy of the model with grid size numerical refinement, one must assure that sufficient particles be available to populate all shells.

3. Any future study to enhance the operation of the established model to should be done with an eye to the research of Choi and Huh (1998). Their methods, such as a flame annihilation term and tuning constants, in the development of a CFM combustion model proved successful in correspondence of the numerical output with experimental data.

4. A last recommendation in the operation of the present model would be to incorporate the k-ε model for turbulence in the reacting flow of the combustion process. The k-ε model, a version of which is detailed in Appendix D, would allow for an alternative estimate on the influence of kinetic energy and its dissipation in time.

References

Abdel-Gayed, R.G. and Bradley, D. (1985), *Criteria for Turbulent Propagation Limits of Premixed Flames*, Combustion and Flame 62, 61-68.

Abdel-Gayed, R.G., Bradley, D., and Lawes, M. (1987), *Turbulent Burning Velocities : A General Criteria for Correlation in Terms of Straining Rates*, Proc. R. Soc. London A414, 389-413.

Bergeron, C.A. and Hallett, W.L.H. (1989), *Ignition Characteristics of Liquid Hydrocarbon Fuels as Single Droplets*, C.J.Ch.E. 67, 142-149.

Borghi, R. (1988), *Turbulent Combustion Modelling*, Prog. Energy Comb. Sc. 14, 245-292.

Borgnakke, C., Arpaci, V.S., and Tabaczynski, R.J. (1980), A Model for Instantaneous Heat Transfer and Turbulence in a Spark Ignition Engine, SAE Paper 800287.

Bradley, D. (1992), *How Fast Can We Burn?*, 24th Symposium (Int.) on Combustion, The Combustion Institute, Pittsburgh, pp. 247-262.

Bradley, D., Lau, A. K. C., and Lawes, M. (1992), Phil. Trans. R. Soc. London A338, 359-387.

Bradley, D. (1994), private communication.

Bray, K.N.C. and Peters, N. (1994), *Turbulent Reacting Flows* (Libby, P.A. and Williams, F.A. Eds.), Academic Press, London, pp. 63-113.

Choi, C. R. and Huh, K. Y. (1998), *Development of a Coherent Flamelet Model for a Spark-Ignited Turbulent Premixed Flame in a Closed Vessel*, Combustion and Flame 114, 336-348.

Correa, S. M. (1995), A *Direct Comparison of Pair-Exchange and IEM Models in Premixed Combustion*, Combustion and Flame 103, 194-206.

Checkel, M. D. and Thomas, A. (1994), *Turbulent Combustion of Premixed Flames in Closed Vessels*, Combustion and Flame 96, 351-370.

Checkel, M. D. and Ting, D. (1993), *Turbulence Effects on Developing Turbulent Flames in a Constant Volume Combustion Chamber*, SAE Paper 930867

Curl, R.L. (1963), *Dispersed Mixing: Theory and Effects in Simple Reactions*, A.I.Ch.E. 9, No. 2.

Ferguson, C.R. (1986), *Internal Combustion Engines*, John Wiley & Sons Inc., Toronto, pp. 103-114.

Gear, C.W. (1971), *Algorithm 407 DIFSUB for Solution of Ordinary Differential Equations*, Comm ACM 14, 185-190.

Heywood, J.B. (1988), *Internal Combustion Engine Fundamentals*, McGraw-Hill Inc., New York, pp. 406-412.

Hires, Ekchian, Heywood, Tabaczynski, Wall (1976), *Performance and NO_X Emissions Modelling of a Jet Ignition Prechamber Stratified Charge Engine*, SAE Paper 760161.

JANAF Thermochemical Tables (1971), NBS Publication, NSRDS-NBS 37.

Kosaly, G. (1986), *Theoretical Remarks on a Phenomenological Model of Turbulent Mixing*, Combustion Science and Technology 49, 227-234.

Launder, B.E. and Spalding, D.B. (1972), *Mathematical Models of Turbulence*, Academic, New York.

Lei, M.I-H. (1988), *Stochastic Model for Flame Propagation at Lean Ignition Limit and Partial Burn Limit of Spark Ignition Engines*, M.A.Sc. Thesis, Univ. of Ottawa.

Lei, M.I-H. and Milane, R.E. (1990), *Stochastic Model for Flame Propagation at Lean Ignition Limit of Spark Ignition Engines*, Combustion Science and Technology 69, 33-51.

Milane, R.E. (1999), private communication

Milane, R.E. and Hill, P.F. (1988), *Turbulent Characteristics of Premixed Fuel and Air*, Combustion Science and Technology, Vol. 59, pp. 275.

Milane, R.E., Tabaczynski, R.J., and Arpaci, V.S. (1983), *A Stochastic Model of Turbulent Mixing for the Prediction of Burn Rate in A Spark Ignition Engine*, Combustion Science and Technology 32, 211-235.

Norris, A. T. and Pope, S. B. (1994), Twenty-Fifth Symposium (Int.) on Combustion, The Combustion Institute, Pittsburgh, pp. 781-789.

Patankar, S.V. (1980), *Numerical Heat Transfer and Fluid Flow*, Hemisphere Publishing Corp., New York, pp. 25-39, 143-146.

Petrov, E.A. and Talantov, A.V. (1959), Izv. vÿssh. ucheb. Zaved., Aviat. Teknol. 3, 91-100. (English Transl.: American Rocket Society Journal, Vol. 31, 408-413 (1961).)

Pope, S.B. (1987), *Turbulent Premixed Flames*, Ann. Rev. Fluid Mech. 19, 237-270.

Pope, S.B. and Cheng W.K. (1986), *Statistical Calculations of Spherical*

Turbulent Flames, Symp. (Int.) Combust., 21st. Pittsburgh: Combust. Inst.

Pope, S.B. (1982), *An Improved Turbulent Mixing Model*, Combustion Science and Technology 28, 131-135.

Pope, S.B. (1980), *A Monte Carlo Method for the PDF Equations of Turbulent Flow*, MIT Report EL-80-012.

Pope, S.B. (1979), *A Monte Carlo Method for the PDF Equations of Turbulent Flow*, Phil. Trans. Roy. Soc. London A291, 529.

Pope, S.B. (1976), *The Probability Approach to the Modelling of Turbulent Reacting Flows*, Combustion and Flame 27, 299-312.

Rassweiler, G.M. and Withrow, L. (1938), *Motion Pictures of Engine Flames Correlated with Pressure Cards*, SAE Trans. 83, 185-204. Reissued as SAE Paper 800131.

Reid, R.C., Prausnitz, J.M., and Poling, B.E. (1987), *The Properties if Gases and Liquids*, 4th Edition, McGraw-Hill, 656-659.

Schäfer, Fred and van Basshuysen, Richard (1995), *Reduced Emissions and Fuel Consumption in Automobile Engines*, Springer Verlag, New York, 20-47.

Westbrook, C.K. and Dryer, V.S. (1981), *Simplified Reaction Mechanisms for the Oxidation of Hydrocarbon Fuels in Flames*, Combustion Science and Technology 27, 31-43.

Young, T.R. and Boris, J.P. (1977), A Numerical Technique for Solving Stiff Ordinary Differential Equation Associated with Chemical Kinetics of Reactive Flow Problems, J. Phys. Chem. 81, 2424.

Appendix A

Numerical Results on the Effects of the Input Parameters

The numerical results[1] of the modeled combustion have been plotted and are arranged in the following order:

- The effects of the pre-exponential and activation energy values in the chemical reaction rate equation

  Figure A-1. Pressure versus Time
  Figure A-2. Burned Mass Fraction versus Time
  Figure A-3. Mean Expansion Speed versus Time
  Figure A-4. Burning Particle Fraction versus Time

- The effect of the coefficient σ_ϕ in the diffusion rate equation

  Figure A-5. Pressure versus Time
  Figure A-6. Burned Mass Fraction versus Time
  Figure A-7. Burning Speed versus Time
  Figure A-8. Burning Particle Fraction versus Time

- The effect of the coefficient C_ϕ in the mixing rate equation

  Figure A-9. Pressure versus Time
  Figure A-10. Burned Mass Fraction versus Time

[1] Unless otherwise stated, these results are for a discretization which comprises 107440 particles (equal mass) which are distributed among 23 shells (concentric control volumes).

Figure A-11. Burning Speed versus Time
Figure A-12. Burning Particle Fraction versus Time

- The effects of numeric refinement in the discretiztion, that is, the number of the constituent particles (equal mass) and the number of shells (discrete concentric control volumes).

Figure A-13. Pressure versus Time
Figure A-14. Burned Mass Fraction versus Time
Figure A-15. Burning Speed versus Time
Figure A-16. Burning Particle Fraction versus Time

- The correspondence of the burning speed to the experimental data compiled by Bradley (1992).

Figure A-17. Mean Expansion Speed versus R.M.S. Turbulent Velocity for Specific Model Inputs to Compare with the Experimental Data Presented by Bradley (1992)

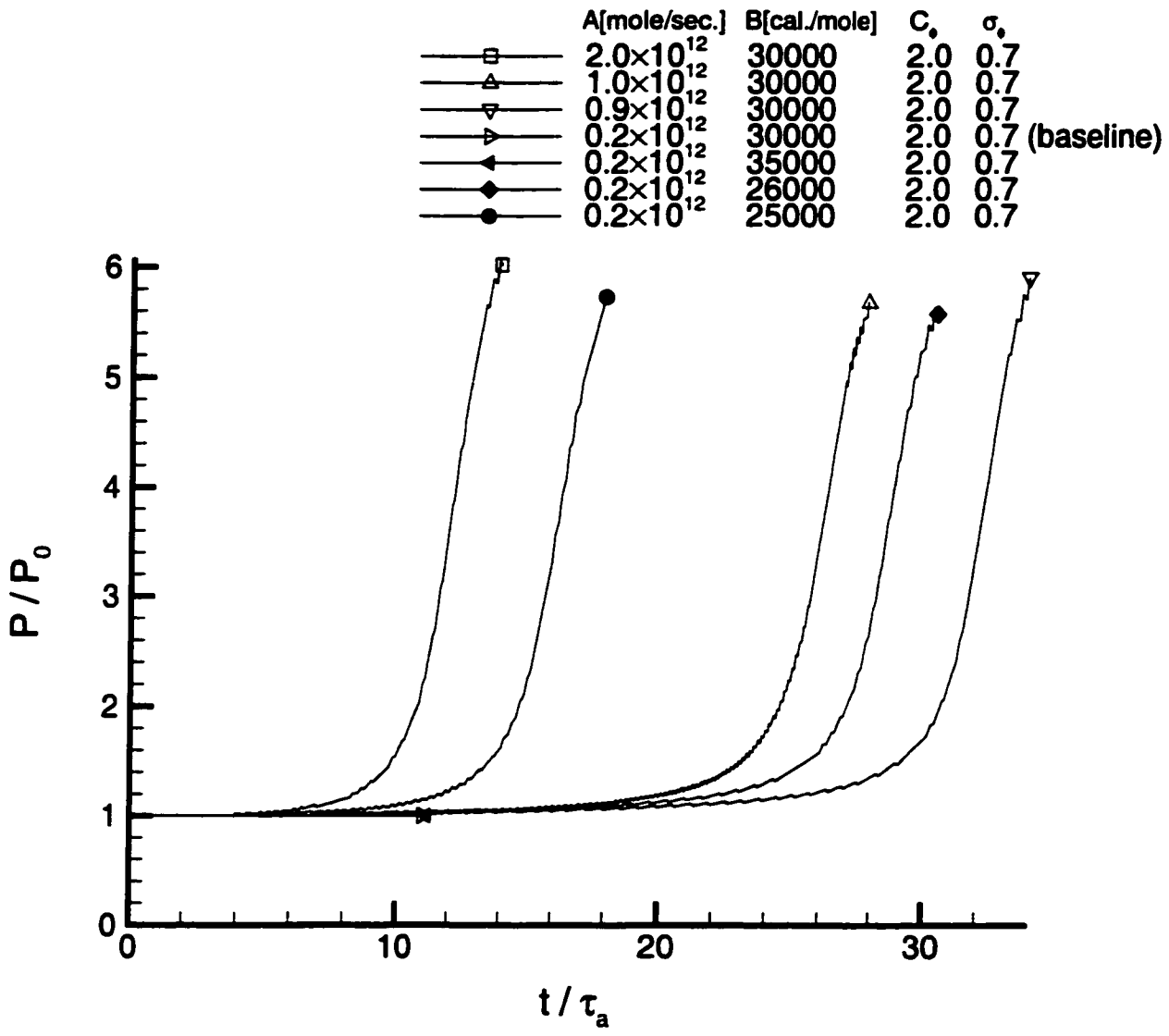

Figure A-1. Pressure versus Time for Different Reaction Rate Coefficients

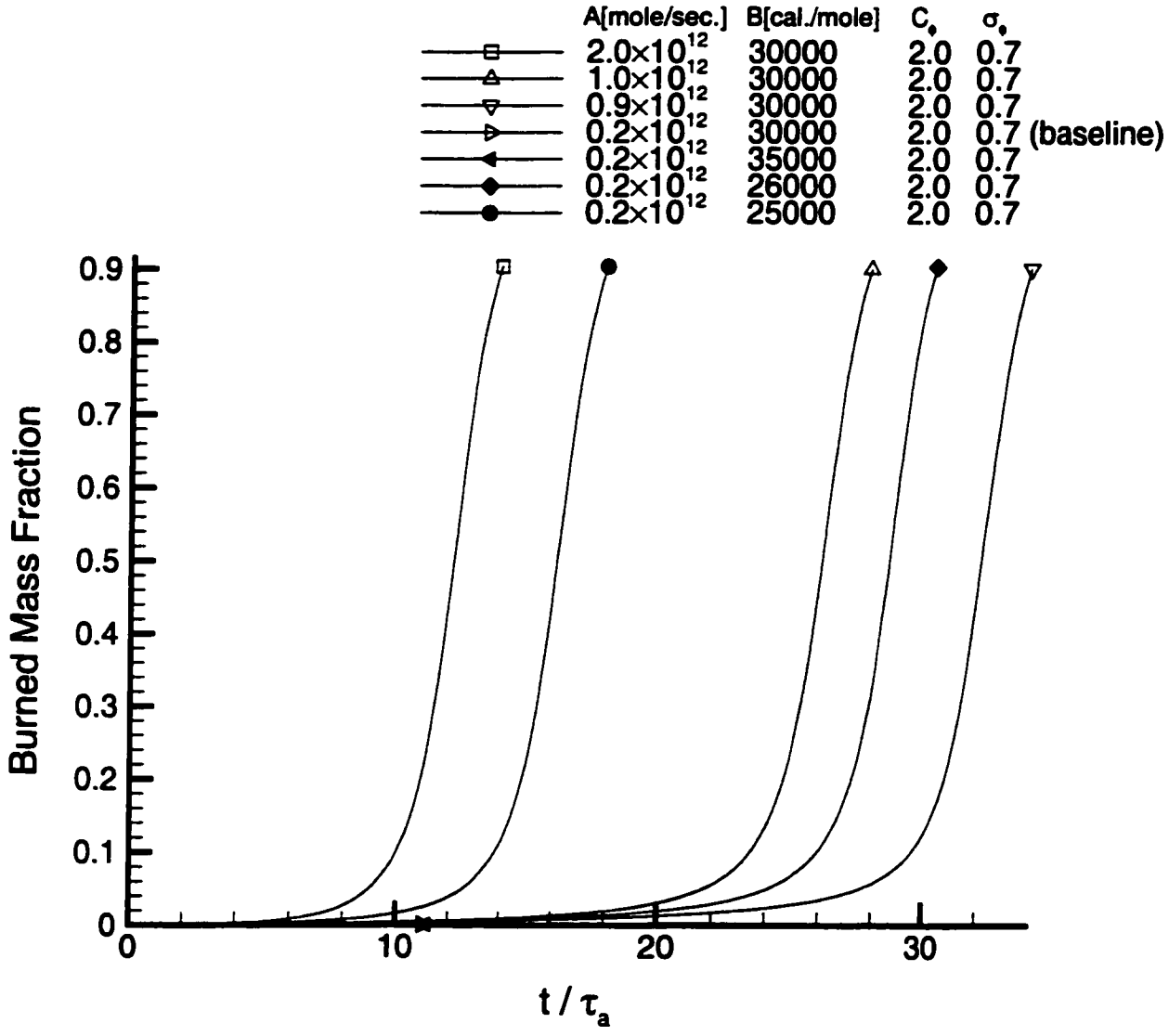

Figure A-2. Burned Mass Fraction versus Time for Different Reaction Rate Coefficients

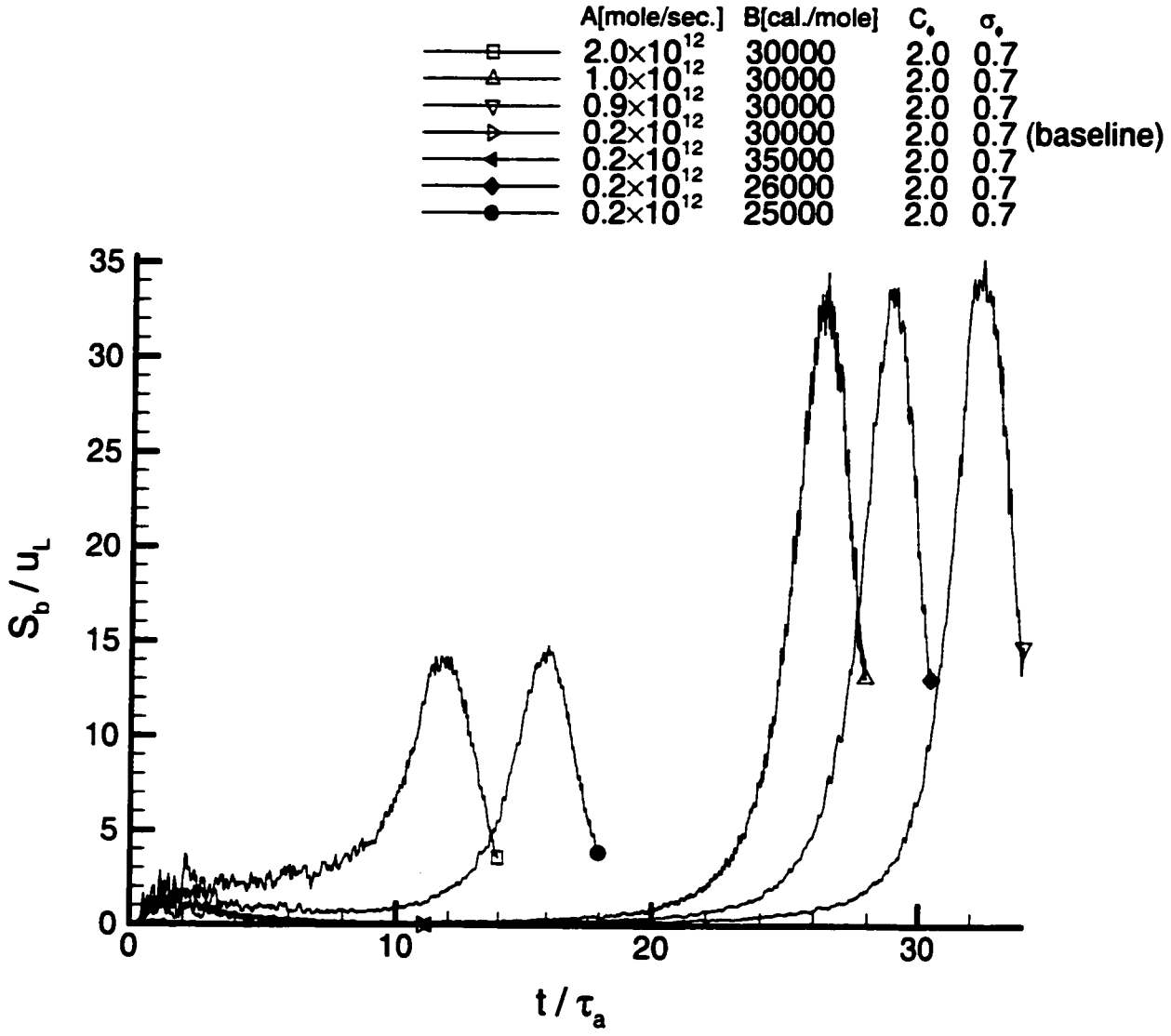

Figure A-3. Burning Speed versus Time for Different Reaction Rate Coefficients

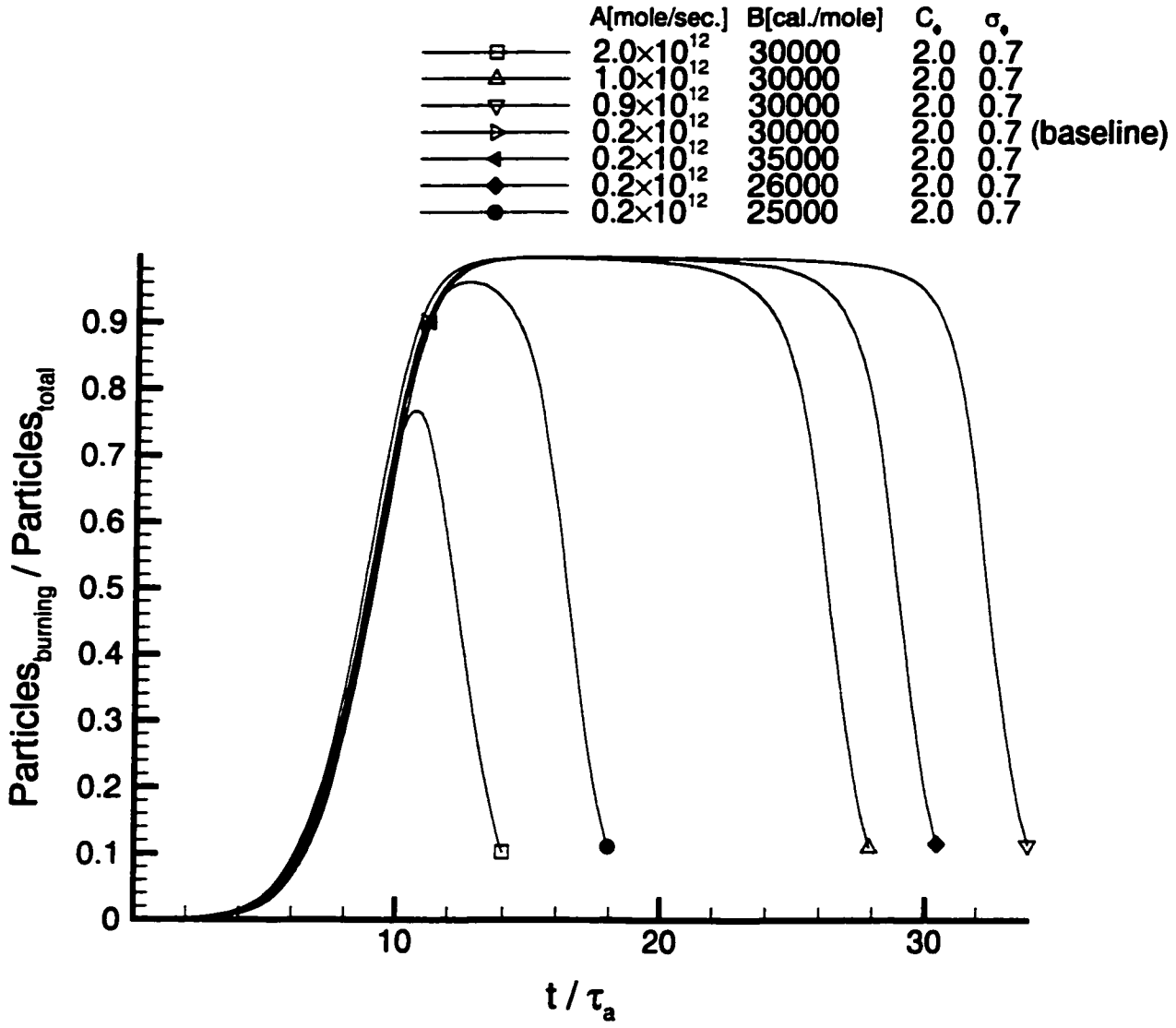

Figure A-4. Burning Particle Fraction versus Time for Different Reaction Rate Coefficients

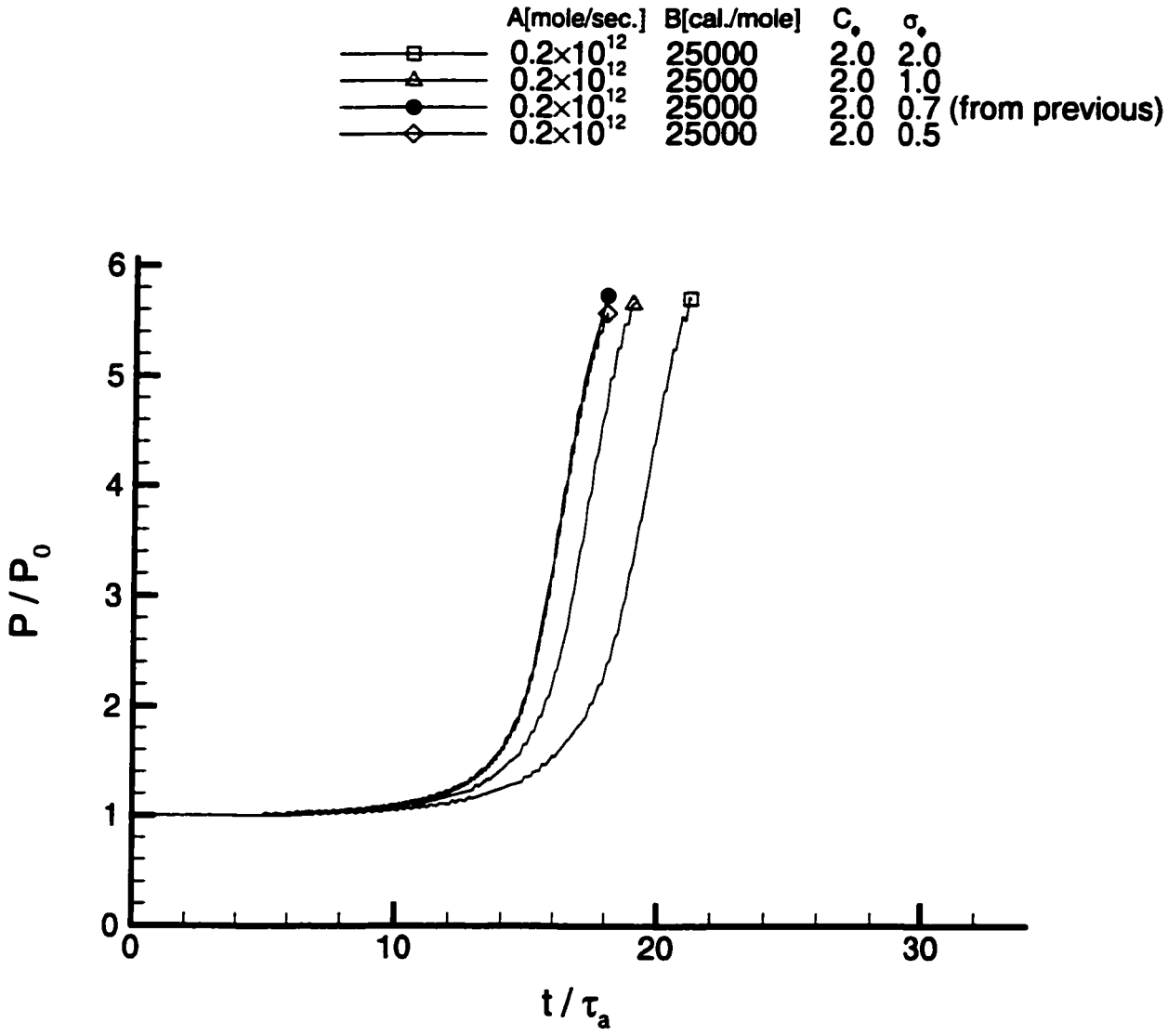

Figure A-5. Pressure versus Time for Different Diffusion Rates

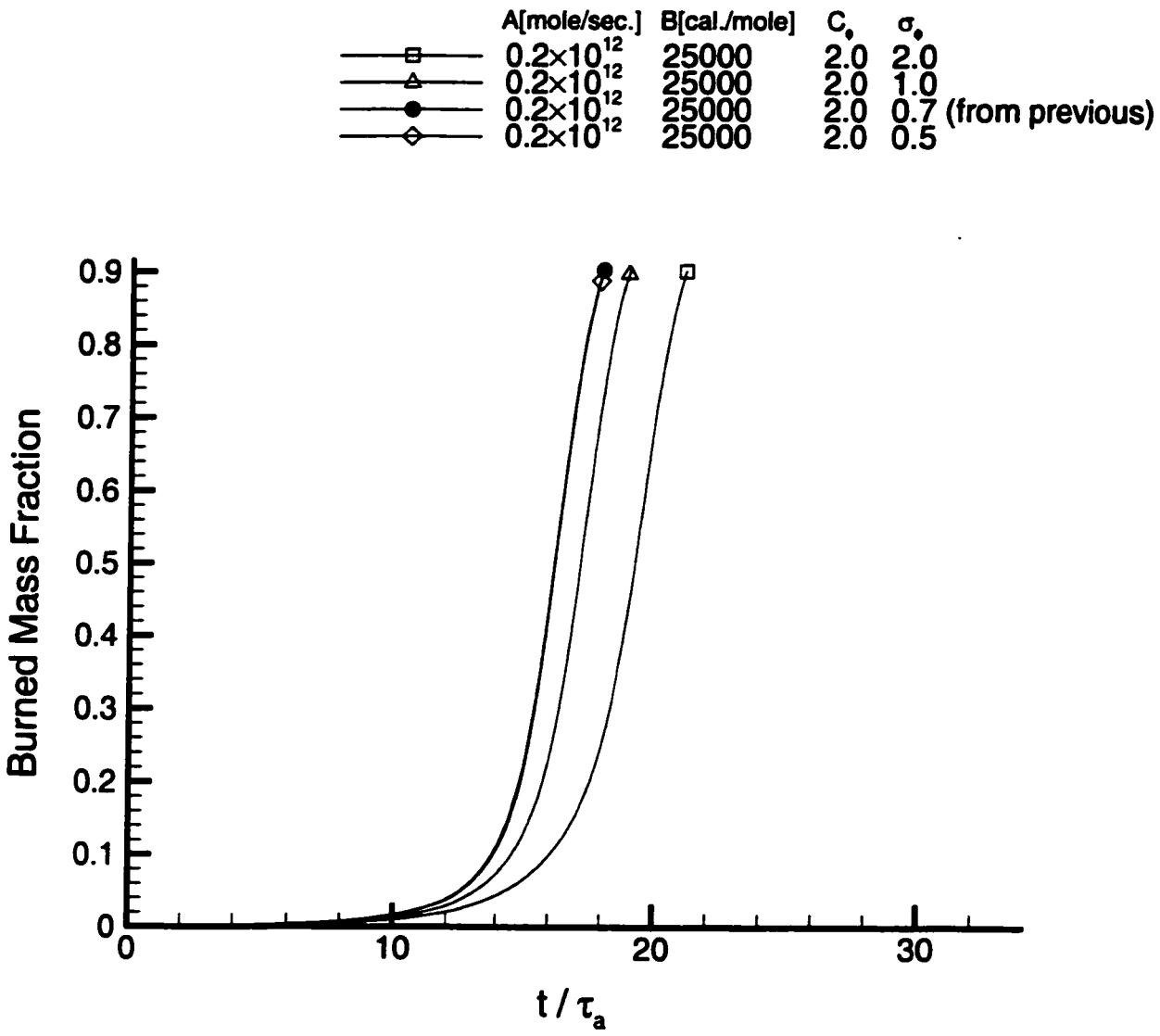

Figure A-6. Burned Mass Fraction versus Time for Different Diffusion Rates

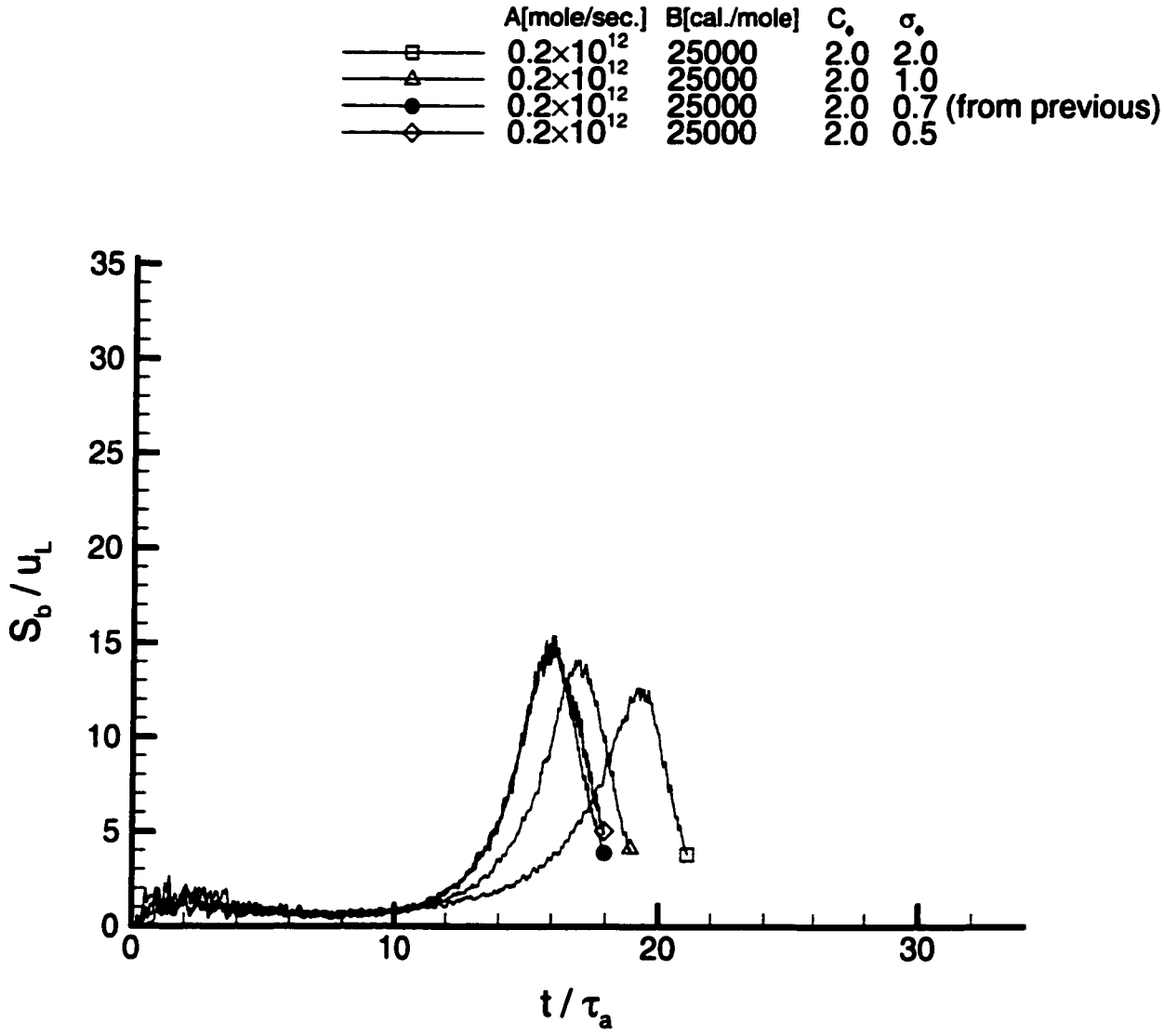

Figure A-7. Burning Speed versus Time for Different Diffusion Rates

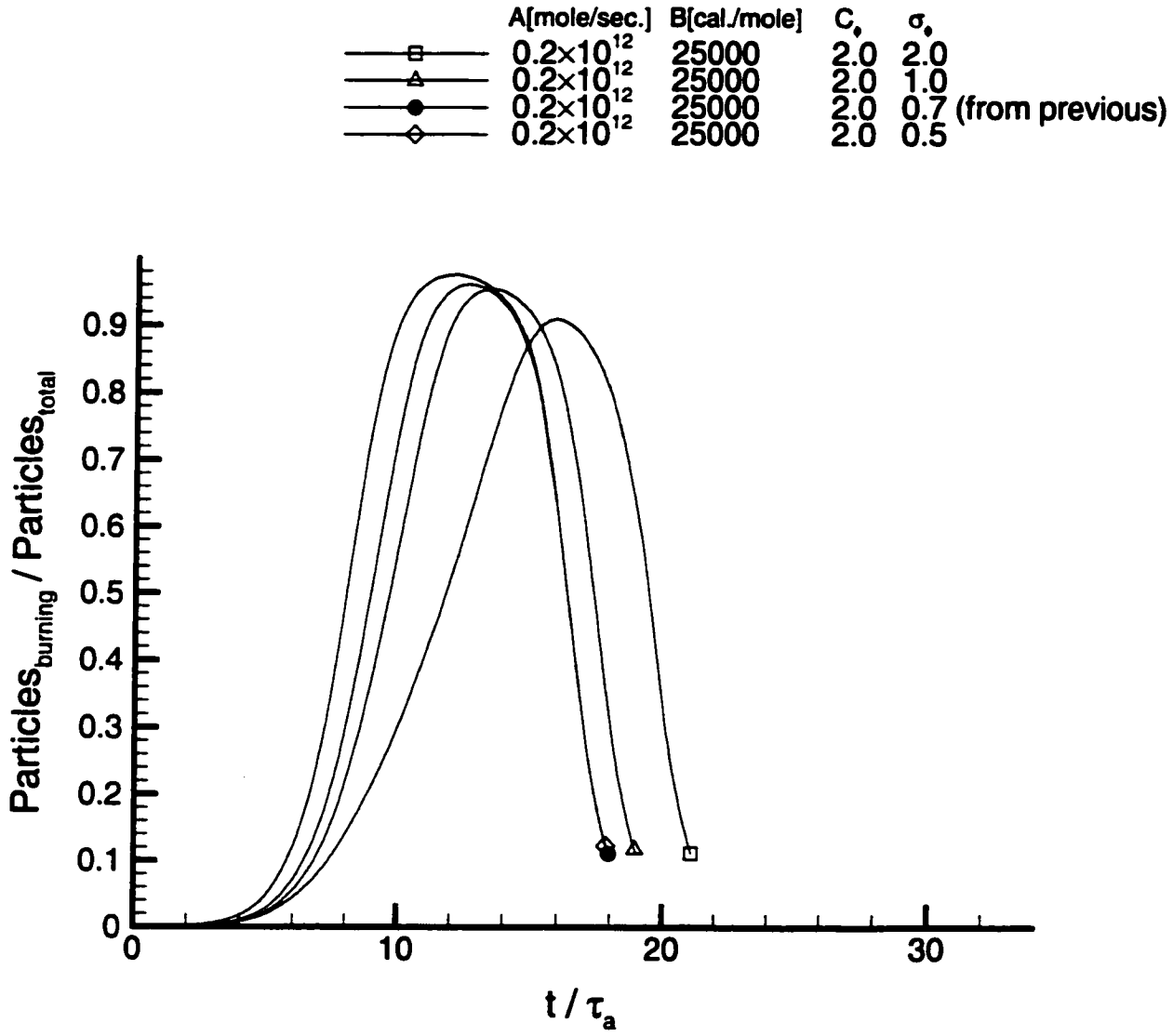

Figure A-8. Burning Particle Fraction versus Time for Different Diffusion Rates

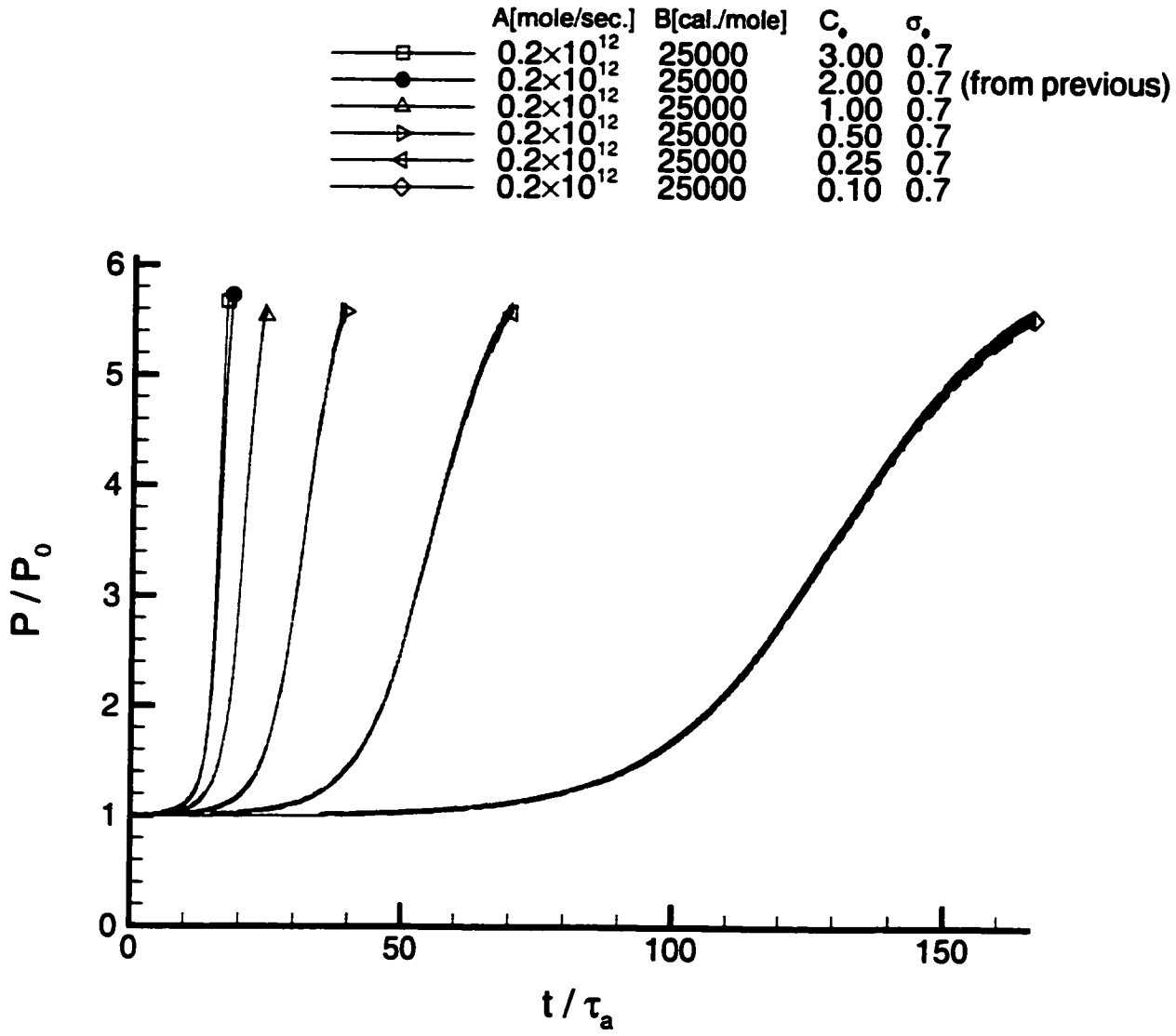

Figure A-9. Pressure versus Time for Different Mixing Rates

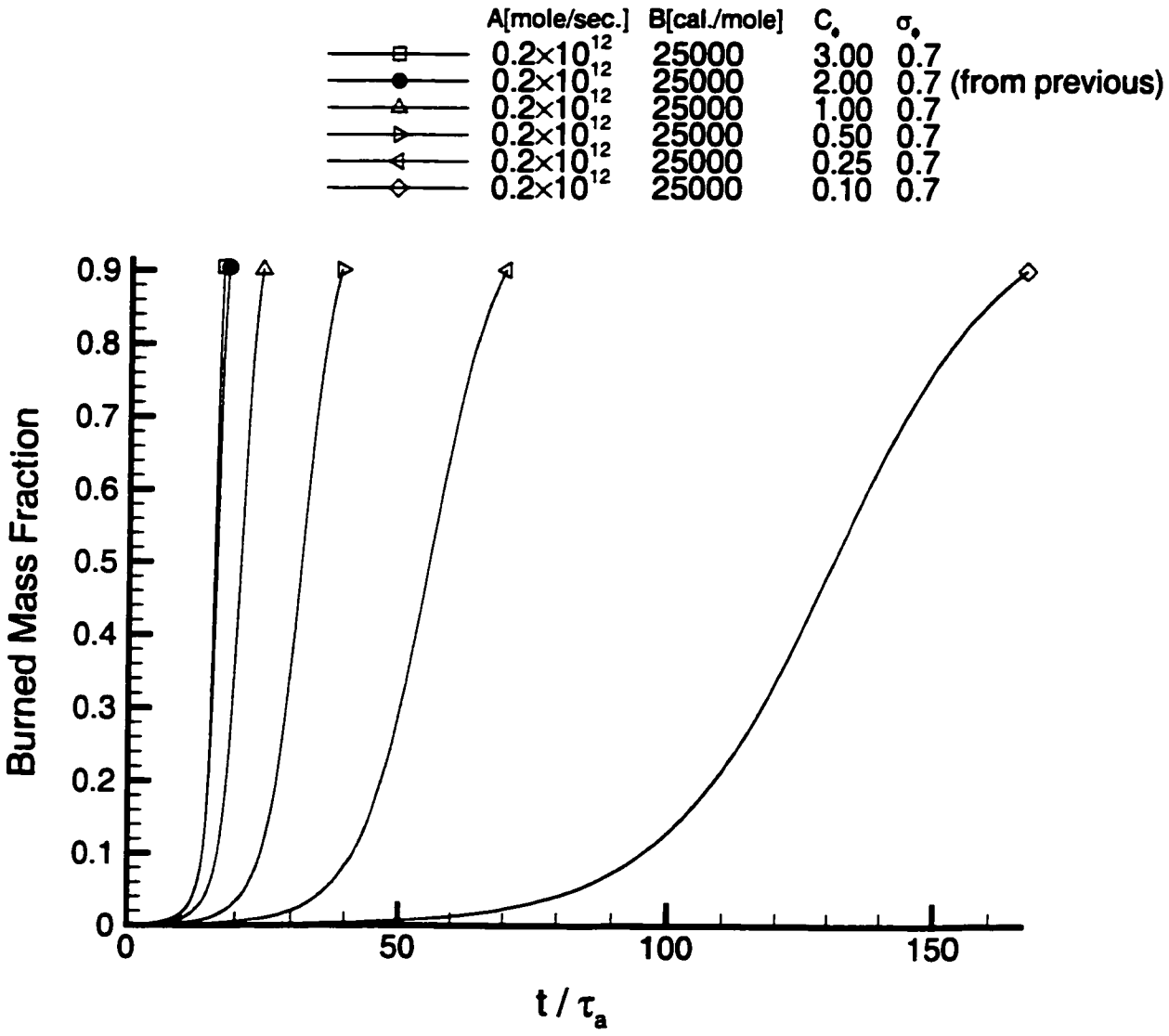

Figure A-10. Burned Mass Fraction versus Time for Different Mixing Rates

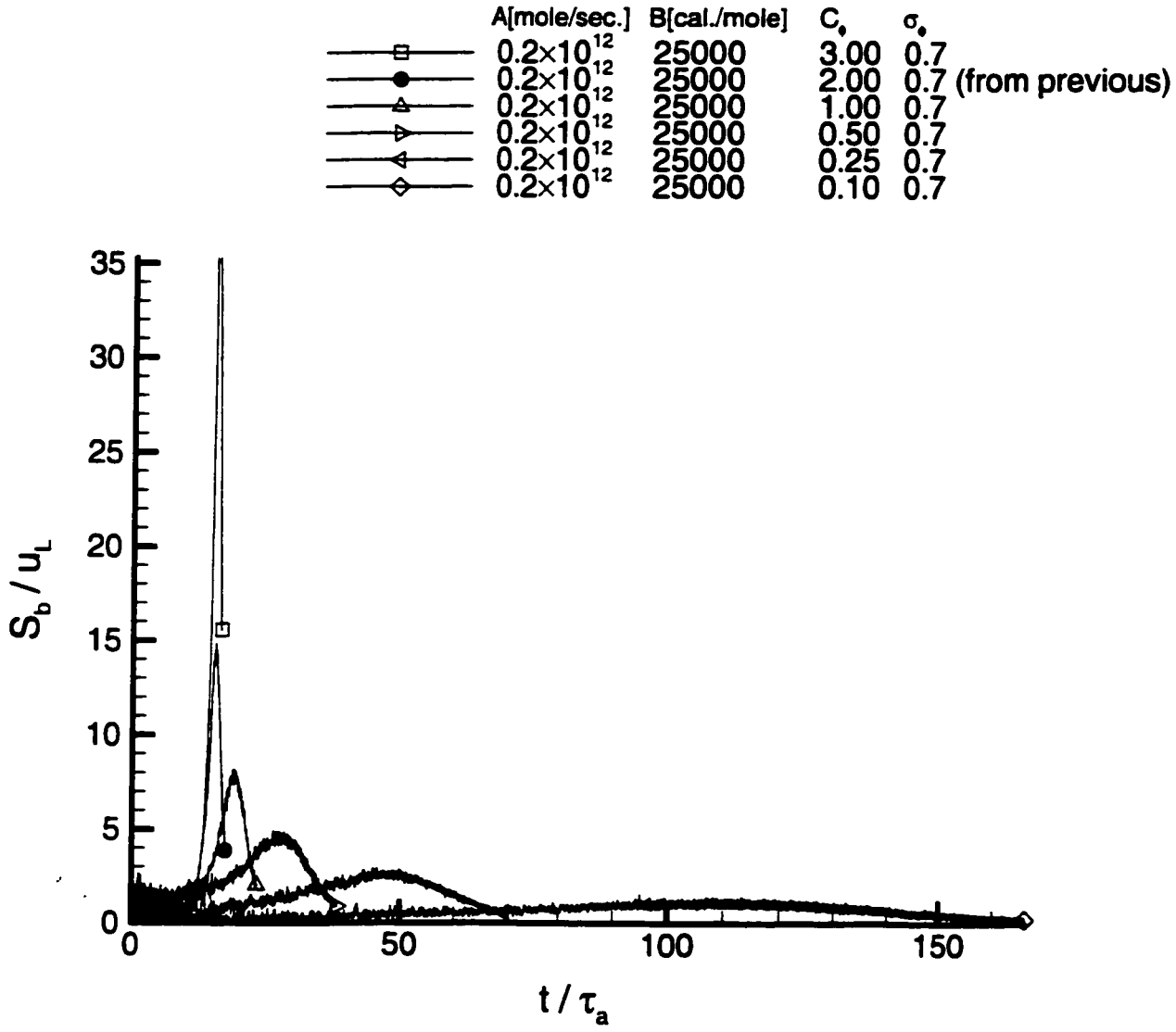

Figure A-11. Burning Speed versus Time for Different Mixing Rates

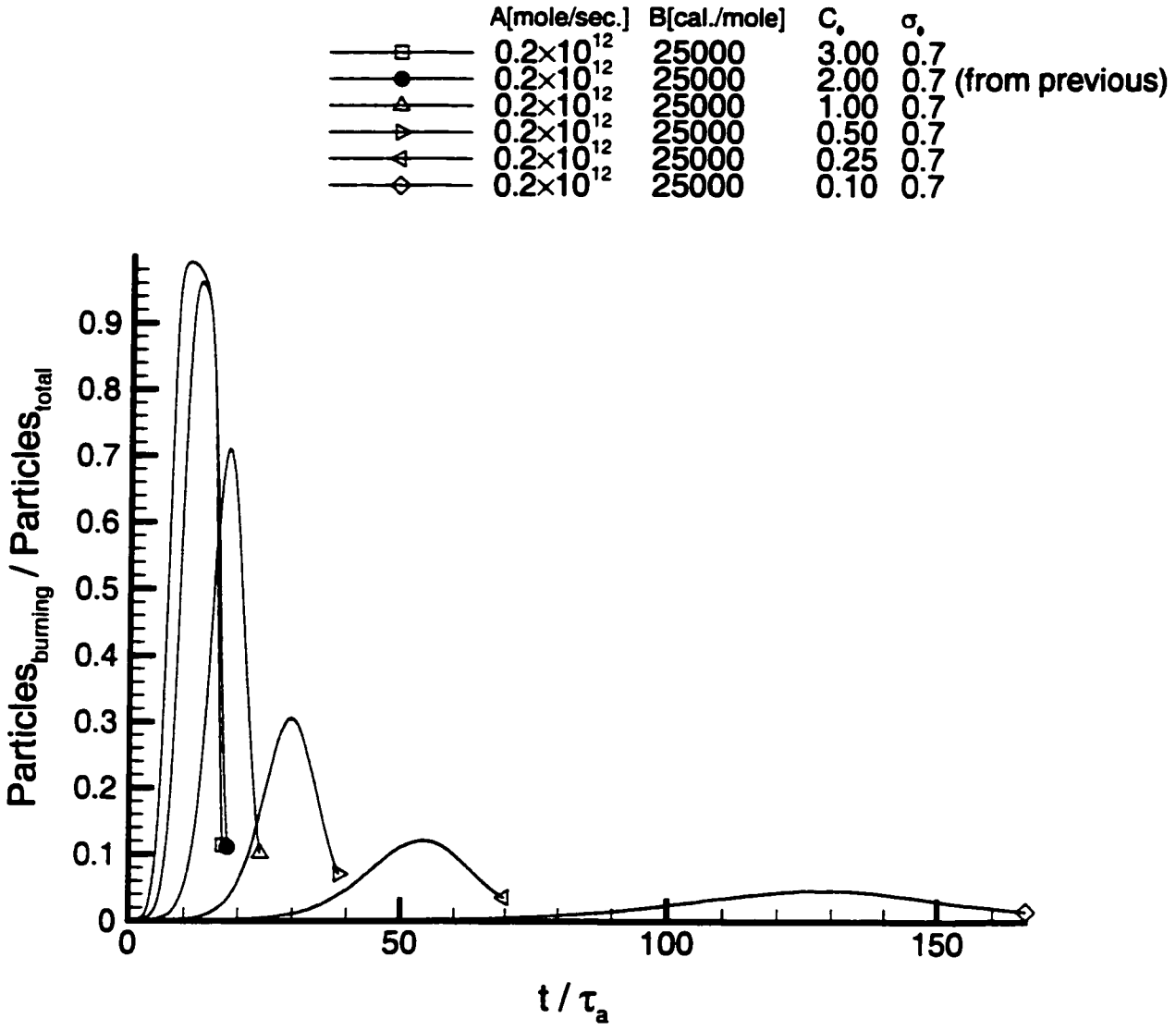

Figure A-12. Burning Particle Fraction versus Time for Different Mixing Rates

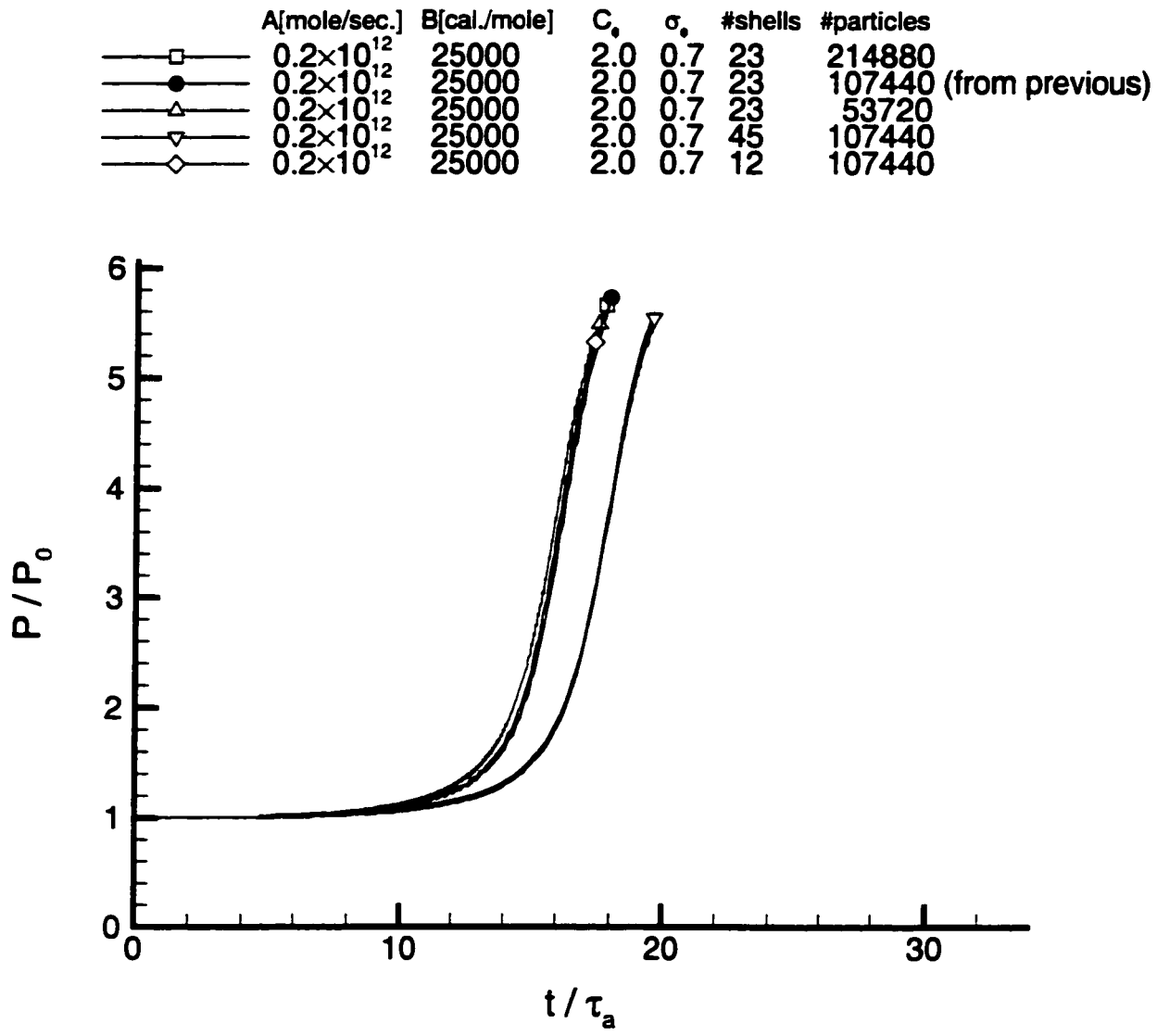

Figure A-13. Pressure versus Time for Different Shell and Particle Numeric Refinements

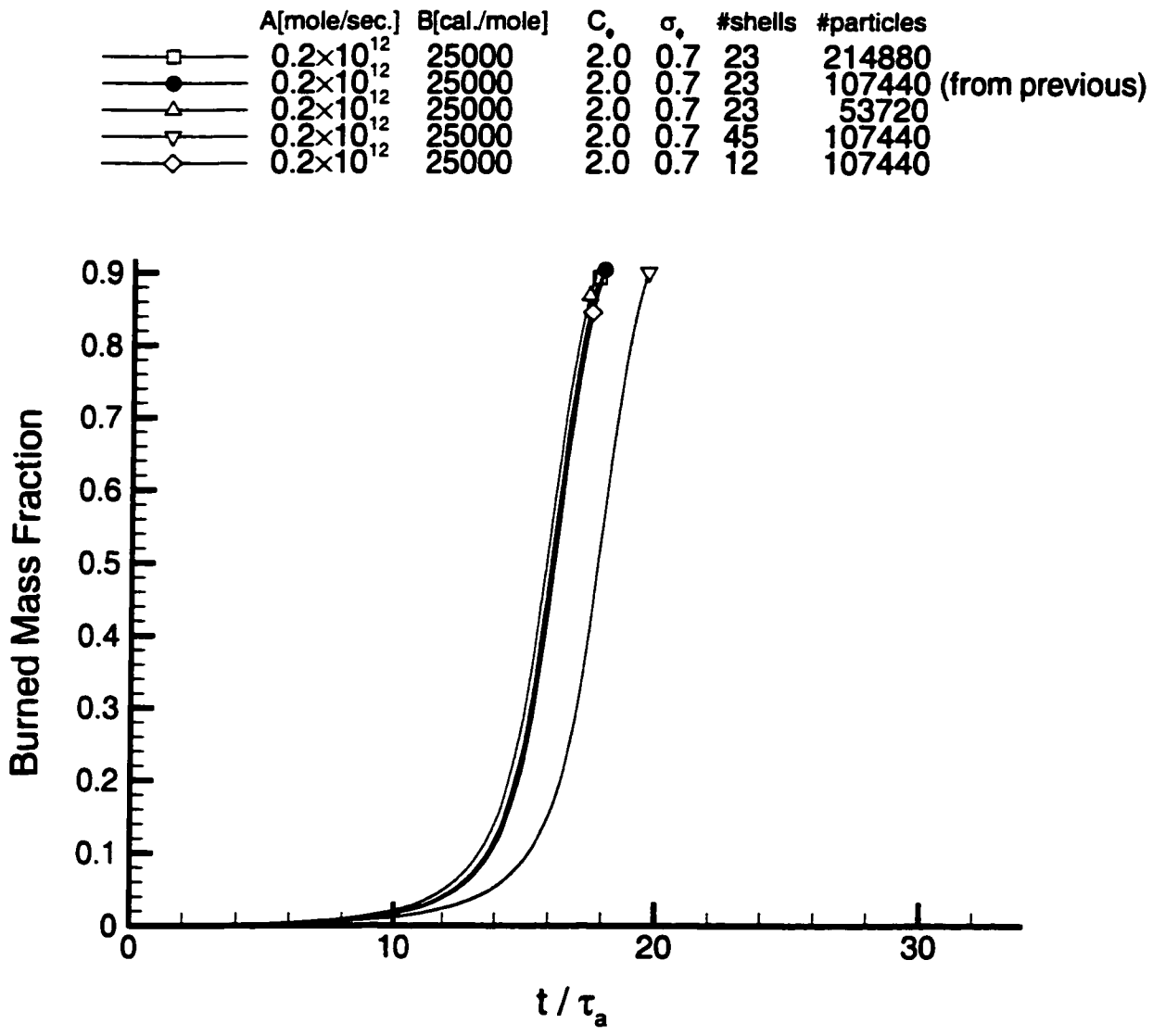

Figure A-14. Burned Mass Fraction versus Time for Different Shell and Particle Numeric Refinements

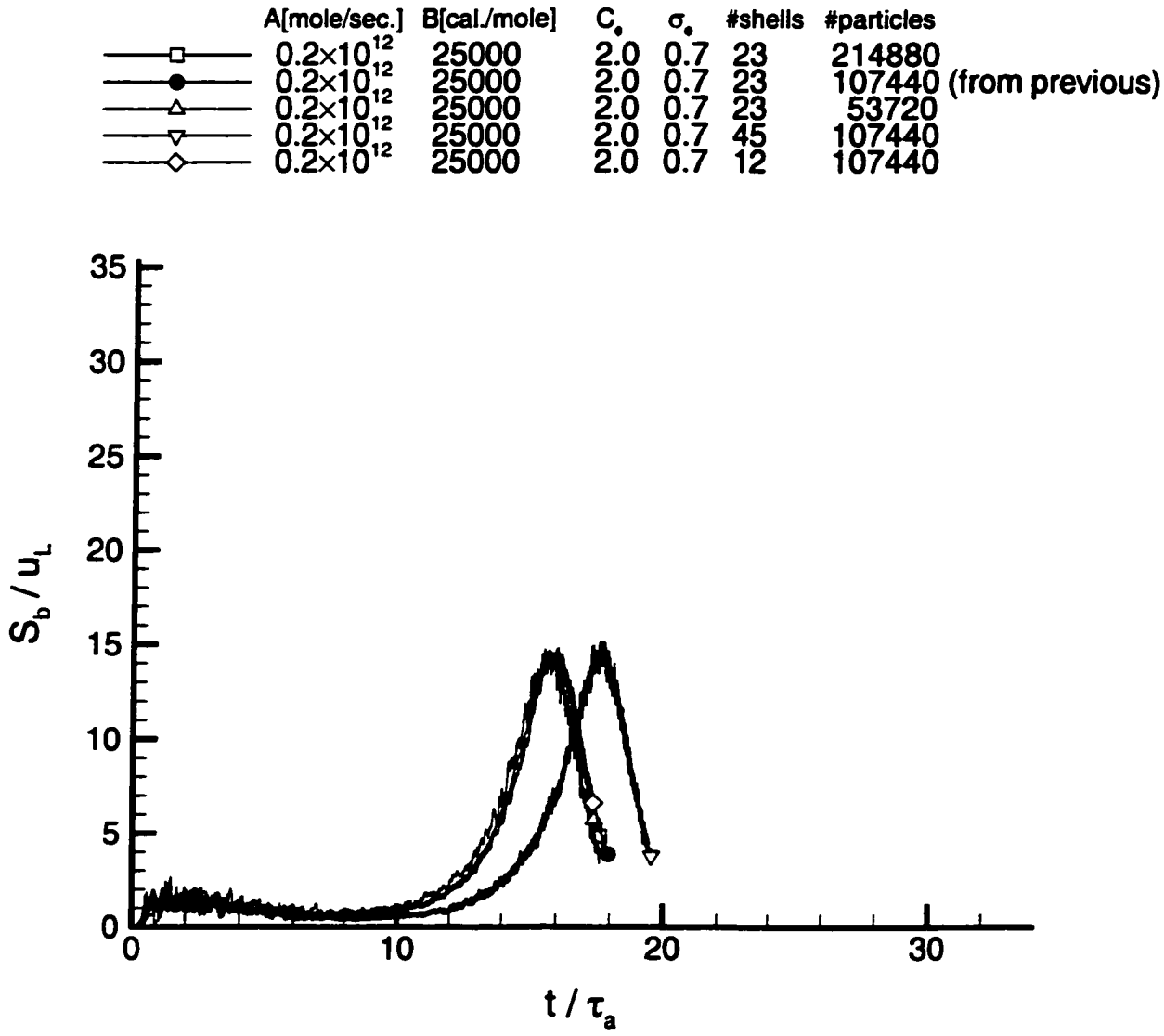

Figure A-15. Burning Speed versus Time for Different Shell and Particle Numeric Refinements

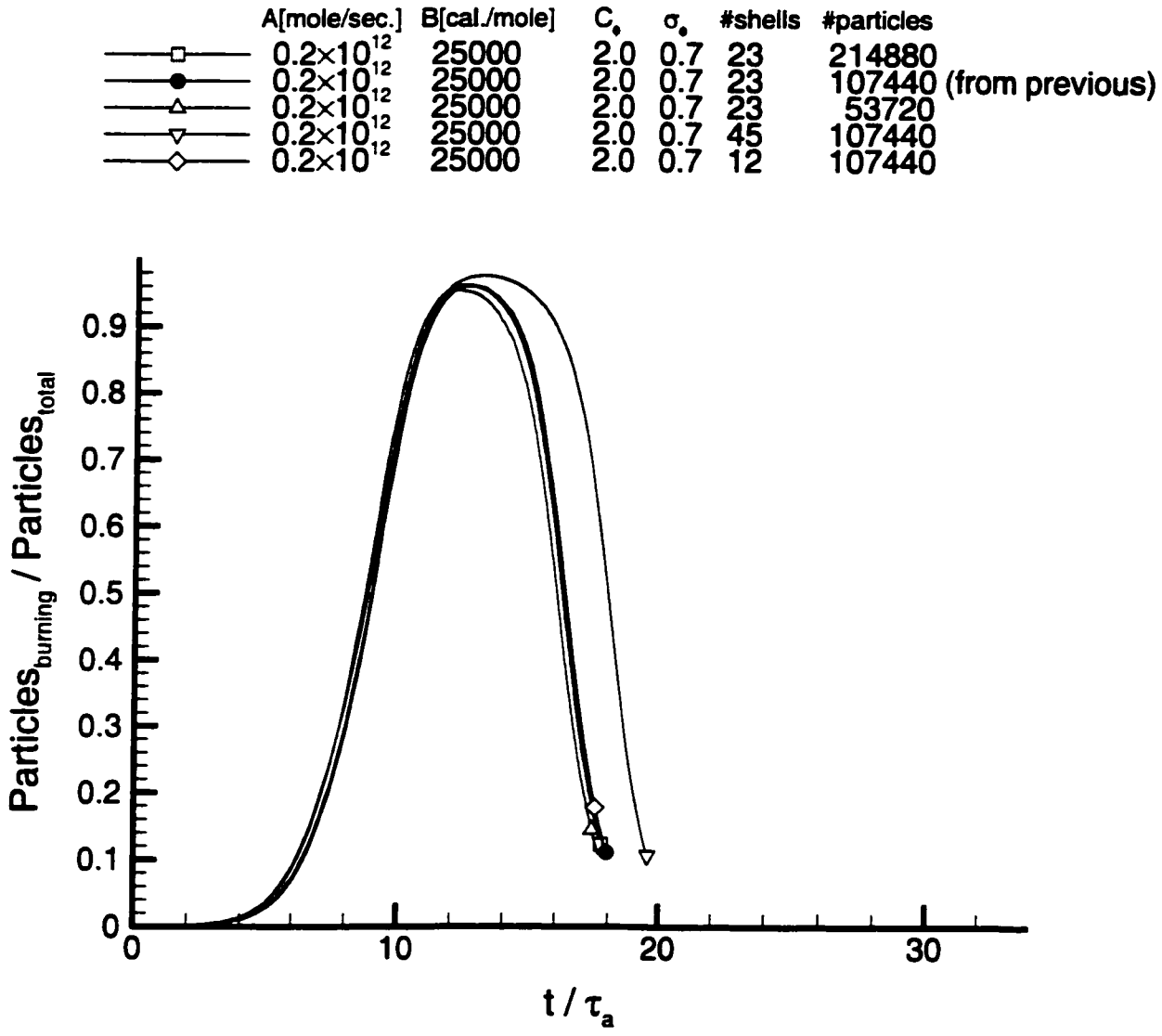

Figure A-16. Burning Particle Fraction versus Time for Different Shell and Particle Numeric Refinements

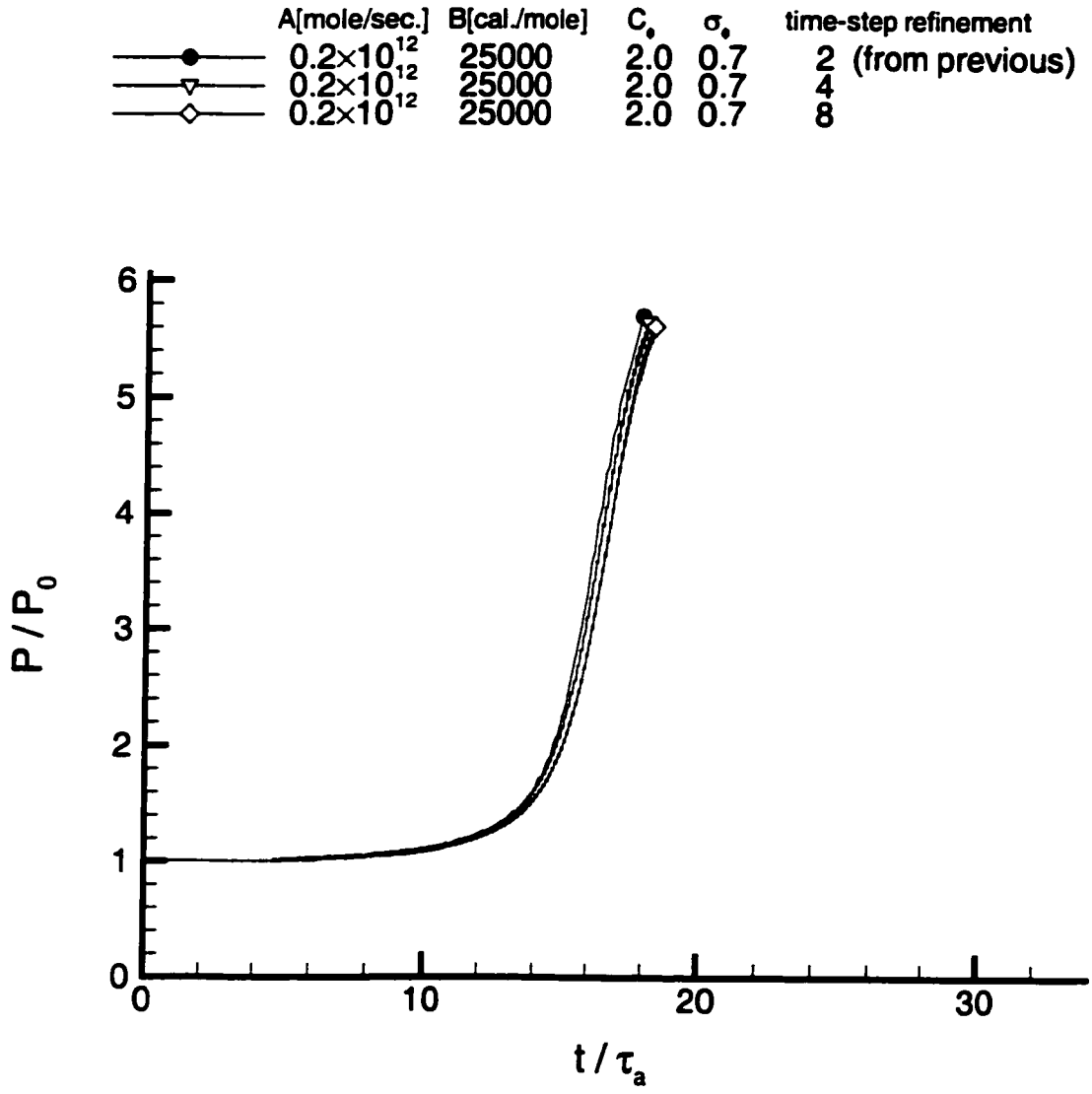

Figure A-17. Pressure versus Time for Different Time-Step Numeric Refinements

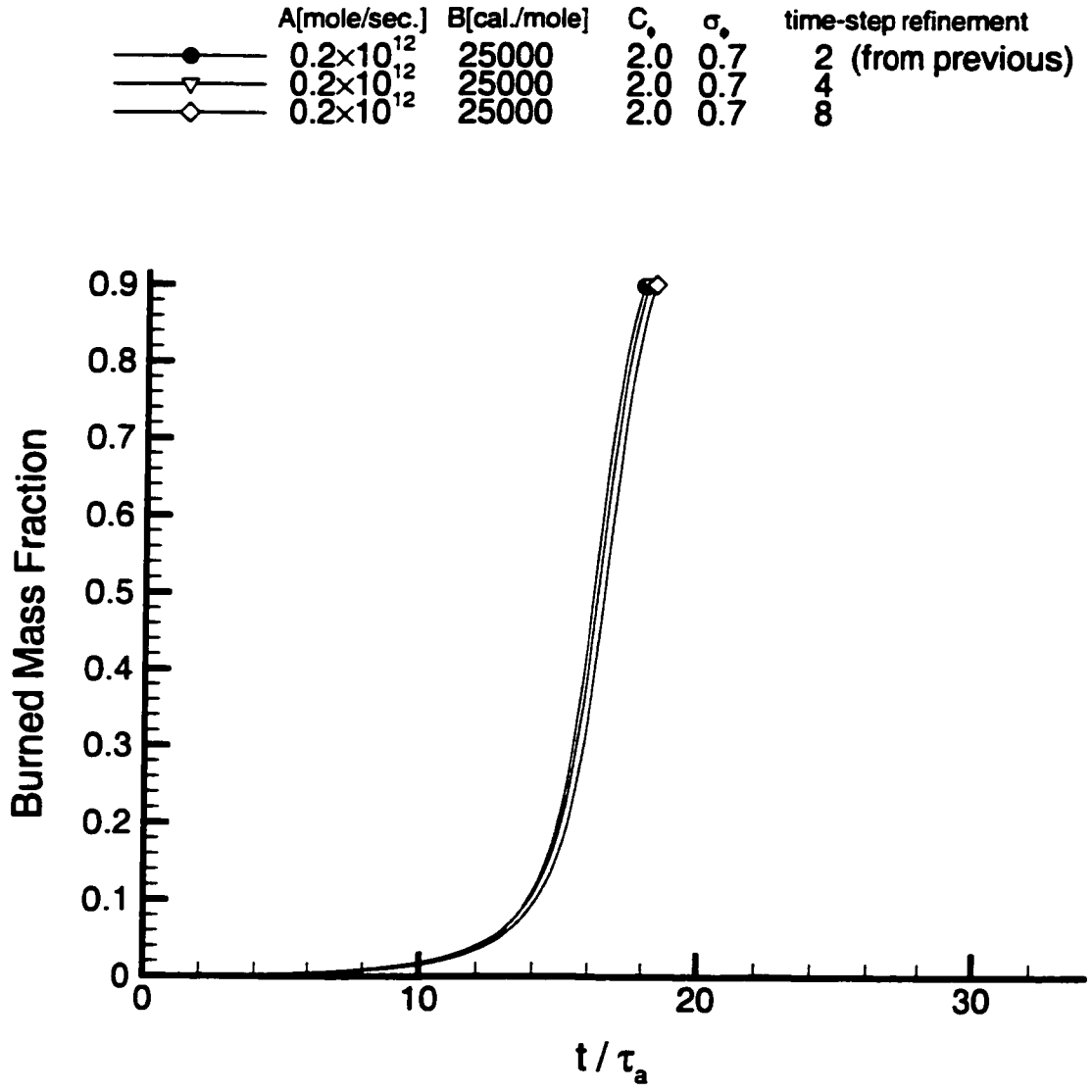

Figure A-18. Burned Mass Fraction versus Time for Different Time-Step Numeric Refinements

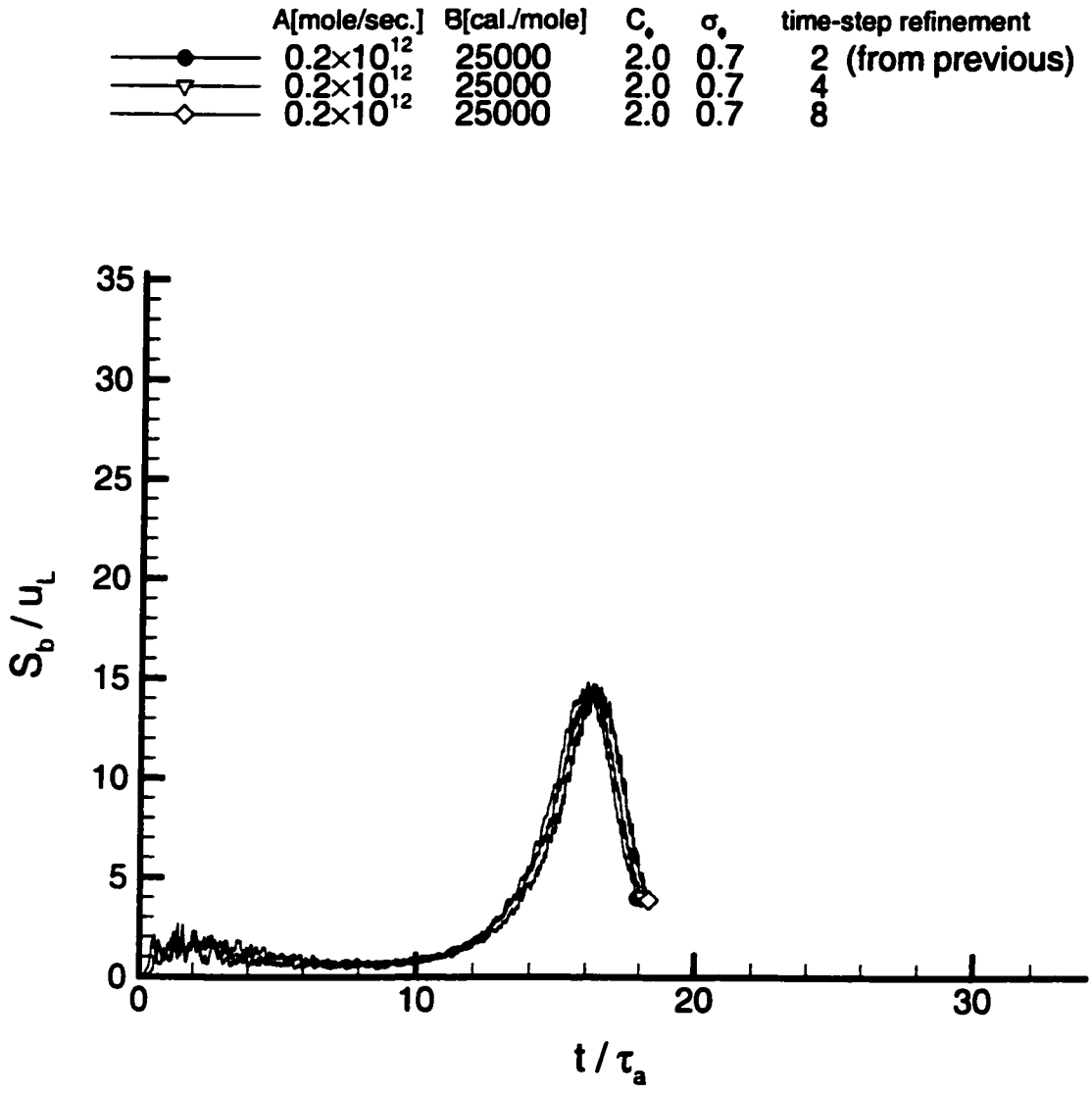

Figure A-19. Burning Speed versus Time for Different Time-Step Numeric Refinements

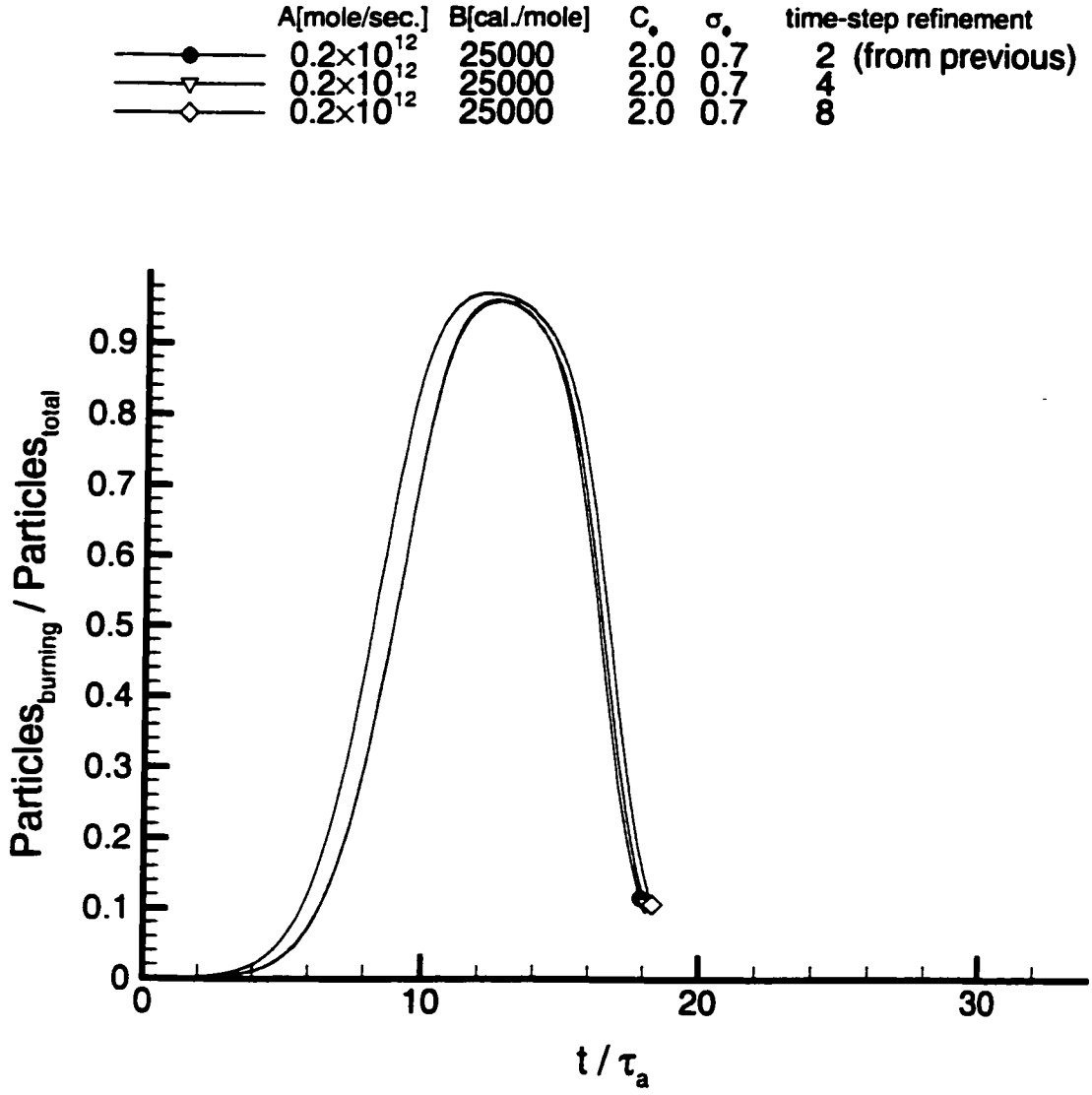

Figure A-20. Burning Particle Fraction versus Time for Different Time-Step Numeric Refinements

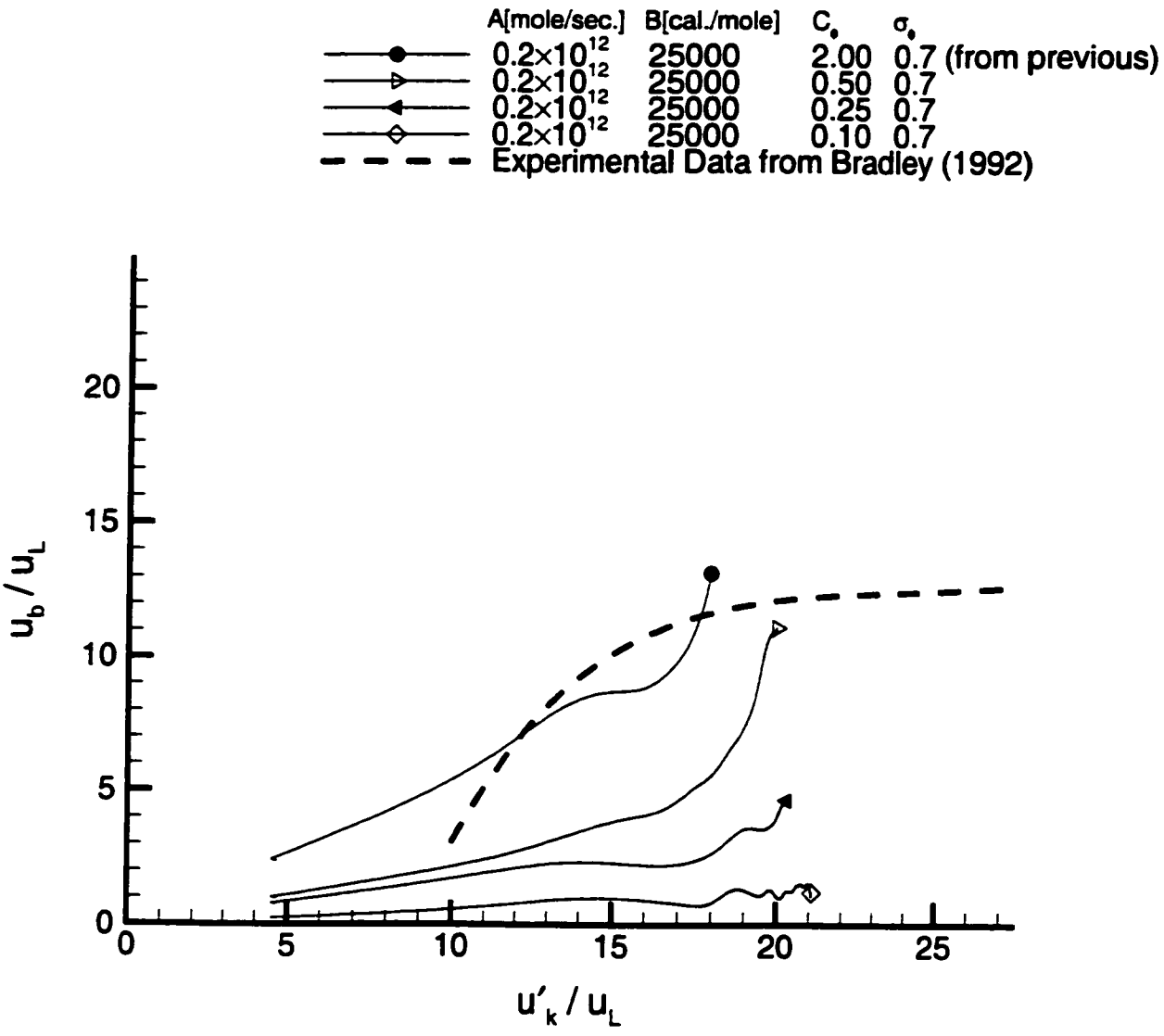

Figure A-21. Mean Expansion Speed versus R.M.S. Turbulent Velocity for Specific Model Inputs to Compare with the Experimental Data Presented by Bradley (1992)

Appendix B

Combustion Algorithm Listing

The computer program and supporting subroutines comprise the entirety of the algorithm used in the thesis. The code is written in FORTRAN and makes use of the IMSL® subroutine RNUND where randomized values are required. Copies of the complete program and subroutine listings are available through the author or Dr. R. Milane at The University of Ottawa.

The code listing is divided into the following sections:

- Main Program Listing

  This FORTRAN code has been developed by the author to manage the subroutines for diffusion, mixing, and turbulence evolution for the particles and shells as modeled in the discretized domain of the combustion chamber. The various speeds of interest for the modeled combustion are derived through calculations within this listing.

  Inputs for the computer runs are read-in from data files 'fuel.dat', 'products.dat', and 'model.dat' as described in Appendix C.

- Subroutine DIFFUSE

  The coding for this subroutine was developed by the author to provide for diffusion among shells in the discretized particle domain of the combustion chamber. This would provide for the physical movement of particles between

neighbouring shells (concentric spherical control volumes) so as to model the diffusion of energy (and other properties) in premixed combustion over the current time-step.

Particle movement mechanics are based on the use of Monte Carlo methods as applied by Dr. R. Milane in his notes of May 1996

.

- Subroutine SHELLMIX and MIXFRO

The coding for the subroutine SHELLMIX was developed by the author to provide for mixing in the discretized particle domain of the combustion chamber over the current time-step.

This would effect the binary mixing of randomly selected pairs of particles within each shell. Each shell is treated as a separate control volume, thereby allowing the mixing to involve same-shell particles only. It is assumed that the volume and pressure are not changing, and the properties and chemical composition are frozen during the mixing process.

MIXFRO calculates the new composition and thermodynamic properties of a pair of identical particles resulting from a binary mixing. It is assumed that the volume and pressure have not changed, and the properties and composition are frozen during the mixing process

- Subroutine KEPSILON

The coding for this subroutine was developed by the author to provide for the effects of the rapid distortion theory to evolve the turbulence-based variables in the discretized domain over the current time-step.

- Subroutines UPROP, CLDPRD, KINET, KINTER, and CODE

Subroutines UPROP and CLDPRD (used for the thermodynamic property calculations of the unburned and fully burned particles respectively) were modified so that their computations were analogous to the form of subroutine KINTER (used for the burning particles).

UPROP calculates the properties of a the unburned homogeneous mixture of air, residual gas, and fuel as a function of equivalence ratio, temperature, and pressure.

CLDPRD calculates the specific enthalpy of the products of complete combustion at temperatures and pressures where dissociation of the product gases may be ignored. The density of the product gas is also calculated, as are the partial derivatives of both of these quantities with respect to pressure and temperature.

KINET calculates the evolution of species concentration and temperature in the current time-step.

KINTER calculates burning particle temperature with respect to the mixture's internal energy and fuel concentration.

CODE makes use of a predictor-corrector with a variable time-step to derive the temperature and concentration of the burning particles. The single step reaction mechanism from Westbrook and Dryer (1981) calculates the fuel depletion rate and a partial differential calculates the particle temperature evolution.

In general, the coding for these five subroutines (UPROP, CLDPRD, KINET, KINTER, and CODE) was provided by In-Heng Lei (1988) and has been modified only with the inclusion of comment statements for ease of use and variable convention with the author's coding.

Appendix C

Algorithm Input Parameters

In this appendix, the referenced data used to initialize the combustion algorithm and provide for the computations are shown in Tables C-1, C-2, C-3, and C-4 below.

The empirical values relate to the combustion process approaching the misfire condition, that is, where $K \cdot Le \approx 6.0$. Corresponding data for this condition with the fuel benzene was found among the compiled data of Dr. Derek Bradley, specifically Petrov and Talantov (1959), at the University of Leeds, U.K. and are shown in Tables C-1 and C-4.

Data for the condition simulation with values for the fuel propane was taken from the research of Sheikh (1996) at the University of Ottawa and are shown in Table C-4.

Numerical files with the necessary input data used by the computer program (described in Appendix B) are presented in three data files corresponding to the components of the combustion model. These computer files are labelled "products.dat", "fuel.dat", and "model.dat."

Table C-1 : Combustion Parameters near the Misfire Condition from Petrov and Talantov (1959)

Parameter	*Value*	*Unit of Measure*
Combustion Mixture	C_6H_6-Air	
Equivalence Ratio	0.625	Dimensionless
Viscosity (Kinematic)	2.352e-1	[cm^2/sec.]
Le (Lewis Number)	2.75	Dimensionless
Temperature (Reactants)	373	[K]
Pressure (Ambient)	1.00	[atm.]
Mean Velocity, $\langle u \rangle$	0.00e+00	[cm/sec.]
R.M.S. Velocity, u'	1020	[cm/sec.]
Integral Length Scale, l_o	0.267	[cm]
R_l (Laminar Reynolds Number)	1.17e+03	Dimensionless
Laminar Flame Speed, u_l	4.70e+01	[cm/sec.]
Turbulent Flame Speed, u_t	5.40e+02	[cm/sec.]
K (Karlovitz Number)	2.160228	Dimensionless
K-Le (Karlovitz-Lewis Product)	5.940627	Dimensionless

Table C-2 : Input data in the file "products.dat" from Hires et al (1976)

Species	*Temperature Range*	Thermodynamic Coefficients					
		c_0	c_1	c_2	c_3	c_4	c_5
CO	100K ≤ T ≤ 500K	-93.7579	4.7373	16.653	-11.232	2.828	0.006767
	500K < T ≤ 6000K	-97.1418	11.94	2.0886	-0.47029	0.037363	-0.58945
H_2O	100K ≤ T ≤ 500K	-57.08	7.8097	-0.20235	3.4187	-1.179	0.001436
	500K < T ≤ 6000K	-56.6259	6.1391	4.6078	-0.9356	0.066695	0.03358
CO	100K ≤ T ≤ 500K	-27.196	6.9738	-0.82383	2.942	-1.1762	0.000413
	500K < T ≤ 6000K	-27.7346	7.0996	1.276	-0.28775	0.022356	-0.15987
H_2	100K ≤ T ≤ 500K	-0.11819	6.9919	0.1617	-0.21821	0.29682	-0.01625
	500K < T ≤ 6000K	0.76498	5.5557	1.7872	-0.28813	0.019515	0.16118
O_2	100K ≤ T ≤ 500K	0.103637	6.2957	2.3884	-0.03148	-0.32674	0.004359
	500K < T ≤ 6000K	-0.89346	7.8658	0.68837	-0.03194	-0.00269	-0.20139
N_2	100K ≤ T ≤ 500K	-0.01397	7.0922	-1.2958	3.2069	-1.2022	-0.00035
	500K < T ≤ 6000K	-0.33184	6.8078	1.4534	-0.32899	0.02561	-0.11895

* This table shows the molecular, chemical, and the coefficients for polynomial fit to the corresponding thermodynamic properties of the combustion products. The data is required for the operations of subroutines UPROP, CLDPRD, KINET, KINTER, and MIXFRO.

The specific enthalpy H and specific heat C_P are found as functions of absolute temperature where the curve fit calculation is valid over the temp. range 100[K] ≤ T ≤ 6000[K].

$$H(T) = c_0 + c_1 t + \frac{c_2}{2} t^2 + \frac{c_3}{3} t^3 + \frac{c_4}{4} t^4 - \frac{c_5}{t}$$

and

$$C_P(T) = c_1 + c_2 t + c_3 t^2 + c_4 t^3 + \frac{c_5}{t^2}$$

where

- enthalpy $H(T)$ has units [kcal/mol.]
- specific heat $C_P(T)$ has units [cal/mol./K]
- temperatures t and T have units [K/1000] and [K] respectively
- noting that the enthalpy datum state is T at 0[K] with O_2, N_2, and H_2 in gaseous state.

Table C-3 : Input data in the file "fuel.dat"*

Parameter		*Benzene*	*Propane*	*Unit of Measure*
Fuel		'Benzene'	'Propane'	
Molecular Formula		'C6H6'	'C3H8'	
Molecular Weight		78.11	44.09	[g/mol.]
Pre-exponential Factor, A		8.0e+11	8.6e+11	[mol./sec.]
Activation Energy, B		30000.	25000.	[cal./mol.]
# of N Atoms in Fuel Molecule		0	0	
# of C Atoms in Fuel Molecule		6	3	
# of H Atoms in Fuel Molecule		6	8	
# of O Atoms in Fuel Molecule		0	0	
Degree of Thermodynamic Curve		4	4	
Thermodynamic Coefficients from Reid et al (1987)	c_0	88790.2	-82489.0	[J/mol.]
	c_1	-33.920	-4.224	[J/mol./K]
	c_2	0.4739	0.3063	[J/mol./K^2]
	c_3	-0.0003017	-0.0001855	[J/mol./K^3]
	c_4	7.130e-8	4.296e-8	[J/mol./K^4]

* The fuel's specific enthalpy H and specific heat C_P are found as functions of absolute temperature where the curve fit calculation is valid over the temp. range $100[K] \le T \le 3000[K]$.

$$H(T) = c_0 + c_1 T + \frac{c_2}{2} T^2 + \frac{c_3}{3} T^3 + \frac{c_4}{4} T^4$$

and

$$C_P(T) = c_1 + c_2 T + c_3 T^2 + c_4 T^3$$

where

- enthalpy $H(T)$ has units [J/mol.]
- specific heat $C_P(T)$ has units [J/mol./K]
- temperature T has units [K]

Table C-4 : Input data from the file "model.dat"

Parameter	*Benzene*	*Propane*	*Detail*
Temperature Before Ignition, TIN	373.0	373.0	[K]
Pressure Before Ignition, PIN	1.0	1.0	[atm.]
Initial Turbulent Velocity, UPRIM	1020.	549.08	[cm/sec.]
Laminar Flame Speed, UL	47.0	17	[cm/sec.]
Integral Length Scale, L0	0.267	0.496	[cm]
Kinematic Viscosity, VISKIN	0.2352	0.6	[cm^2/sec.]
Spark Gap for Ignition, GAP	0.4	0.4	[cm]
Advance Angle of Spark, SA (TDC = 0^0 crank angle)	0.	0.	[deg.]
Spark Duration, SPDR	2.	2.	[msec.]
Ignition Energy, EIGN	0.	0.	[cal.]
Residual Fraction, RESFRK	0.	0.	
Ambient Atmosphere's N2 to O2 Molar Ratio, XI	3.76	3.76	
Equivalence Ratio, PHI	0.625	0.625	
Equivalence Ratio for FR, PHIFR	0.625	0.625	
Equivalence Ratio for Exhaust Gas Recirculation., PHIEGR	0.625	0.625	
Volume of the Chamber, VTO	90.0	90.0	[cm^3]
Refinement of the Time-step, DMAIN	2	2	
Number of the Burning Particles in Core, NB	40	40	
Number of Shells to be Created in Chamber, ISHELL	23	23	
Number of Central Shells to be Initially Ignited, ICSHELL	1	1	
Empirical Constant for Mixing Rate (value 0.6 to 3.1) , CPHI	2.0	2.0	C_ϕ
Empirical Constant for Diffusion Rate, CMU	0.09	0.09	C_μ
Turbulent Schmidt Number for Diffusion Rate, SIGPHI	0.7	0.7	σ_ϕ
Empirical Constant for Dissipation, CD	0.202	0.202	C_D
Empirical Constant for Kinetic Energy, SIGK	1.0	1.0	σ_k
Empirical Constant for Dissipation, CEPS2	1.92	1.92	$C_{\varepsilon 2}$
Empirical Constant for Dissipation, SIGEPS	1.3	1.3	σ_ε
Constant Based on Adopted Mixing Model, BETA *nb β=2.0 for complete mixing , β=3.0 for a partial mixing*	2.0	2.0	β

Appendix D

The k-ε Model for Turbulence

A possible objective with future progress in this study is to incorporate the k-ε model (Spalding and Launder, 1972). Such a scheme would improve the modeling of all turbulence-influenced variables, such as, the mixing frequency ω and the diffusion coefficient Γ_T.

Included in this Appendix is a description of the k-ε model, its numerical application to the study's combustion model, and the corresponding FORTRAN computer code listing

D.1 k-ε Model Introduction

To provide a realistic model to the turbulent development process in a stirred flow, the use of the k-ε model (Spalding and Launder, 1972) can be adopted. The k-equation is

[D.1]

$$\frac{dk}{dt} = \frac{1}{r^2 \rho} \frac{\partial}{\partial r}\left[r^2 \rho \frac{\nu_T}{\sigma_k} \frac{\partial k}{\partial r} \right] + \frac{2}{3} \frac{k}{\rho} \frac{d\rho}{dt} + \Im_P - \varepsilon,$$

where the first term on right hand side is the diffusion term, the second is the production term, $\Im_P$ is the energy supplied by the impeller in the vessel (a constant), and ε is the energy dissipation term. In this study, $\sigma_k = 1$ and the energy supply (the third term) is based on initial values as,

[D.2]

$$\Im_P = C_D \frac{k_0^{3/2}}{\ell_0} .$$

The rate of dissipation, known at the ε-equation is

[D.3]

$$\frac{d\varepsilon}{dt} = \frac{1}{\rho}\frac{1}{r^2}\frac{\partial}{\partial r}\left[r^2 \rho \frac{\nu_T}{\sigma_\varepsilon}\frac{\partial \varepsilon}{\partial r}\right] + \frac{4}{3}\frac{\varepsilon}{\rho}\frac{d\rho}{dt} - C_{\varepsilon_2}\frac{\varepsilon^2}{k}$$

where $\sigma_\varepsilon = 1.3$ and $C_{\varepsilon_2} = 1.92$.

In both equations, the turbulent viscosity is calculated as,

[D.4]

$$\nu_T = C_D \frac{k^2}{\varepsilon}$$

where $C_D = 0.09$.

D.2 Numerical Methodology

The k equation is rewritten using the concepts of a control volume formulation as,

$$\frac{dk}{dt} = \frac{1}{r^2\rho}\frac{\partial}{\partial r}\left[r^2\rho\frac{\nu_T}{\sigma_k}\frac{\partial k}{\partial r}\right] + S \qquad [D.5]$$

where the source term S is defined as,

$$S = \frac{2}{3}\frac{k}{\rho}\frac{d\rho}{dt} + \Im_P - \varepsilon. \qquad [D.6]$$

This source term can be linearized according to the numerical methods of Patankar (1980) as,

$$S = S_C + S_P k^* \qquad [D.7]$$

where the superscript * indicates an approximate, known quantity such as a previous time-step's value.

Using the control-volume technique described in Section 2.1 and referring to Figure 2-2, the Eq. [D.5] can be written as,

[D.8]

$$\int_w^e\int_t^{t+\Delta t} 4\pi r^2 \frac{dk}{dt}\,dt\,dr = \int_w^e\int_t^{t+\Delta t} \frac{1}{\rho} 4\pi \frac{r^2}{r^2}\frac{\partial}{\partial r}\left[r^2\rho\frac{\nu_T}{\sigma_k}\right]dt\,dr + \int_w^e\int_t^{t+\Delta t} 4\pi r^2 S\,dt\,dr$$

Following Patankar (1980), the first term of Eq. [D.8] is expressed using an explicit formulation as,

[D.9]

$$\int_w^e\int_t^{t+\Delta t} 4\pi r^2 \frac{dk}{dt}\,dt\,dr = \Delta V_P^0\left[k_P^1 - k_P^0\right]$$

The first term of the right hand side of Eq. [D.8] is expanded as,

[D.10]

$$\int_w^e\int_t^{t+\Delta t} \frac{1}{\rho} 4\pi \frac{r^2}{r^2}\frac{\partial}{\partial r}\left[r^2\rho\frac{\nu_T}{\sigma_k}\frac{\partial k}{\partial r}\right]dt\,dr = \int_t^{t+\Delta t}\frac{4\pi}{\rho_P}\left[r_e^2\rho_e\frac{\nu_{Te}}{\sigma_k}\frac{(k_E-k_P)}{(\delta r)_e} - r_w^2\rho_w\frac{\nu_{Tw}}{\sigma_k}\frac{(k_P-k_W)}{(\delta r)_w}\right]dt$$
$$= \int_t^{t+\Delta t}\frac{1}{\rho_P}\left[S_e\rho_e\frac{\nu_{Te}}{\sigma_k}\frac{(k_E-k_P)}{(\delta r)_e} - S_w\rho_w\frac{\nu_{Tw}}{\sigma_k}\frac{(k_P-k_W)}{(\delta r)_w}\right]dt$$

and is further developed , assuming an explicit integration, as,

[D.11]

$$\int_w^e\int_t^{t+\Delta t} \frac{1}{\rho} 4\pi \frac{r^2}{r^2}\frac{\partial}{\partial r_E}\left[r^2\rho\frac{\nu_T}{\sigma_k}\right]dt\,dr = \frac{1}{\langle\rho\rangle_P^0}\left[S_e^0\langle\rho\rangle_e^0\frac{\nu_{Te}^0}{\sigma_k}\frac{\left(k_E^0-k_P^0\right)}{(\delta r)_e^0} - S_w^0\langle\rho\rangle_w^0\frac{\nu_{Tw}^0}{\sigma_k}\frac{\left(k_P^0-k_W^0\right)}{(\delta r)_e^0}\right]\Delta t$$

The second term on the right hand side of Eq. [D.8] is now expanded as,

$$\int_w^e \int_t^{t+\Delta t} 4\pi r^2 S \, dt \, dr = S_P^0 \Delta t \Delta V_P^0 \qquad [D.12]$$

where Eq. [D.7], the linearization of the source term S_P^0 is presented as,

$$S_P^0 = S_{C_r}^0 + S_{P_r}^0 k_P^0. \qquad [D.13]$$

According to the Patankar (1980) formulation, a basic rule to assure numerical convergence is that the quantity S_p must not be positive. To this end, a conditional assignment of value to the linearization coefficients is based on the rate of change of density. That is if $\left.\frac{d\rho}{dt}\right|^0 > 0$ then,

$$S_{C_r}^0 = \frac{2}{3}\frac{k_P^0}{\rho_P^0}\left.\frac{d\rho_P}{dt}\right|^0 + \Im_P - \varepsilon_P^0 \qquad [D.14]$$

$$S_{P_r}^0 = 0 \qquad [D.15]$$

otherwise,

$$S_{C_r}^0 = \Im_P - \varepsilon_P^0 \qquad [D.16]$$

[D.17]

$$S_{P_P}{}^0 = \frac{2}{3\rho_P^0}\left.\frac{d\rho_P}{dt}\right|^0$$

where the density derivative is calculated as,

[D.18]

$$\left.\frac{d\langle\rho\rangle_P}{dt}\right|^0 = \frac{\langle\rho\rangle_P^1 - \langle\rho\rangle_P^0}{\Delta t}$$

The discretized equation corresponding to the governing equation for k, Eq. [D.8], by the control volume technique is then written as,

[D.19]

$$\left(k_P^1 - k_P^0\right)\frac{\Delta V_P}{\Delta t} = \frac{1}{\langle\rho\rangle_P^0}\left[S_e^0\frac{\langle\rho\rangle_e^0 \nu_{T_e}^0}{\sigma_k}\frac{\left(k_E^0 - k_P^0\right)}{(\delta r)_e^0} - S_w^0\frac{\langle\rho\rangle_w^0 \nu_{T_w}^0}{\sigma_k}\frac{\left(k_P^0 - k_W^0\right)}{(\delta r)_w^0}\right] + S_{P_P}^0\Delta V_P^0 k_P^0 + S_{C_P}^0\Delta V_P^0$$

where all superscripts 0 in above equations are known quantities. Therefore, k_P^1 may be determined by letting,

[D.20]

$$a_E^0 = \frac{S_e^0\langle\rho\rangle_e^0 \nu_{T_e}^0}{\sigma_k\langle\rho\rangle_P^0(\delta r)_e^0}$$

[D.21]

$$a_W^0 = \frac{S_w^0\langle\rho\rangle_w^0 \nu_{T_w}^0}{\sigma_k\langle\rho\rangle_P^0(\delta r)_w^0}$$

and

$$b = S_P^0 \Delta V_P^0 . \qquad [D.22]$$

That when substituted into Eq. [D.19] gives,

$$\left(k_P^1 - k_P^0\right)\frac{\Delta V_P^0}{\Delta t} = a_E^0\left(k_E^0 - k_P^0\right) - a_W^0\left(k_P^0 - k_W^0\right) + bk_P^0 + S_{C_r}^0 \Delta V_P^0 . \qquad [D.23]$$

A further substitution is possible by setting,

$$a_P^0 = \frac{\Delta V_P^0}{\Delta t} \qquad [D.24]$$

so by rearranging Eq. [D.23], the discretized equation becomes,

$$a_P^0 k_P^1 = a_P^0 k_P^0 + a_E^0 k_E^0 - a_E^0 k_P^0 - a_W^0 k_P^0 + a_W^0 k_W^0 + bk_P^0 + S_{C_r}^0 \Delta V_P^0 \qquad [D.25]$$

and collecting like terms,

$$a_P^0 k_P^1 = a_E^0 k_E^0 + a_W^0 k_W^0 + \left(a_P^0 - a_E^0 - a_W^0 + b\right)k_P^0 + S_{C_r}^0 \Delta V_P^0 \qquad [D.26]$$

where a_P^0, a_E^0, a_W^0, b, and $S_{C_r}^0$ are defined above.

For a physically realistic solution (Patankar, 1980),

$$a_P^0 - a_E^0 - a_W^0 + b \geq 0 \qquad [D.27]$$

and by substitution the inequality becomes,

$$\frac{\Delta V_P^0}{\Delta t} \geq \frac{S_e^0 \langle \rho \rangle_e^0 v_{T_e}^0}{\sigma_k \langle \rho \rangle_P^0 (\delta r)_e^0} + \frac{S_w^0 \langle \rho \rangle_w^0 v_{T_w}^0}{\sigma_k \langle \rho \rangle_P^0 (\delta r)_w^0} - S_{P_P}^0 \Delta V_P^0 \qquad [D.28]$$

A further rearranging gives,

$$\Delta t \leq \frac{\Delta V_P^0}{\frac{S_e^0 \langle \rho \rangle_e^0 v_{T_e}^0}{\sigma_k \langle \rho \rangle_P^0 (\delta r)_e^0} + \frac{S_w^0 \langle \rho \rangle_w^0 v_{T_w}^0}{\sigma_k \langle \rho \rangle_P^0 (\delta r)_w^0} - S_{P_P}^0 \Delta V_P^0} \qquad [D.29]$$

The cited densities of Eqs. [D.20], [D.21], and [D.29] are defined as follows,

$$\langle \rho \rangle_e^0 = \left[\frac{1 - f_e}{\langle \rho \rangle_P^0} + \frac{f_e}{\langle \rho \rangle_E^0} \right]^{-1} \qquad [D.30]$$

and

$$\langle \rho \rangle_w^0 = \left[\frac{1 - f_w}{\langle \rho \rangle_P^0} + \frac{f_w}{\langle \rho \rangle_W^0} \right]^{-1} \qquad [D.31]$$

where $\langle\rho\rangle_E^0$ and $\langle\rho\rangle_W^0$ are the average densities at time t in shells E and W respectively.

The cited viscosities of Eq. [D.29] are defined as follows,

$$\nu_{T_e}^0 = \left[\frac{1-f_e}{\nu_{T_P}^0} + \frac{f_e}{\nu_{T_E}^0}\right]^{-1} \qquad [D.32]$$

and

$$\nu_{T_w}^0 = \left[\frac{1-f_w}{\nu_{T_P}^0} + \frac{f_w}{\nu_{T_W}^0}\right]^{-1} \qquad [D.33]$$

where $\nu_{T_E}^0$ and $\nu_{T_W}^0$ are the turbulent viscosities at time t in shells E and W respectively and are calculated using Eq. [D.4] as,

$$\nu_{T_P}^0 = C_\mu \frac{\left(k_P^0\right)^2}{\varepsilon_P^0} \qquad [D.34]$$

It is necessary that $\frac{\left(k^0\right)^2}{\varepsilon^0}$ is an average as calculated using the value of each particle in the given shell. The average value is obtained as the arithmetic summation over the number of individual particles.

The ε-equation is also rewritten using the concepts of the control volume formulation as,

[D.35]

$$\frac{d\varepsilon}{dt} = \frac{1}{r^2\rho}\frac{\partial}{\partial r}\left[r^2\rho\frac{\nu_T}{\sigma_\varepsilon}\frac{\partial\varepsilon}{\partial r}\right] + S$$

where the source term S is defined as,

[D.36]

$$S = \frac{4}{3}\frac{\varepsilon}{\rho}\frac{d\rho}{dt} - C_{\varepsilon_2}\frac{(\varepsilon^*)^2}{k^*}.$$

This source term S is again linearized in the same way as for the k-equation per Eq. [D.7] following the method of Patankar (1980),

[D.37]

$$S = S_C + S_P\varepsilon^*.$$

There is a similarity between the ε-equation of Eq. [D.35] and the k-equation of Eq. [D.8]. In what follows, the integration of S is shown for the explicit case,

[D.38]

$$\int_w^e\int_t^{t+\Delta t} 4\pi r^2 S\,dt\,dr = S_P{}^0\Delta t\,\Delta V_P^0$$

where, the linearization of the source term S_P^0 is presented as,

$$S_P^0 = S_{C_P}^0 + S_{P_P}^0 \varepsilon_P^0 . \qquad [D.39]$$

As with the k-equation's source term linearization, Patankar (1980) recommends that $S_{P_P}^0 < 0$ for numerical convergence. This, again, requires the conditional assignment of values to the linerarization coefficients being based upon the rate of change of density. So that if $\left|\frac{d\rho}{dt}\right| > 0$ then,

$$S_{C_P}^0 = \frac{4}{3}\frac{\varepsilon_P^0}{\rho_P^0}\left|\frac{d\rho_P}{dt}\right|^0 + C_{\varepsilon_2}\frac{\left(\varepsilon_P^0\right)^2}{k_P^0} \qquad [D.40]$$

$$S_{P_P}^0 = -2C_{\varepsilon_2}\frac{\varepsilon_P^0}{k_P^0} \qquad [D.41]$$

otherwise,

$$S_{C_P}^0 = \frac{4\varepsilon_P^0}{3\rho_P^0}\left|\frac{d\rho_P}{dt}\right|^0 \qquad [D.42]$$

$$S_{P_P}^0 = -C_{\varepsilon_2}\frac{\left(\varepsilon_P^0\right)^2}{k_P^0} \qquad [D.43]$$

As with the development of Eq. [D.26], the term $S_P{}^0\varepsilon_P^0\Delta V_P^0$ should be added as $b\varepsilon_P^0$ where,

$$b = S_{P_r}^0 \Delta V_P^0 \qquad [D.44]$$

Now by arranging Eq. [D.39] in the same way as Eq. [D.23] of the k-equation's development, the discretized ε-equation becomes,

$$a_P^0 \varepsilon_P^1 = a_E^0 \varepsilon_E^0 + a_W^0 \varepsilon_W^0 + \left(a_P^0 - a_E^0 - a_W^0 + b\right)\varepsilon_P^0 + S_{C_r}^0 \Delta V_P^0 \qquad [D.45]$$

where the above coefficients are defined in the same way as in the k-equation as,

$$a_P^0 = \frac{\Delta V_P^0}{\Delta t}\ , \qquad [D.46]$$

$$a_E^0 = \frac{S_\varepsilon^0 \langle\rho\rangle_e^0 \nu_{T_e}^0}{\sigma_\varepsilon \langle\rho\rangle_P^0 (\delta r)_e^0}\ , \qquad [D.47]$$

$$a_W^0 = \frac{S_w^0 \langle\rho\rangle_w^0 \nu_{T_w}^0}{\sigma_\varepsilon \langle\rho\rangle_P^0 (\delta r)_w^0}\ , \qquad [D.48]$$

and

$$b = S_{P_r}^0 \Delta V_P^0. \qquad [D.49]$$

For the physically realistic solution within the ε-equation it is required that,

$$a_P^0 - a_E^0 - a_W^0 + b \geq 0 \qquad [D.50]$$

where by substitution, as in the k-equation, the inequality becomes the same restriction to the global time-step,

$$\Delta t \leq \frac{\Delta V_p^0}{\dfrac{S_e^0 \langle \rho \rangle_e^0 \nu_{T_e}^0}{\sigma_\varepsilon \langle \rho \rangle_P^0 (\delta r)_e^0} + \dfrac{S_w^0 \langle \rho \rangle_w^0 \nu_{T_w}^0}{\sigma_\varepsilon \langle \rho \rangle_P^0 (\delta r)_w^0} - S_{P_r}^0 \Delta V_p^0} \qquad [D.51]$$

D.3 Computer Code Listing of the k-ε Model

```
C ***************************** 01/06/97 ******************************
C
C     subroutine KEPSILON
C
C     PURPOSE
C      to allow the assignment of turbulence properties the shells
C      (concentric spherical control volumes) by using the k-epsilon
C      model so as to model the dissipation in the energy/properties
C      in premixed combustion over a time-step DT.
C
C      The movement mechanics are based on the use of Monte Carlo
C      methods as applied by Dr. R. Milane in his notes of June 1997.
C
C     USAGE
C        CALL KEPSILON(M,ISHELL,OMEGA,GAMRHO,KIMP,DT)
```

```
C
C     PARAMETERS
C      given
C           M = mass of each particle [g]
C           ISHELL = total number of concentric shells
C           OMEGA(I1)  = mixing frequency for the shell [1/sec]
C           GAMRHO(I1) = diffusion coefficient for the shell
C           KIMP = the energy supplied by the impeller in the vessel
C           DT = the time-step of consideration [sec.]
C      where
C           I1 = shell index
C           I2 = particle index within shell I1
C
C      returns after DT
C
C           the OMEGA AND GAMRHO vectors are updated to account for
C           the dissipation of turbulence per k-epsilon
C
C     remarks
C        1)  must be mindful of the PARTICLE array's dimensioning
C            as an INTEGER array... ensure that it accommodates all
C            the shells!
C-----------------------------------------------------------------------
C
      SUBROUTINE KEPSILON(M,ISHELL,OMEGA,GAMRHO,KIMP,DT)
C
       REAL VSHELL(100,3),SW,SE,DRW,DRE,DT,DVOL,KIMP
       REAL M,OMEGA(100),GAMRHO(100)
       INTEGER INSHELL(100),ISHELL
       INTEGER I,I1,I2,I1F,NP,NR,K
C
       COMMON/CONSTNTS/R,PSCALE,PI
       COMMON/PARNUM/N,N1,N2,N3
       COMMON/GLOBAL/TEMP(150000),VOL(150000),SHELL(150000)
       COMMON/TURB/EKSHELL(100,11),CPHI,CMU,SIGPHI,CD,SIGK,CEPS2
     +   ,SIGEPS
C-----------------------------------------------------------------------
C
C  sort the particles into the arrays for subroutine
C
C   where :  I1 = shell index
C            I2 = particle index within shell I1
C            INSHELL(I1) = number of particles in shell I1
C            VSHELL(I1,1) = volume of shell I1 [cc]
C            VSHELL(I1,2) = outer radius of shell I1 [cm]
C            ISHELL = total number of concentric shells
C-----------------------------------------------------------------------
C
C   clearing the INSHELL, VSHELL arrays
C
      DO 800 I = 1,ISHELL
         INSHELL(I) = 0
         VSHELL(I,1) = 0.
         VSHELL(I,2) = 0.
```

```
 800    CONTINUE
C
      DO 805 I = 1,N
C
         I1 = SHELL(I)
         INSHELL(I1) = INSHELL(I1) + 1
C
C   collecting the volume into the VSHELL(I1,1) array
C
         VSHELL(I1,1) = VSHELL(I1,1) + VOL(I)

C
 805    CONTINUE
C
      CRAD = 0.
      CVOL = 0.
C
      DO 810 I = 1,ISHELL
C
         CVOL = CVOL + VSHELL(I,1)
         CRAD = ( CVOL * 0.75 / PI )**(1./3.)
C
C   collecting the shells' (outer) radii into the array
C
         VSHELL(I,2) = CRAD
C
 810  CONTINUE
C
      FE = 0.5
      FW = 0.5
C---------------------------------------------------------------------
C
C    first consider the centre shell
C
      SW = 0.
      SE = 4. * PI * VSHELL(1,2)**(2.)
      DVOL = VSHELL(1,1)
      DRW = 0.
      DRE = 0.5 * VSHELL(2,2)
      NW = 0.
      NP = INSHELL(1)
      NE = INSHELL(2)
C
      KW0 = 0.
      KP0 = EKSHELL(1,1)
      KE0 = EKSHELL(2,1)
C
      EPSW0 = 0.
      EPSP0 = EKSHELL(1,2)
      EPSE0 = EKSHELL(2,2)
C
      RHOP0 = EKSHELL(1,3)
      RHOW = 0.
      RHOP = M * NP / VSHELL(1,1)
```

```
      RHOE = M * NE / VSHELL(2,1)
      RHOWT = 0.
      RHOET = ( ( ( 1 - FE ) / RHOP ) + ( FE / RHOE ) )**(-1.)
C
      NUW = 0.
      NUP = CD * KP0**(2.) / EPSP0
      NUE = CD * KE0**(2.) / EPSE0
      NUTW0 = 0.
      NUTE0 = ( ( ( 1 - FE ) / NUP ) + ( FE / NUE ) )**(-1.)
C
      DRHODT = (RHOP - RHOP0) / DT
C
      AW0K = 0.
      AP0K = DVOL / DT
      AE0K = SE * RHOET * NUTE0 / SIGK / RHOP / DRE
      SC0K = 2. / 3. * KP0 / RHOP * DRHODT + KIMP - EPSP0
      SP0K = 0.
      BK = 0.
C
      AW0E = 0.
      AP0E = DVOL / DT
      AE0E = SE * RHOET * NUTE0 / SIGEPS / RHOP / DRE
      SC0E = 4. / 3. * EPSP0 / RHOP * DRHODT +
     +         CEPS2 * EPSP0**2. / KP0
      SP0E = -2. * CEPS2 * EPSP0 / KP0
      BE = SP0E * DVOL
C
      IF ( DRHODT .LT. 0. ) THEN
            SC0K = KIMP - EPSP0
            SP0K = 2. / 3. / RHOP * DRHODT
            BK = SP0K * DVOL
            SC0E = -CEPS2 * EPSP0 / KP0
            SP0E = 4. / 3. / RHOP * DRHODT
            BE = SP0E * DVOL
      ENDIF
C
      KP = ( ( AE0K * KE0 ) + ( AW0K * KW0 ) +
     +         ( ( AP0K - AE0K - AW0K + BK ) * KP0 ) +
     +         ( SC0K * DVOL ) ) / AP0K
C
      EPSP = ( ( AE0E * EPSE0 ) + ( AW0E * EPSW0 ) +
     +           ( ( AP0E - AE0E - AW0E + BE ) * EPSP0 ) +
     +           ( SC0E * DVOL ) ) / AP0E
C
      OMEGA(1) = CPHI * EPSP / KP
      GAMRHO(1) = CMU / SIGPHI * KP**(2.) / EPSP
C
      EKSHELL(1,1) = KP
      EKSHELL(1,2) = EPSP
      EKSHELL(1,3) = RHOP
      EKSHELL(1,4) = DRHODT
      EKSHELL(1,5) = VSHELL(1,1)
      EKSHELL(1,6) = VSHELL(1,2)
      EKSHELL(1,7) = 2. / 3. * KP0 / RHOP0 * DRHODT
```

```
      EKSHELL(1,8) = KP0
      EKSHELL(1,9) = EPSP0
C
C     next to deal with the internal shells
C
      DO 820 I = 2,ISHELL-1
C
        SW = SE
        SE = 4. * PI * VSHELL(I,2)**(2.)
        DVOL = VSHELL(I,1)
        DRW = DRE
        DRE = 0.5 * ( VSHELL(I+1,2) - VSHELL(I-1,2) )
        NW = NP
        NP = NE
        NE = INSHELL(I+1)
C
        KW0 = KP0
        KP0 = KE0
        KE0 = EKSHELL(I+1,1)
C
        EPSW0 = EPSP0
        EPSP0 = EPSE0
        EPSE0 = EKSHELL(I+1,2)
C
        RHOP0 = EKSHELL(I,3)
        RHOW = RHOP
        RHOP = RHOE
        RHOE = M * NE / VSHELL(I+1,1)
        RHOWT0 = ( ( ( 1 - FW ) / RHOP ) + ( FW / RHOW ) )**(-1.)
        RHOET0 = ( ( ( 1 - FE ) / RHOP ) + ( FE / RHOE ) )**(-1.)
C
        NUW = NUP
        NUP = NUE
        NUE = CD * KE0**(2.) / EPSE0
        NUTW0 = ( ( ( 1 - FW ) / NUP ) + ( FW / NUW ) )**(-1.)
        NUTE0 = ( ( ( 1 - FE ) / NUP ) + ( FE / NUE ) )**(-1.)
C
        DRHODT = (RHOP - RHOP0) / DT
C
        AW0K = SW * RHOWT0 * NUTW0 / SIGK / RHOP / DRW
        AP0K = DVOL / DT
        AE0K = SE * RHOET0 * NUTE0 / SIGK / RHOP / DRE
        SC0K = 2. / 3. * KP0 / RHOP * DRHODT + KIMP - EPSP0
        SP0K = 0.
        BK = 0.
C
        AW0E = SW * RHOWT * NUTW0 / SIGEPS / RHOP / DRW
        AP0E = DVOL / DT
        AE0E = SE * RHOET * NUTE0 / SIGEPS / RHOP / DRE
        SC0E = 4. / 3. * EPSP0 / RHOP * DRHODT +
     +           CEPS2 * EPSP0**2. / KP0
        SP0E = -2. * CEPS2 * EPSP0 / KP0
        BE = SP0E * DVOL
C
```

```
         IF ( DRHODT .LT. 0. ) THEN
               SC0K = KIMP - EPSP0
               SP0K = 2. / 3. / RHOP * DRHODT
               BK = SP0K * DVOL
               SC0E = -CEPS2 * EPSP0 / KP0
               SP0E = 4. / 3. / RHOP * DRHODT
               BE = SP0E * DVOL
         ENDIF
C
C
         KP = ( ( AE0K * KE0 ) + ( AW0K * KW0 ) +
     +           ( ( AP0K - AE0K - AW0K + BK ) * KP0 ) +
     +           ( SC0K * DVOL ) ) / AP0K
C
         EPSP = ( ( AE0E * EPSE0 ) + ( AW0E * EPSW0 ) +
     +             ( ( AP0E - AE0E - AW0E + BE ) * EPSP0 ) +
     +             ( SC0E * DVOL ) ) / AP0E
C
         OMEGA(I) = CPHI * EPSP / KP
         GAMRHO(I) = CMU / SIGPHI * KP**(2.) / EPSP
C
         EKSHELL(I,1) = KP
         EKSHELL(I,2) = EPSP
         EKSHELL(I,3) = RHOP
         EKSHELL(I,4) = DRHODT
         EKSHELL(I,5) = VSHELL(I,1)
         EKSHELL(I,6) = VSHELL(I,2)
         EKSHELL(I,7) = 2. / 3. * KP0 / RHOP * DRHODT
         EKSHELL(I,8) = KP0
         EKSHELL(I,9) = EPSP0
C
 820     CONTINUE
C
C    last it is necessary to deal with the outermost shell
C
       SW = SE
       SE = 0.
       DVOL = VSHELL(ISHELL,1)
       DRW = DRE
       DRE = 0.
       NW = NP
       NP = NE
       NE = 0.
C
       KW0 = KP0
       KP0 = KE0
       KE0 = 0.
C
       EPSW0 = EPSP0
       EPSP0 = EPSE0
       EPSE0 = 0.
C

       RHOP0 = EKSHELL(ISHELL,3)
```

```
      RHOW = RHOP
      RHOP = RHOE
      RHOE = 0.
      RHOWT = ( ( ( 1 - FW ) / RHOP ) + ( FW / RHOW ) )**(-1.)
      RHOET = 0.
C
      NUW = NUP
      NUP = NUE
      NUE = 0.
      NUTW0 = ( ( ( 1 - FW ) / NUP ) + ( FW / NUW ) )**(-1.)
      NUTE0 = 0.
C
      DRHODT = (RHOP - RHOP0) / DT
C
      AW0K = SW * RHOWT * NUTW0 / SIGK / RHOP / DRW
      AP0K = DVOL / DT
      AE0K = 0.
      SC0K = 2. / 3. * KP0 / RHOP * DRHODT + KIMP - EPSP0
      SP0K = 0.
      BK = 0.
C
      AW0E = SW * RHOWT * NUTW0 / SIGEPS / RHOP / DRW
      AP0E = DVOL / DT
      AE0E = 0.
      SC0E = 4. / 3. * EPSP0 / RHOP * DRHODT +
     +         CEPS2 * EPSP0**2. / KP0
      SP0E = -2. * CEPS2 * EPSP0 / KP0
      BE = SP0E * DVOL
C
      IF ( DRHODT .LT. 0. ) THEN
            SC0K = KIMP - EPSP0
            SP0K = 2. / 3. / RHOP * DRHODT
            BK = SP0K * DVOL
            SC0E = -CEPS2 * EPSP0 / KP0
            SP0E = 4. / 3. / RHOP * DRHODT
            BE = SP0E * DVOL
      ENDIF
C
      KP = ( ( AE0K * KE0 ) + ( AW0K * KW0 ) +
     +         ( ( AP0K - AE0K - AW0K + BK ) * KP0 ) +
     +         ( SC0K * DVOL ) ) / AP0K
C
      EPSP = ( ( AE0E * EPSE0 ) + ( AW0E * EPSW0 ) +
     +           ( ( AP0E - AE0E - AW0E + BE ) * EPSP0 ) +
     +           ( SC0E * DVOL ) ) / AP0E
C
      OMEGA(ISHELL) = CPHI * EPSP / KP
      GAMRHO(ISHELL) = CMU / SIGPHI * KP**(2.) / EPSP
C
      EKSHELL(ISHELL,1) = KP
      EKSHELL(ISHELL,2) = EPSP
      EKSHELL(ISHELL,3) = RHOP
      EKSHELL(ISHELL,4) = DRHODT
      EKSHELL(ISHELL,5) = VSHELL(ISHELL,1)
```

```
      EKSHELL(ISHELL,6) = VSHELL(ISHELL,2)
      EKSHELL(ISHELL,7) = 2. / 3. * KP0 / RHOP * DRHODT
      EKSHELL(ISHELL,8) = KP0
      EKSHELL(ISHELL,9) = EPSP0
C
      RETURN
      END
```